



Norwegian University of
Science and Technology

Production and Application of
Micronized Polysaccharide Particles -
Studying Perturbation of a Model
Mucus Barrier with Total Internal
Reflection Fluorescence (TIRF)
Microscopy and Atomic Force
Microscopy (AFM) Indentation

Ahne Myklatun

Master of Science in Physics and Mathematics

Submission date: June 2011

Supervisor: Bjørn Torger Stokke, IFY

Abstract

The overall aim of this project was to produce homogeneously sized polysaccharide microparticles and apply these and similar sized particles as probes for investigation of mucin layers as a model for a biological barrier. Small polysaccharide particles have many applications, e.g. within the medical field of drug delivery. In this study a microfluidic system was developed to produce alginate beads, which can be used in drug delivery systems. Different designs, continuous phases and concentrations were tested in order to find an optimal system. Beads in the size range of 10 μm were produced using a device with T-shaped design and three inlets. An electrostatic bead generator was also used to make alginate beads, however the beads produced were too large to be used in the experiments with the mucin layers.

One of the many challenges when working with drug delivery systems is the mucus barrier protecting the epithelial cells. In this study a model mucus barrier was made by immobilizing mucins, the glycoprotein responsible for the physical properties of the barrier. A procedure for fluorescence labelling of polystyrene beads with quantum dots was developed, and penetration of these beads into the model barrier was measured with total internal reflection fluorescence (TIRF) microscopy. In TIRF the excitation field intensity decays exponentially, and the emitted fluorescence intensity from the beads gives an indication of the distance between the beads and the surface. Measurements performed on mucin layers of different concentrations indicate that mucin concentrations above 0,5 mg/ml will result in a layer too thick or too dense to give a intensity signal. At mucin concentration 0,05 mg/ml fluorescence was observable in TIRF, and it was clearly weaker than for the control with a bead directly on a glass surface. This indicates that the beads hover over the surface due to the mucin layers, and show that it is in principle possible to measure the penetration depth of beads into mucin layer using TIRF.

To simulate the condition in the lungs of cystic fibrosis (CF) patients, the mucin layers were incubated with alginate. Measurements were performed to see how this affected the penetration of the beads into the layer. A weaker fluorescent signal was obtained for these samples in TIRF, which suggests that there has been interaction between mucin and alginate. It was in addition investigated how different concentrations of G-blocks in the solution affected the penetration into the mucin-alginate layer. These testes were carried out using both TIRF and atomic force microscopy (AFM) nanoindentation experiments. The TIRF measurements were inconclusive, while the nanoindentation experiments showed decreased interaction between mucin-alginate layer and a bead.

Preface

This report is the final product of the master thesis performed at the Department of Physics at the Norwegian University of science and Technology (NTNU) in the spring semester 2011.

This has been a challenging project to work with, using known techniques for new applications. It was exciting to do plan and carry out experiments to test hypotheses, and although not everything worked out as planned I have learned about many different techniques during my work.

I want to thank my supervisor, Professor Bjørn Torger Stokke, for the opportunity to work on this project, and for guidance through the work. I also want to thank Gjertrud Maurstad for performing the AFM nanoindentation experiments, and for help and support in the laboratory throughout this project. Thank you also to David Barriet for production of the microfluidic devices and for helpful discussions about designs and methods during the development of the microfluidic system. I also want to thank Astrid Bjørkøy for teaching me how to use the equipment in the laboratory. In addition I want to thank Marit Sletmoen for help with the immobilization of mucins and Kjetil Formo for help during production of alginate beads with the electrostatic bead generator.

Ahne Myklatun, Trondheim 19.06.2011

Table of Contents

1. Introduction	1
2. Theory	3
2.1 Mucins	3
2.2. Particle transport through mucus	5
2.3 Alginate particles	7
2.4 Microfluidics.....	9
2.5 Electrostatic bead generation.....	11
2.6 Total internal reflection fluorescence microscopy.....	11
2.7 Analysis of TIRF data.....	13
2.8 Quantum dots.....	16
2.9 Confocal microscopy	16
2.10 Atomic force microscopy.....	17
3. Experimental.....	19
3.1 Immobilization of mucin	19
3.2 Production of alginate particles using microfluidics	22
3.3 Production of alginate particles using the electrostatic bead generator.....	26
3.4 Fluorescence labelling of polystyrene beads	27
3.5 TIRF measurements	30
3.6 AFM nanoindentation experiments.....	34
4. Results	37
4.1 Alginate particles	37
4.2 TIRF measurements	40
4.3 AFM nanoindentation experiments.....	47
5. Discussion.....	51
5.1 Immobilization of mucins.....	51
5.2 Production of alginate beads.....	51
5.3 Labelling of beads with quantum dots.....	52
5.4 TIRF measurements	53

5.5 AFM nanoindentation experiments.....	55
5.6 Particle transport.....	56
5.7 Future perspectives.....	57
6. Conclusions.....	59
References.....	61
Appendix A.....	65
Data files.....	65
Appendix B.....	69
Table of abbreviations.....	69
Appendix C.....	70
Scatter plots for parameter fit from TIRF analysis.....	70
Appendix D.....	72
Force-distance curves from AFM nanoindentation experiments.....	72

1. Introduction

Small polysaccharide particles have many applications in different areas, like interaction studies and medicine. Among the promising medical applications is drug delivery, which uses small particles to transport medicine directly to the target cells. Substantial research and development has been done within this field, however there are still major challenges that need to be overcome.

One of the challenges when working with micro- and nanoparticles in drug delivery is the mucus layer protecting the cells in all exposed areas that are not covered by skin, including the lungs, eyes, gastrointestinal tract and the female reproductive tract. The mucus layer is a gel consisting mainly of water and glycoproteins, called mucins, secreted by the epithelial cells [1]. The mucus layer is a part of the natural defence system and acts as a barrier that will stop pathogens and other contaminants, like particles, from reaching the cells. The mucus barrier needs to be overcome in order for the particles to function properly in delivering their medicine to the cells.

Cystic fibrosis (CF) is an illness that has potential for drug delivery treatment. However, the mucus barrier protecting the cells is especially hard to overcome in the lungs of patients with CF. These patients have mutations in some of the genes regulating the production and components of the mucus barrier. This results in more viscous mucus which makes clearance difficult. The altered mucus can provide a place for bacteria to grow, which will further complicate the disease. One bacterium that is closely associated with CF is *Pseudomonas aeruginosa* [2]. This bacterium produces alginate, a biopolymer that will interact with the mucins and further increase the viscosity, which makes the delivery of medicine even more difficult.

In this study an immobilized mucin layer is used as a model for the mucus barrier. Alginate particles are produced using microfluidics, to function as a model for the drug delivery system, in addition to polystyrene beads. The aim is to produce monodisperse alginate particles with diameters in the size range 10 μm .

There are many different techniques to study the diffusion of particles through mucus, including observation in diffusion cells with a donor and a receptor cell separated by a mucus barrier, investigation of a mucus layer exposed to drugs,

and similar diffusion experiments [3]. Many of these methods are time consuming and require exact knowledge of volumes and concentrations. Another technique to study the penetration of particles into the mucin layer is reflection interference contrast microscopy (RICM), which allows for determination of distances between interacting surfaces [4].

An alternative, developed in this study, is to use total internal reflection fluorescence (TIRF) microscopy. In this technique a decaying excitation field is created, and the penetration of fluorescently labelled microparticles into the mucin layer is measured by detecting the fluorescence intensity, which is dependent on the height above the surface [5]. In addition atomic force microscopy (AFM) nanoindentation experiments are carried out to obtain force distance curves as a basis to measure mechanical properties and layer thickness that can be related to the results obtained by the TIRF experiments.

To simulate the condition of CF the mucin layers are incubated with alginate. It is investigated how a combination of mucins and alginate will affect the penetration of the particles. It is further investigated if addition of alginate oligomers will compete with the longer alginate chains and reduce the mucus viscosity [6], and thereby increase the penetration depth of the microparticles into the mucin-alginate layers. This would be an effective way to help the particles loaded with medicine to reach their target in the lungs of CF patients.

2. Theory

2.1 Mucins

Mucins are large glycoproteins produced by epithelial cells. There are many different mucins in the mucin family, and they are characterized by the mucin domain, which is a variable number of tandem repeats. This region is rich in serine and threonine residues, which function as sites for O-glycosylation (Figure 1). The mucins are often heavily glycosylated, and the oligosaccharides may contribute to over half of the mass of the glycoprotein [1].

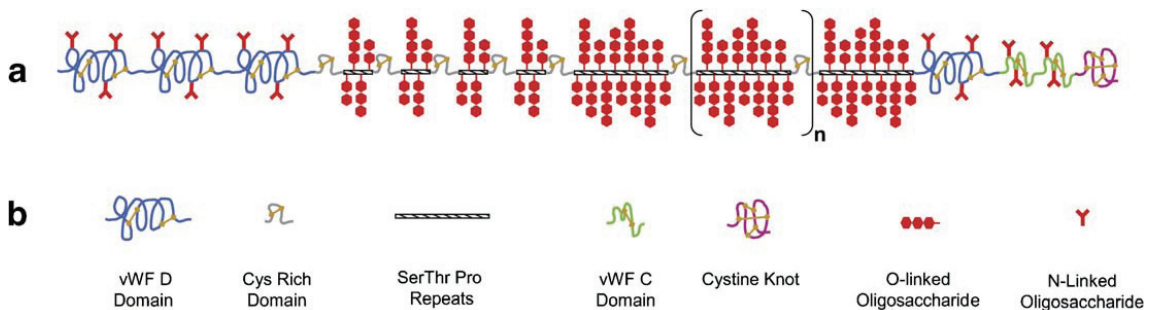


Figure 1: (a) Schematic illustration of a mucin molecule showing how the thickness of the molecule varies from the glycosylated parts (red) to the naked protein (blue, green and striped). (b) The symbols indicate different domains of the mucin molecule. The figure is from Bansil et al. [7].

The mucins can be divided into two main groups; secreted mucins and transmembrane mucins. The secreted mucins are extracellular and gel-forming. The transmembrane mucins have a short tail in the cytoplasm of the epithelial cell, a single hydrophobic domain through the membrane and a large extracellular domain. This domain can extend up to 1500 nm into the extracellular matrix, depending on the type of mucin [1].

Mucins are heterogeneous with respect to length, molecular weight, composition and extent of oligosaccharides [3]. The structure of mucins can be characterized by various techniques, but the result might vary for different mucins and techniques. The conformation of mucins is also dependent on the environment [3]. One technique that can be used to determine length, thickness and structure is atomic force microscopy (AFM). The thickness of mucins varies along the

molecule, from the thin naked protein to the thick glycosylated parts [8]. Figure 2 shows an image of mucin molecules obtained with electron microscopy [9].

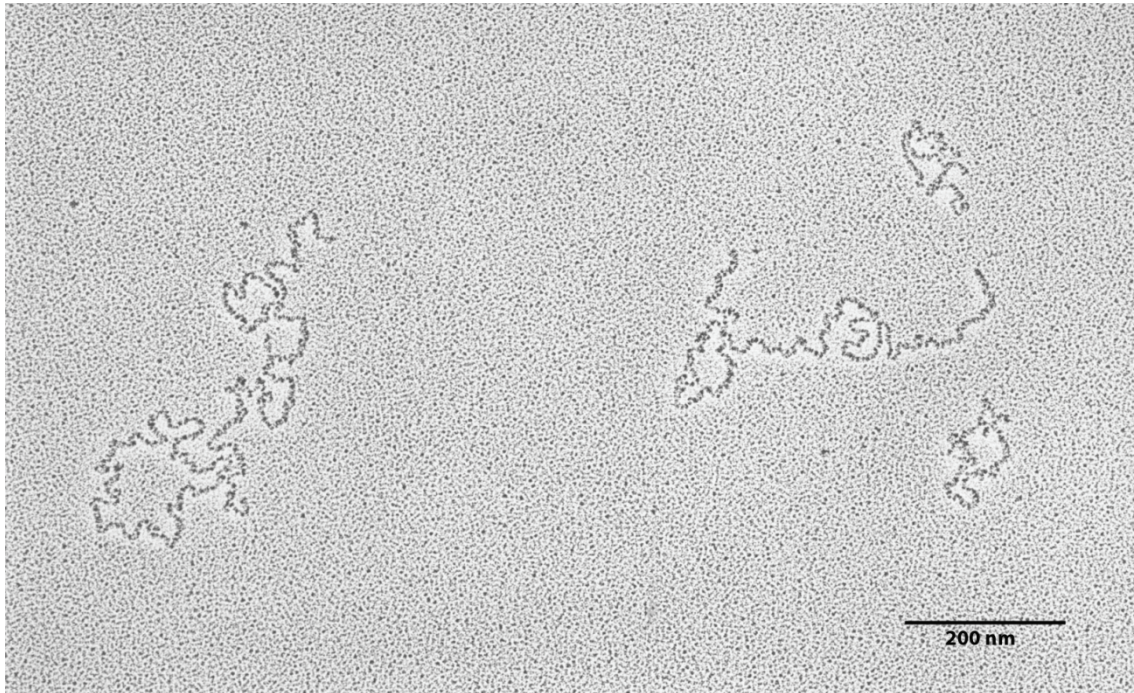


Figure 2: Electron micrograph of human-bronchial mucin molecules. The image is from Stokke et al. [9].

Together with water and other extracellular molecules, like lipids and mineral salts, the mucins make up the mucus layer protecting the underlying epithelial cells from pathogens and other contaminants (Figure 3). The mucus layer also contributes to hydration and lubrication, due to the hydrophilic environment created by the glycosylated parts of mucins [1]. The sugar chains are negatively charged and are important for the solubility and they contribute to the extended structure of the mucins [10]. Some transmembrane mucins are also thought to be a part of a signalling pathway in the cells [1]. When bacteria interact with the extracellular domain of a mucin it stimulates a cellular response. The mucins are also involved in adhesion between cells through signalling pathways [1].

The combination of the different mucins and the extent of glycosylation depend on the tissue type in which they are produced, the physiological state of the cell and different stimuli like hormones. If the regulation of mucins is altered it may lead to various diseases, like cystic fibrosis (CF), asthma or cancer [1].

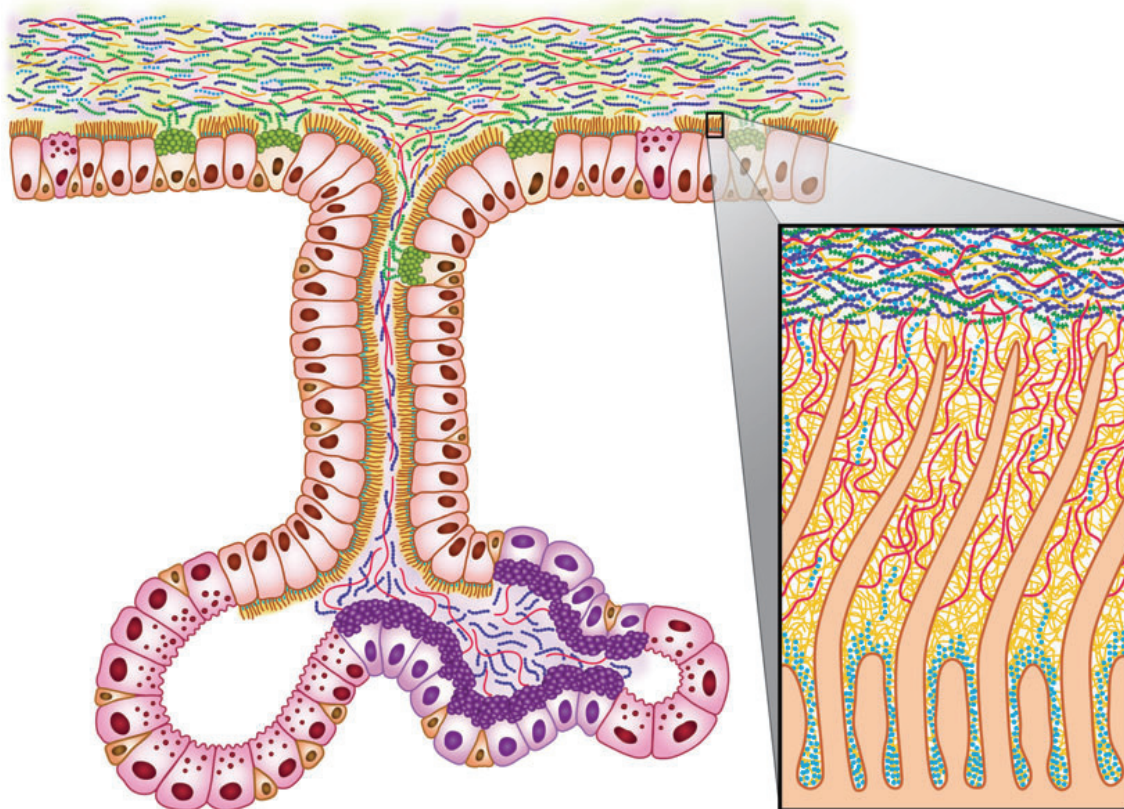


Figure 3: Illustration from Hattrup et al.[1] showing how the mucus layer consisting of different mucins protect the epithelial cells in the lungs from contaminants by making a barrier difficult to penetrate.

2.2. Particle transport through mucus

The exact function of the mucus layer is not well understood. It is a common assumption that the mucins with their bottle-brush structure make up a mesh that filter out larger particles, by steric hindrance. However the pore size in the mucus layer is uncertain. Different techniques for measuring the pore size give different results, ranging from about 100 nm to 10 μm [11]. A study by Lai et al. [12] observed that the pore size is dependent on the particles. Large nanoparticles with non-mucoadhesive coating can diffuse more easily through the mucus layer than smaller mucoadhesive particles. Another result of this study was that high concentrations of nanoparticles cause the mucins to bundle together to capture the particles. This is supported by McGill et al. who found that nanoparticles can be used to open up the mucus layer for other particles, by binding to the mucin molecules [13]. Hydrophobic interaction between non-glycosylated parts of the mucin molecules may cause them to bundle together and create larger pores [11].

In addition to the size, the surface properties of the particles are important for the mobility in a mucus layer. This is important due to the negative surface charge of the mucin molecules. Coating the particles with a hydrophilic and uncharged polymer has been showed to increase the rate of transport compared to uncoated particles [12]. This is confirmed by another study of particle mobility, which showed that the mucus layer filter particles by electrostatic interactions (Figure 4) [14]. In addition to the surface charge of the particles, the salt concentration and the pH of the surrounding solution is important for the interaction between particles and mucins, and between single mucin molecules. Hong et al. [10] used AFM to show that the mucins aggregate at low pH.

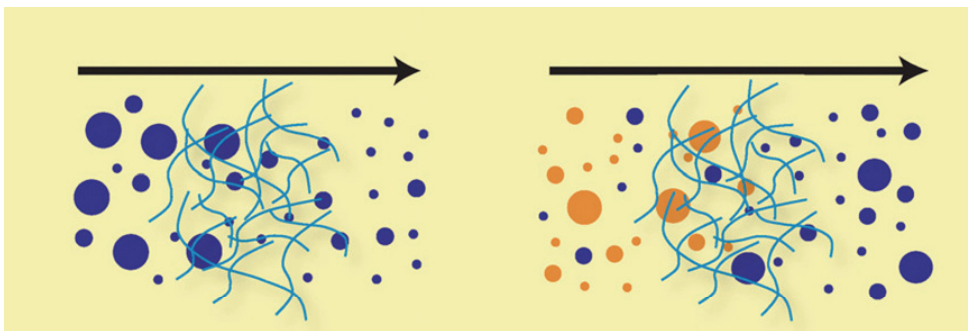


Figure 4: Illustration of different theories on how the mucus layer filters particles. To the left is filtration by size, and to the right is filtration by interaction. Figure from Lieleg et al. [14].

Patients with CF do not have a normal mucus barrier in the lungs due to alterations in one or more gene that controls the production and function of the barrier. This results in a more viscous mucus layer and causes difficulties with clearance of the lungs. Some bacteria, like *Pseudomonas aeruginosa*, are able to grow in this altered mucus [2]. *Pseudomonas aeruginosa* is an antibiotic-resistant bacterium, and will therefore often be the dominating bacteria in the lungs of CF patients after a while. When present in the mucus of CF patients the bacteria produce alginate, which contributes to hydration and protection from the immune system [2]. The alginate contains mostly mannuronate residues and acetyl groups. This alginate might interact with mucins and cause the mucus to become even more viscous, and thereby make delivery of medication through micro- and nanoparticles more challenging. This is a major problem when treating CF patients, since up to 90 % of the patients are infected with the alginate-producing bacterium [2].

It has been shown that addition of guluronate to the altered mucus of CF patients infected with *Pseudomonas aeruginosa* will reduce the viscosity of the mucus [6]. In this study, we explore to which extent addition of short alginate G-blocks to the solution covering the mucin-alginate layers perturb the nanomechanical properties and thickness of these. The hypothesis is that the shorter oligomers can compete with the alginates in binding to the mucins and thereby reduce alginate-mediated mucus hyperviscosity. This would open up the mucus layer, and thus addition of G-block could make subsequent drug delivery more efficient. Alternatively, the G-blocks can act as medicine itself, due to the lower viscosity of the mucus and thereby easier clearance of the lungs [6].

2.3 Alginate particles

Alginate is an unbranched biopolymer, found in brown algae. It consists of the two sugars β -D-mannuronic acid (M) and α -L-guluronic acid (G). Alginates are generally built up of M-blocks, G-blocks, MG-blocks and other random sequences (Figure 5). The composition determines the chemical and physical properties of alginate, like the viscosity [15].

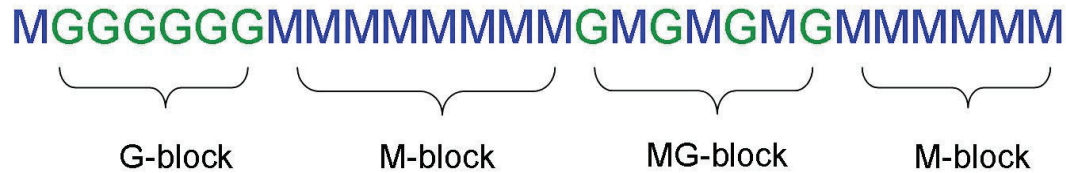


Figure 5: The principle of how alginates are built up by blocks.

Alginate can bind divalent cations, like Ca^{2+} and Ba^{2+} , to form a gel. This is a fast process that can be understood by the egg-box model (Figure 6), where the cations are bound between two chains of guluronate residues [15]. Since gelation is dependent on two chains of guluronate, there is a minimum concentration at which alginate can form a gel. This is called the critical overlap concentration and is defined by the concentration when alginate chains start overlapping in the solution and the viscosity becomes more dependent on the alginate concentration [16].

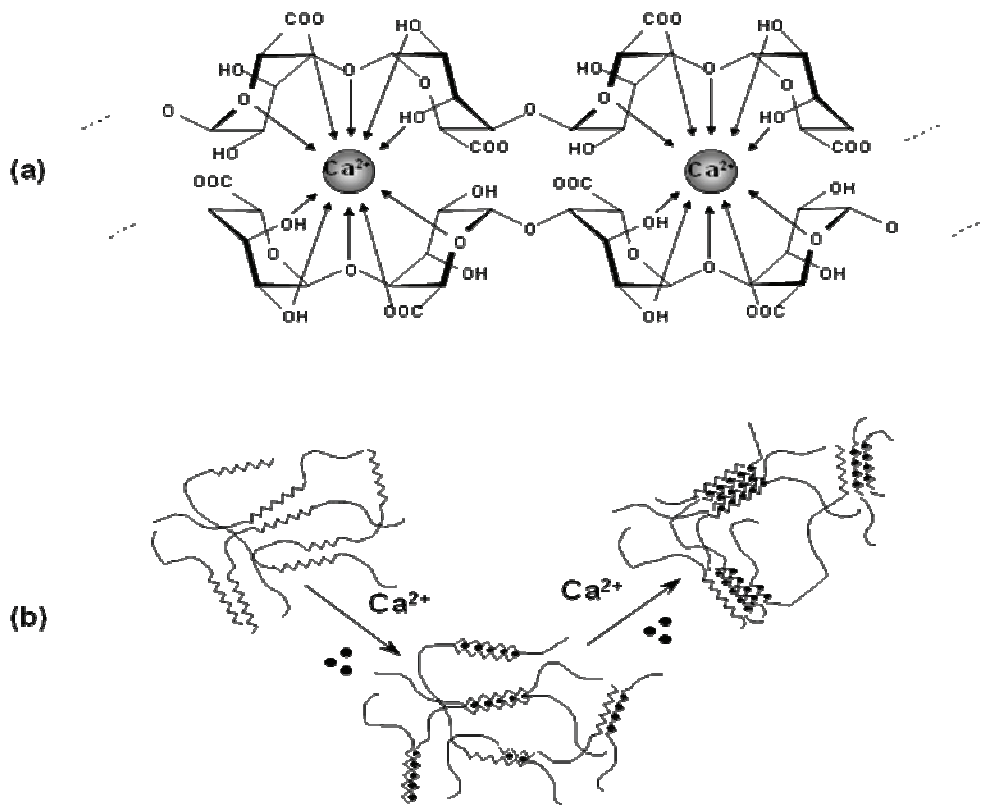


Figure 6: (a) The egg-box model illustrates how calcium ions bind between two chains of guluronate residues and (b) how this makes alginate form a gel. The figure is from the doctoral thesis of Mørch [17].

Due to the gel forming property of alginate, it can be used to make gel beads. Micro- and nanometer sized alginate particles have applications in the studies of behaviour and interaction of biopolymer with atomic force microscopy and optical tweezers [18]. Alginate is biocompatible, and can therefore be used in medical applications like drug delivery [19], imaging, tissue engineering [20] and cell encapsulation [17].

There are different ways to produce alginate particles. A strategy that was developed earlier is the use of microfluidics [21]. This technique gives in general smaller particles and good monodispersity in size, and was further developed in this study. Other techniques for bead production are to make use of self assembly in the layer-by layer technique [22] or to use emulsification techniques [23]. Alternatively an electrostatic system can be used to generate alginate beads [24].

2.4 Microfluidics

Microfluidics is manipulation of fluids in channels of micrometer size. At this size scale the Reynolds number is low and the viscous forces dominate over inertial forces. The flow is laminar in the small channels and this can be used to make droplets. Microfluidics is often preferred over other techniques due to the small size of beads and monodispersity that is possible to obtain.

The production of alginate beads with microfluidics was explored in an earlier project [21]. A proof of concept was made with a flow focusing design. There are in general two solutions in the channels when microfluidic devices are used to produce polymer particles. The dispersed phase is the solution which the beads are made of, and a continuous phase is the solution that breaks up the dispersed phase and surrounds the beads. In a flow focusing design the dispersed phase flows in a central channel, while the continuous phase flows in the side channels (Figure 7a). When the channels are brought together the continuous phase will impose a shear stress on the dispersed phase, and thereby cause it to break. The droplets will then flow, surrounded by the continuous phase, towards an exit channel. The same principle is valid also for other designs of the microfluidic channels seen in Figure 7. The size of the beads produced are dependent both on the dimensions of the channels and the flow rate ratio of the two phases [25].

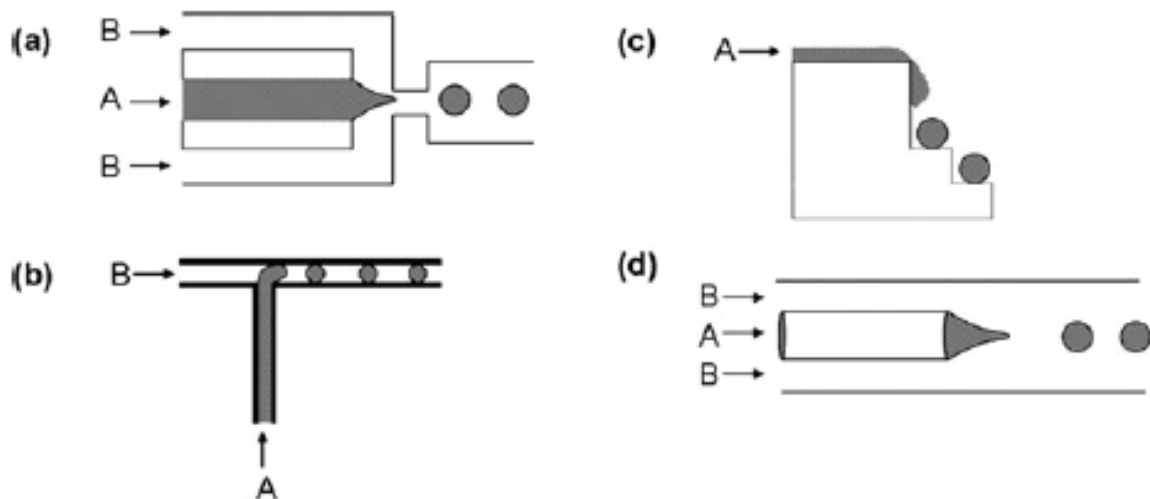


Figure 7: Different designs for production of beads in a microfluidic device. (a) Flow focusing, (b) T-shaped, (c) terrace-like and (d) concentric capillaries. In each case A is the dispersed phase and B is the continuous phase. Figure from Tumarkin et al. [25].

After the beads are formed, gelation has to take place in order to stabilize the beads. This can be done by introducing the gel-inducing ions, often referred to as crosslinking agents, externally. This is done outside the microfluidic device, in a bath containing crosslinking agents. There are also possibilities for gelation inside the microfluidic device, like coalescence of the beads with droplets containing a crosslinking agent [25]. An alternative is to let a solution with gel-inducing ions be mixed with the dispersed phase solution right before the droplets are formed. This requires an extra inlet for the crosslinking solution. Gelation inside the microfluidic device can also be obtained by mixing inactive crosslinking agents with the dispersed phase, and then activate the ions after the beads are formed. Activation can be achieved by a change in pH or by UV radiation. This method is called internal gelation. Alternatively external gelation can be obtained by adding crosslinking agents to the continuous phase, so that the ions will diffuse into the beads after they are formed (Figure 8) [25].

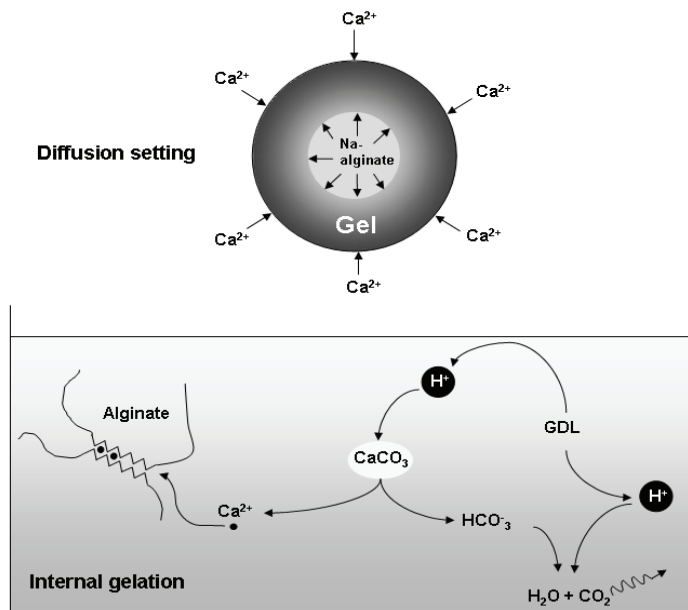


Figure 8: The principle of external gelation of alginate beads with Ca^{2+} (top) and the principle of internal gelation triggered by lowering the pH value of the solution (bottom). The figure is from the doctoral thesis of Mørch [17].

To produce alginate particles, an alginate solution is used as the dispersed phase. An oil or an organic solvent like DMC [26] is often used as the continuous phase. For gelation of alginate beads divalent cations are used as crosslinking agents. Ca^{2+} is often preferred, especially if the beads should be used in medical applications, since Ba^{2+} is toxic.

2.5 Electrostatic bead generation

An alternative to microfluidics for production of alginate beads is to use an electrostatic system [24]. The principle of an electrostatic bead generator is to use electrostatic forces to pull off droplets from a needle. A pump is used to push an alginate solution through a tube and into the needle, which has a small inner diameter. A calcium bath is placed under the needle. A power source is connected to a pole into the calcium bath and the needle, which results in a voltage drop across the space between the calcium bath and the needle. This will cause small alginate droplets to be pulled off from the needle in a high rate, before they are able to grow into big droplets. The different parameters in the setup, like the alginate concentration, voltage, pump speed, distance between needle and calcium bath and the needle inner diameter, determines the size of the particles produced.

During the production of alginate beads with this technique, satellites will also be formed. These are alginate beads, much smaller than the original beads. It has not been performed studies that determine what affects the production of satellites. In this study it was investigated if these satellite beads are small enough to be used in the further experiments.

2.6 Total internal reflection fluorescence microscopy

Total internal reflection fluorescence (TIRF) microscopy is a microscopy technique used to image fluorescent samples [27]. When an incident ray reaches a surface, it will be transmitted and reflected, depending on the refractive indices and the angle between the surface normal plane and the incident ray. At some angle, called the critical angle θ_c , the incident light will be totally reflected. The critical angle is dependent on the refractive indices of the two mediums n_1 and n_2 , and is given by

$$\theta_c = \sin^{-1}\left(\frac{n_2}{n_1}\right). \quad (1)$$

TIRF microscopes are operated above this critical angle, to obtain total internal reflection. The refractive index of the microscope slide has to be larger than the refractive index of the sample. Even though the incident ray is reflected at the sample surface, some of the energy will be transferred into the sample. This is an electromagnetic field, called the evanescent wave, with an intensity that decays

exponentially as

$$I(z) = I_0 e^{-\frac{z}{d}}, \quad (2)$$

where I_0 is the intensity at the interface, z is the distance from the interface and d is the penetration depth. The penetration depth of the evanescent field is typically in the range of 100 nm and depends on the incidence angle θ and the wavelength of the incoming light λ as

$$d = \frac{\lambda}{2\pi n_1 \sqrt{\sin^2 \theta - \left(\frac{n_2}{n_1}\right)^2}}, \quad (3)$$

where n_1 and n_2 are the refractive indices of the glass surface and the liquid in the sample, respectively.

Fluorescent molecules within this evanescent field will be excited, if the light has the appropriate wavelength. Since the excitation field decays exponentially, only molecules close to the surface will be excited (Figure 9). This is often useful as parts of the sample that are outside of the field will not be excited and emit fluorescence that can contribute to the signal during measurements. TIRF is a technique that is often used to study interactions between cells and surfaces and movement of molecules close to surfaces [27].

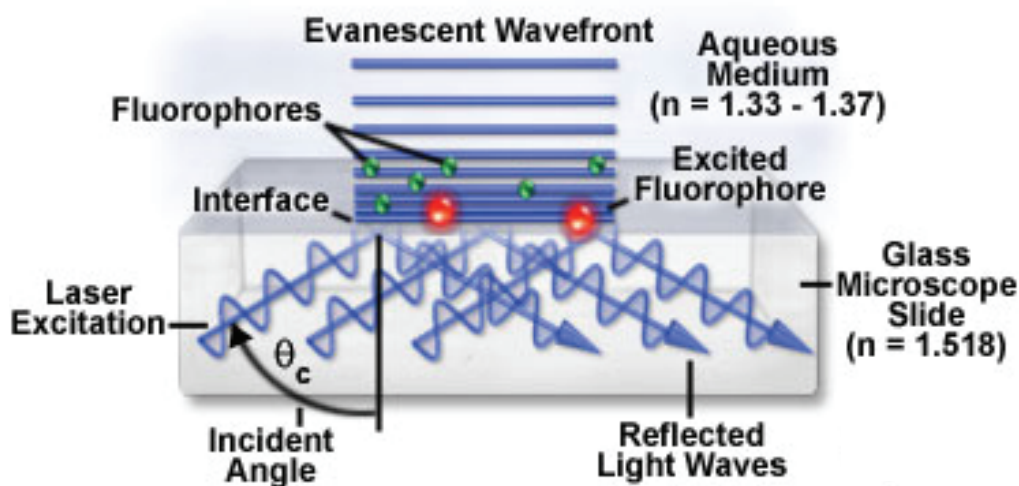


Figure 9: Schematic illustration of the principle of TIRF microscopy from the Nikon MicroscopyU web page [28]. The laser beam hits the glass surface with an angle larger than the critical angle. This results in an evanescent wave that decays exponentially. Fluorophores within this field are excited and emit fluorescence.

In this study the technique was used to determine how far into a mucin layer fluorescent particles can move (Figure 10). Since the evanescent field decays with the distance to the source, the fluorescence from the bead is dependent on the distance from the surface. Analysis of the fluorescence intensity can therefore give indications of the distance from the fluorescent particle to the surface. In this study mucin molecules were immobilized on glass surfaces resulting in a mucin layer. Fluorescently labelled beads were suspended in a solution covering the mucin layer, and by using TIRF microscopy the intensity profile of the beads was measured and the distance from the surface to the alginate beads could be calculated.

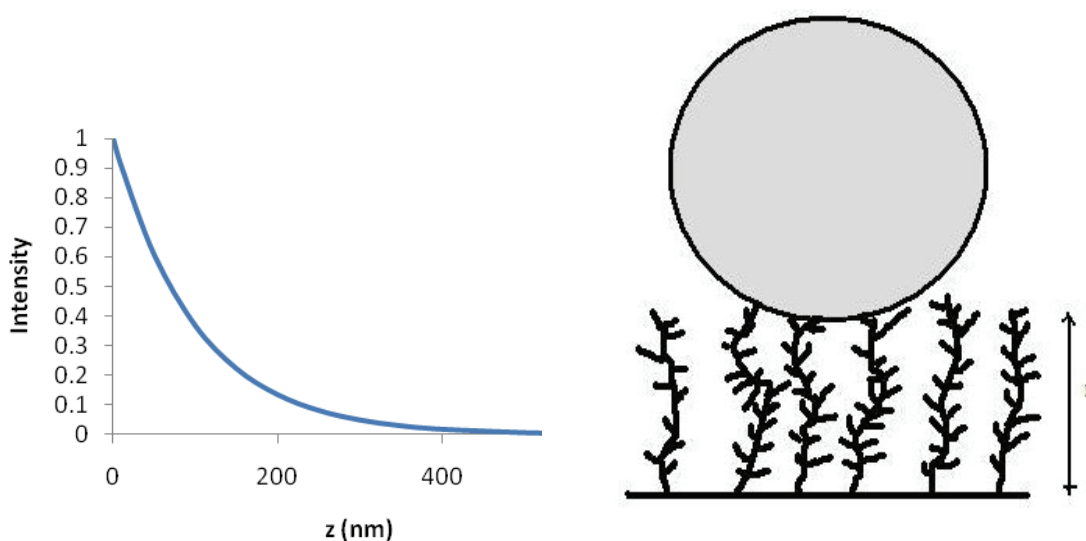


Figure 10: To the left is the intensity profile of an evanescent field, with penetration depth 100 nm, as a function of depth z . A bead on top of a mucin layer will hover a distance h over the surface (right). If the distance h is within the evanescent field the bead is excited and emits fluorescence that can be detected. The intensity of the emitted fluorescence can be used to determine the distance h .

2.7 Analysis of TIRF data

During TIRF measurements many of images containing information about the intensity distribution for a fluorescently labelled particle are obtained. As the evanescent field that excites the particles decays, the intensity from a bead is dependent on its distance from the surface. The obtained intensity information can therefore be converted into a height measurement for the particle. Series of intensity measurements are necessary because the particle is in solution and will perform Brownian motions.

To be able to analyse the intensity a mathematical expression for the fluorescence is needed. Figure 11 shows a sphere of radius R on a surface, where r is the distance from the centre of the bead and z is the distance from the surface to the bead at position r . The parameters relate to each other as follows

$$\begin{aligned} z &= R - R \cos \alpha \\ r &= R \sin \alpha . \end{aligned} \tag{4}$$

This gives an expression for z as a function of r for the bottom half of the sphere

$$z = R(1 - \cos \alpha) = R\left(1 - \sqrt{1 - \sin^2 \alpha}\right) = R\left(1 - \sqrt{1 - \left(\frac{r}{R}\right)^2}\right). \tag{5}$$

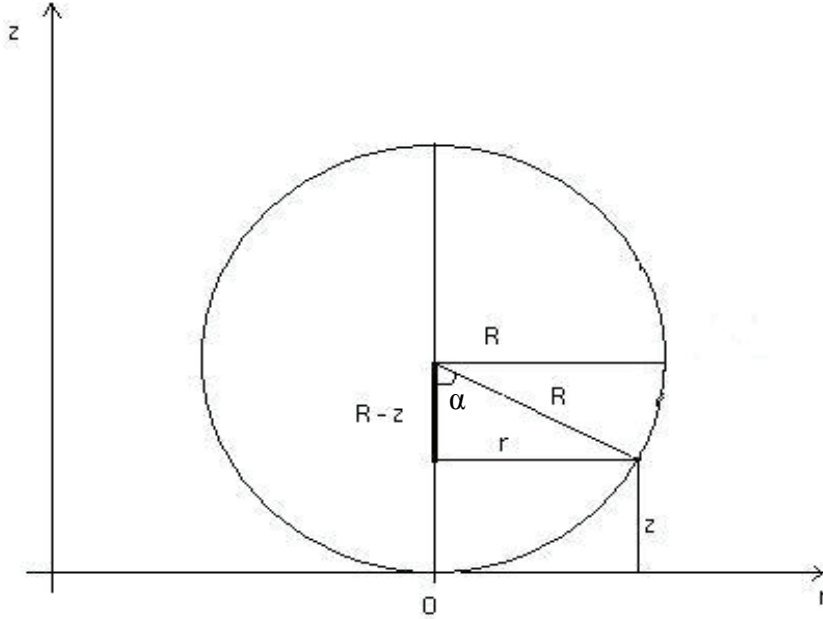


Figure 11: Schematic illustration of a bead on a surface.

The intensity from a fluorescently labelled bead in an evanescent field is thus given by

$$I(r) = I_0 e^{-\frac{R}{d}\left(1 - \sqrt{1 - \left(\frac{r}{R}\right)^2}\right)}, \tag{6}$$

where I_0 is the intensity at the surface. The diameter of the beads is much larger

than the penetration depth of the evanescent field, and only fluorescence from the bottom half of the sphere is considered. If the bead is hovering a distance h over the surface, the expression for the intensity needs to be modified to

$$I(r) = I_0 e^{-\frac{R}{d} \left(1 - \sqrt{1 - \left(\frac{r}{R} \right)^2} \right) - \frac{h}{d}} \quad (7)$$

Mattheyes et al. [5] have shown that the evanescent field intensity profile measured with a bead is better described with an double exponential function, of the form

$$I = A e^{-Bz} + C e^{-Dz} \quad (8)$$

They found that the majority of the intensity is a fast decaying exponential for small distances. A slow decaying exponential is dominating at larger distances due to contribution from light scattering [5].

The probability of finding the bead at a given height h is given by the Boltzmann distribution,

$$p(h) = A e^{-\frac{\varphi(h)}{kT}}, \quad (9)$$

where $\varphi(h)$ is the potential energy of the bead at this height, kT is the thermal energy and A is a normalization constant. The number of observations of a given height is proportional to the probability density. For the analysis a histogram of the measured intensities of the images is created. The number of observations of a given intensity is equal to the number of observations of the corresponding height. This can be used to obtain the potential energy $\varphi(h)$ from the histogram of intensities, if the bins in the intensity histogram are small and equal [29]. The potential is then given by

$$\frac{\varphi(h) - \varphi(h_0)}{kT} = \ln \frac{N(I_0) I(h_0)}{N(I) I(h)}, \quad (10)$$

where $\varphi(h)$ is the potential energy of the bead at height h and kT is the thermal energy. N is the number of observations and I is the intensity for a given height h ,

h_0 is the reference height, for example at the glass surface, and I_0 is the intensity at this reference height [29].

2.8 Quantum dots

Quantum dots are nanocrystals of a semiconductor material [30]. Because of their small size quantum dots exhibit quantum confinement. The Bohr-radius of a semiconductor is the electron-hole distance in an excitation. If the size of the particle is smaller than the Bohr-radius, the spectra for absorption and emission is shifted to shorter wavelengths. Thus the absorption and emission wavelengths can be tuned by the size of the particle. The spectra of quantum dots are narrow, which makes it possible to distinguish between different signals and make a multicolour image. Another advantage of using quantum dots to fluorescently label a sample is that time of emission is longer than for organic fluorophores, and the quantum dots do not photobleach in contrast to organic fluorophores [30].

In order for the particles on the mucin layers to be observed in TIRF measurements they have to be fluorescent. A procedure for covalently linking quantum dots to beads was developed for this purpose.

2.9 Confocal microscopy

In conventional microscopy thick specimens can cause a problem at high magnifications. This is because the depth of field is small, which means that only a section of the sample is in focus. Contributions from the parts of the specimen that are out of focus will create a blurred image. In confocal microscopy this problem is overcome by inserting an aperture in front of the detector. The aperture is often referred to as a pinhole and is placed in the conjugate focal plane where the rays from the focal plane in the sample converge. Rays from other parts of the sample will not be in focus at the pinhole and therefore be rejected. The size of the pinhole determines how sharp the image becomes, but if it is too small most of the rays are rejected and the image becomes very dark. To compensate for this in the case of fluorescent samples the intensity of the excitation laser will have to be increased [27].

By scanning the sample in a raster scan a section of a specimen can be imaged. Images of sections at different depth in the sample can be put together to form a 3D image of the specimen [27]. Confocal microscopy can be used to observe

fluorescently labelled samples, and by performing a 3D scan it can be determined if the fluorescence is on the outside of the sample or if it is stained all the way through. This was done in this study to determine if linking of quantum dots to beads was successful.

2.10 Atomic force microscopy

Atomic force microscopy (AFM) is an ultramicroscopy technique that is used to make topographic images of a sample and measure interaction forces between a sample and a tip. This is done by scanning the tip over the sample in a raster pattern. The tip is attached to a tip holder and together they are called a cantilever. A laser is directed towards the cantilever and the light is reflected onto a photodiode that detects the deflection of the cantilever resulting from forces between the sample and tip (Figure 12). The movement of the cantilever is converted into force measurements by using Hooke's law and the spring constant of the cantilever [31].

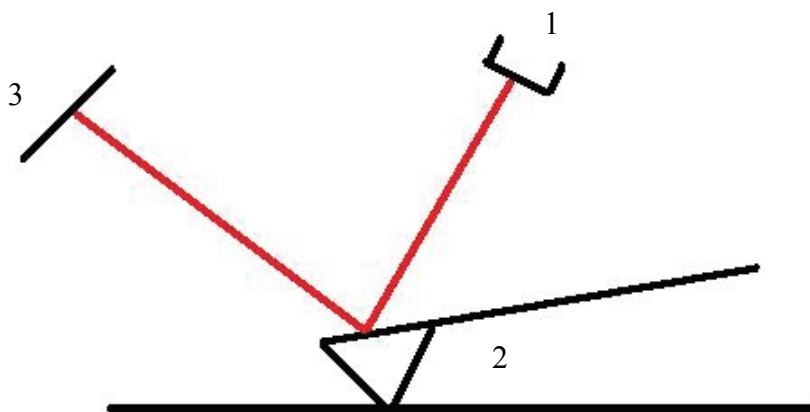


Figure 12: Sketch to illustrate the principle of AFM. (1) A laser beam hits the cantilever (2), which reflects the laser light to a detector (3) that determines the deflection of the cantilevers caused by the sample surface.

AFM can also be used to measure forces between tip and sample. The tip is moved towards the sample, and the deflection of the cantilever is detected. When the tip approaches the sample it will deflect as contact with the sample is reached. This causes an inflexion point in the force curve at the contact point. The shape of the curve is dependent on the elasticity of the sample. The Hertz model can be applied to the curve. In this model it is assumed that the sample is infinite, homogenous and has linear elasticity [32]. The model is used to obtain Young's modulus, which describes the elasticity of the sample. As the tip is

pulled away from the sample adhesive interactions will work against the movement.

AFM indentation has been used by Dagdas et al. [33] to characterize stiffness of gels. AFM indentation measurements can also be performed with a spherical geometry on the tip. If a mucin layer is used as a sample, this will function as a model of a particle approaching mucus. As the tip first approaches the mucin layer and then the surface underneath, these force curves should have two points where the slope changes. The distance between these should give an indication of the thickness of the mucin layer (Figure 13).

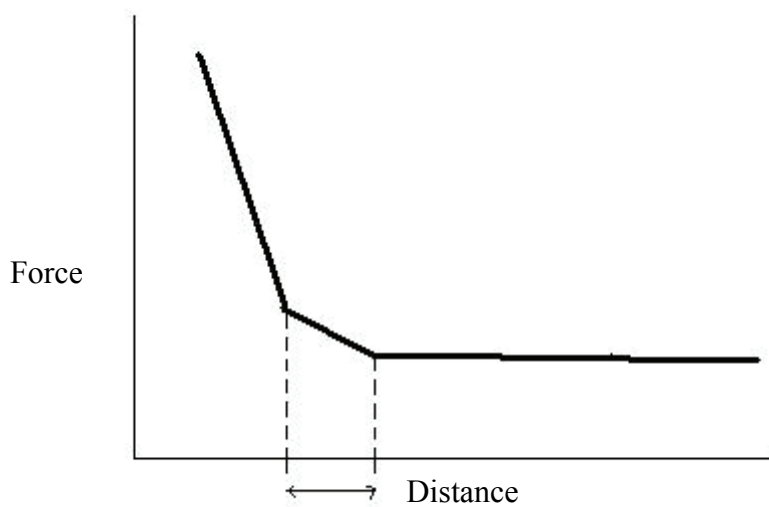


Figure 13: Illustration that shows a theoretical force-distance curve for the tip approaching the sample in an AFM indentation experiment with a mucin layer. The distance between the two points where the slope changes corresponds to the thickness of the mucin layer.

3. Experimental

3.1 Immobilization of mucin

A glass well for TIRF microscopy (WillCo Wells, Amsterdam) was used. The surface was cleaned by covering it with a mix of equal amounts of methanol (KEBO-Lab) and HCl (Sigma-Aldrich), and leaving it for 30 min. The surface was rinsed with mq-water (Millipore Simplicity 185, 18,2 M Ω). Four silicon wells were fastened to the surface (Figure 14). Silanization of the glass surface was done by filling three of the silicone wells with a solution containing 1 % v/v trimethoxysilylpropyl-diethylenetriamine (DETA) (Aldrich, USA) in 1 mM acetic acid for 20 min. Afterwards the surface was rinsed with mq-water. Three mucin solutions with different concentrations were prepared. Equal concentrations of pig gastric mucin (PGM) and 1-(3-dimethylaminopropyl)-3-ethylcarbodiimide hydrochloride (EDAC) were dissolved in 50 mM boric acid with pH 5,8. Both mucin and EDAC were added to obtain 0,5 mg/ml, 1 mg/ml and 2 mg/ml. The three mucin solutions were added to the three silicone wells with silanized glass surfaces. The last well was kept empty as a reference. The glass well was left in the refrigerator with the plastic cover on, for approximately 24 hours, before the mucin solutions were replaced with a 10 mM Tris buffer solution with pH 7,4.

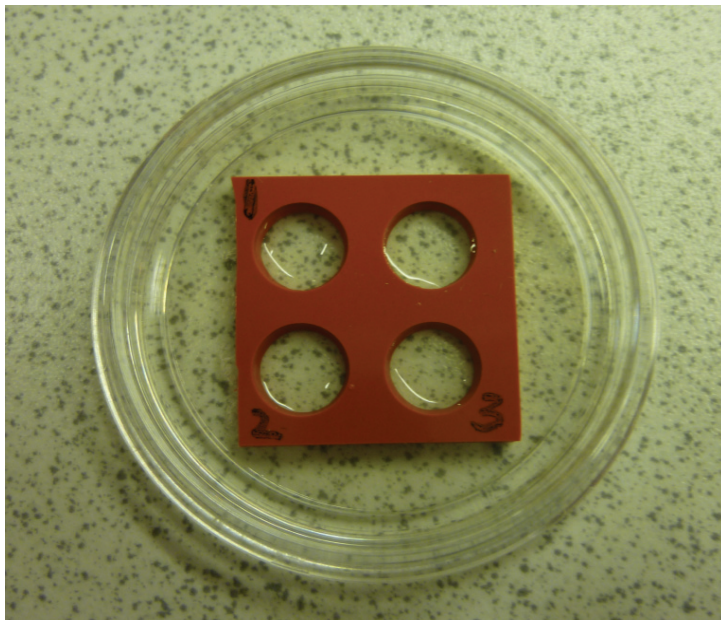


Figure 14: Silicone wells fastened to a TIRF glass wells. Mucins were immobilized in the silicone wells.

For comparison mucin layers for TIRF measurements were prepared with much lower mucin concentration. The same procedure was used, with 0,05 mg/ml of both PGM and EDAC. The wells were incubated for 5 hours with the mucin solution, before it was replaced with Tris buffer. Three parallels of this layer were made.

After TIRF measurements on the pure mucin layers, they were incubated with polyM alginate solution with concentrations 0,5 mg/ml and 2 mg/ml for one hour, to simulate the condition in the CF-affected lung. The alginate solution was prepared from the polyM alginate with fraction of mannuronic acid equal to 1 ($F_M = 1,0$) and 45 % acetyl, dissolved in 10 mM Tris buffer with pH 7,4. After incubation the mucin layer was rinsed with Tris buffer.

To perform AFM measurements mucin was immobilized to mica surfaces. The slides were cleaved on both sides, before the same procedure as for immobilization on a glass surface was used, with the exception of the first cleaning step. The concentrations of mucin and EDAC are summarized in Table 1, together with incubation times. These layers were also incubated with the alginate solution in the same way as for the mucin layers on a glass surface.

Table 1: Overview of the concentrations of mucin and EDAC used in the preparation of the layers, and alginate and G-block concentrations used during the force measurements.

PGM concentration (mg/ml)	EDAC concentration (mg/ml)	Incubation time (h)	Alginate concentration (mg/ml)	G-block concentration (mg/ml)
2	2	25	0	- 0 0,05
2	2	25	0,5	0,1 0,5 2
2	2	25	2	0 0,05 0,1 0,5 2
1	1	17	0	- 0 0,05
1	1	17	2	0,1 0,5 2
0,5	0,5	6	0	- 0 0,05
0,5	0,5	6	0,5	0,1 0,5 2

3.2 Production of alginate particles using microfluidics

All the observations of the microfluidic system were done with the Olympus IX70 inverted microscope. Videos of bead production were obtained with the high speed camera Photron Fastcam SA3 mounted to the microscope. This was used with the software PFV Ver.326. Images of the produced alginate beads were obtained with the Olympus camera mounted to the microscope together with the software AnalySIS. Fluids were pushed through the microfluidic devices by the pressure pump Fluigent MFCS-4C (1300 bar). The pressures were controlled with the software MAESFLO 4C V0.6.1 (Figure 15).

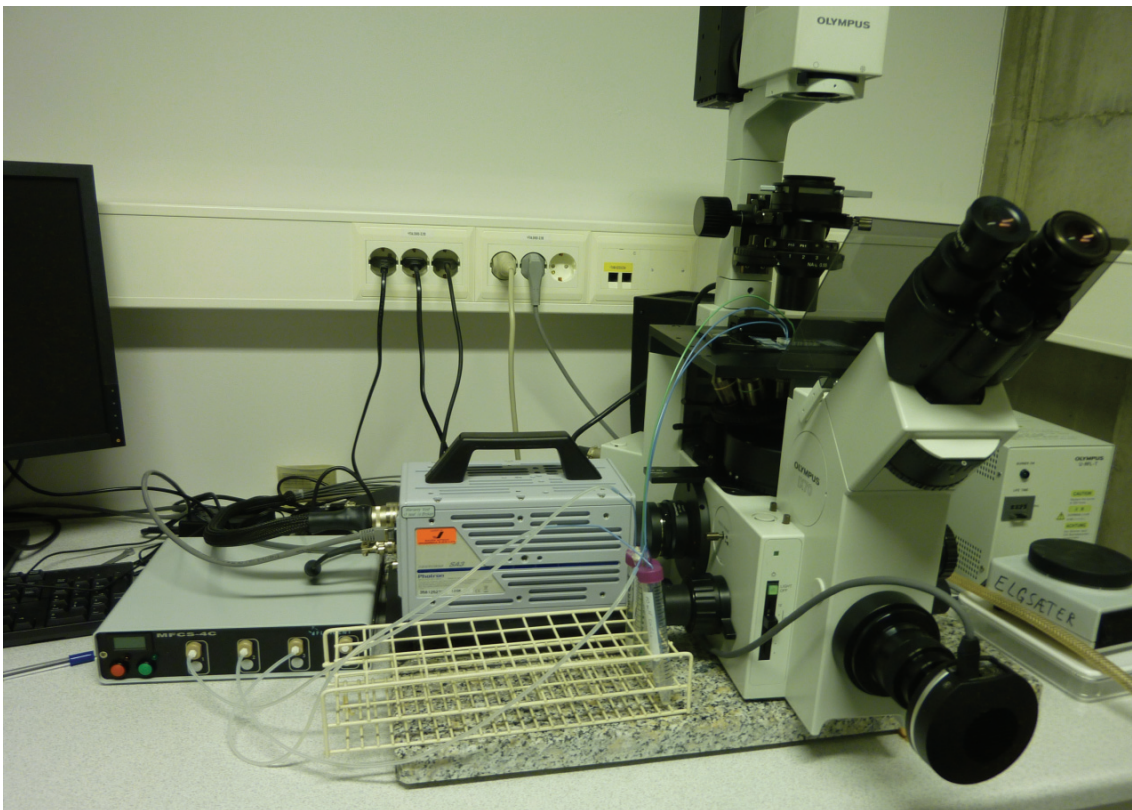


Figure 15: The microfluidic setup. To the left is the pressure pump coupled to the solutions that are pushed into the device placed on the microscope stage. The high speed camera is mounted to the side port of the Olympus IX70 microscope, and the Olympus camera is mounted to the front of the microscope.

The microfluidic devices were produced using soft lithography techniques by David Barriet in the NTNU Nanolab [21]. The channels were made in poly(dimethylsiloxane) (PDMS) and attached to a glass surface.

Alginate solutions were prepared from the high-G alginate LF10/60 (lot: SI2727 from Pronova Biopolymer). A 2 % w/v stock solution of alginate was made by dissolving LF10/60 alginate in mq-water. The alginate solution was mixed on a magnetic stirrer, before it was filtered through syringe filters with pore sizes 5 μm , 1,2 μm and 0,8 μm .

The microfluidic system was first tested with water as the dispersed phase and hexadecane (Sigma, Germany) as the continuous phase. Both flow focusing and T-shaped designs were tested. To obtain a more stable flow and droplet formation, 2 % w/w of the surfactant Span 80 (Fluka Analytical, Germany) was added to the hexadecane.

After the system had worked with water, 1 % w/v alginate was used as the dispersed phase. Alginate was tested together with pure hexadecane and with increasing concentrations of Span 80, in order to observe the effect on the stability of flows and droplet formation. It was also observed if it was obtained plugs during droplet formation or if it was possible to reduce the size of the plugs into spherical droplets. The result is summarized in Table 2.

Table 2: Shape of the beads formed in the droplet formation area of the flow focusing microfluidic system, and the stability of flows and bead formation obtained by different concentrations of Span 80 as surfactant in hexadecane as the continuous phase. 1 % w/v alginate was used as dispersed phase.

Span 80 concentration (% w/w)	Shaped of beads formed	Stability of flows and bead formation
0	Plugs	Very low
0,5	Droplets	Low
1	Plugs	Low
2	Droplets	Medium
4	Droplets	High

From the previous test, 4 % w/w Span 80 in hexadecane gave the best stability. Increasing concentrations of alginate was then tested with this continuous phase in a flow focusing device. A summary is shown in Table 3.

Table 3: Stability of flows and droplet formation for increasing concentrations of alginate as dispersed phase. Hexadecane with 4 % Span 80 was used as continuous phase in the flow focusing device.

Alginate concentration (% w/v)	Stability of flows and bead formation
0,5	High
1	High
2	High
5	Medium

There was not a large difference for the three lower concentrations of alginate. As the gelling is easier to obtain for higher concentrations, 2 % w/v was chosen for further testing. Oleic acid (VWR Prolabo) and Mineral oil (Aldrich-Chemie) were tested as continuous phases, with 2 % w/v alginate as the dispersed phase in flow focusing devices. Two concentrations of surfactant were tested for each continuous phase in addition to the pure oil (Table 4). A plastic pipette tip was placed in the outlet to collect the beads.

A 500 mM stock solution of CaCl₂ was prepared by dissolving CaCl₂*2H₂O in mq- water. This was diluted to a 50 mM CaCl₂ solution which was inserted into the pipette tip after the bead production had started in order to gel the beads. The gelled beads were then investigated in the Olympus microscope. The result is shown in Table 4.

Table 4: Stability during formation of droplets and shape of gelled beads as a result of different continuous phases and concentrations of surfactant. 2 % w/v alginate was used as dispersed phase in the flow focusing device.

Continuous phase	Span 80 concentration (% w/w)	Stability of droplet formation	Shape of gelled beads
Hexadecane	0	Low	-
Hexadecane	0,5	High	Droplet
Hexadecane	2	High	Droplet
Oleic acid	0	Low	-
Oleic acid	0,5	High	Spherical
Oleic acid	2	High	Droplet
Mineral oil	0	Low	-
Mineral oil	0,5	Medium	Droplet
Mineral oil	2	Medium	Droplet

Oleic acid provided a stable droplet formation, and with 0,5 % w/w Span 80 it gave a few spherical beads. Oleic acid was therefore chosen for further investigation. The experiment described above was repeated with varying calcium concentrations to see if this would affect the shape of the gelled beads. Oleic acid with 2 % w/w Span 80 and a 2 % alginate solution was used in a device with T-shaped design. A summary of the result is shown in Table 5.

Table 5: Effect of calcium concentration on the shape of the gelled beads for beads formed in a microfluidic device with T-shaped design and oleic acid with 2 % w/w Span 80 as continuous phase and 2 % w/v alginate as dispersed phase.

CaCl₂ concentration (mM)	Shape of gelled beads
10	Spherical
50	Spherical / droplet
100	Droplet

Since it was hard to obtain spherical beads with the system used so far, two other designs with an extra inlet for calcium were tested (Figure 16). This allowed the calcium solution to mix with the alginate solution right before the droplets were formed. These devices were tested with 2 % w/v alginate and oleic acid with 2 % w/w Span 80. In the calcium inlet 10 mM and 50 mM CaCl₂ was used.

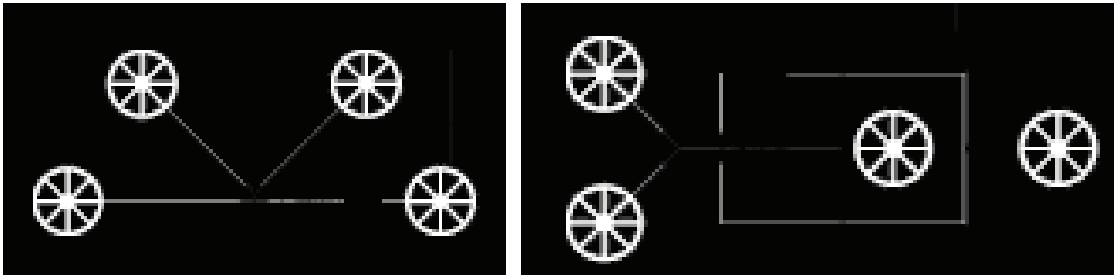


Figure 16: To the left is a T-device with three inlets for, from left to right, oleic acid, alginate and calcium, and one outlet to the right. The right image shows a flow focusing device where the two inlets to the left are for alginate and calcium, the inlet for oleic acid is to the right and the outlet is in the middle.

3.3 Production of alginate particles using the electrostatic bead generator

The electrostatic bead generator was used to make alginate beads parallel to developing the microfluidic system for preparation of alginate gel beads (Figure 17). The calcium bath contained a 50 mM calcium solution, and a 2 % w/v alginate solution was used to make beads. The pump was set to 10 ml/h, the voltage was 7 kV and the needle size was 0,13 mm. The distance from the needle to the calcium solution was 2 cm. This gave large spherical beads, and droplet shaped satellites. After production the beads were washed and stored in a 0,9 mM NaCl 3 mM CaCl₂ solution.

Another batch of alginate beads were also made with the electrostatic bead generator. This time a 50 mM calcium solution with 0,15 M D-Mannitol was used, to obtain spherical shapes on the particles. Blue dextran was added to the 2 % w/v alginate solution, for easier visualization of the beads. The pump was set to 8 ml/h, the voltage was 8 kV and the needle size was 0,13 mm. The distance from the needle to the calcium solution was 1,5 cm. The beads were washed and stored in a 0,9 mM NaCl 3 mM CaCl₂ solution.

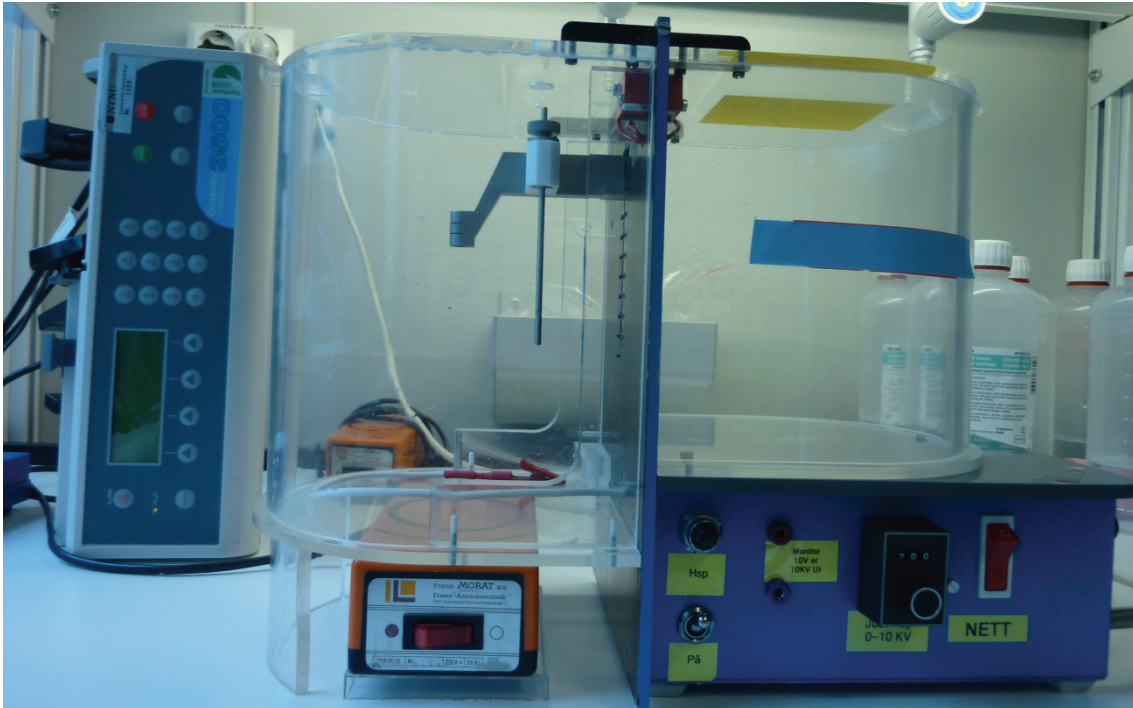


Figure 17: The electrostatic bead generator. To the left is the pump to which a syringe filled with alginate solution is attached. The solution is pushed into a needle (not shown) that is placed in the holder inside the chamber to the left. The pole goes into a calcium bath placed at the bottom of this chamber. A voltage drop across the gap between the needle and the bath causes alginate droplets to be pulled off from the needle.

The beads were filtered through a filter with mesh size 60 μm , to separate the large beads from the smaller satellites. But as the beads were 100-200 μm and the satellites were approximately 50 μm in diameter, they were too large to be used in the TIRF measurements. To reduce the size of the beads different techniques to shrink the beads was tested. Some beads were immersed in DMC, which has been shown to shrink alginate beads during production in microfluidic devices. Other beads were immersed in 96 % ethanol for several days.

3.4 Fluorescence labelling of polystyrene beads

Since the production of alginate beads were still under development and the beads produced with the electrostatic bead generator were too large, polystyrene beads were used for the experiments with mucin layers. To be able observe the beads in TIRF microscopy they were fluorescently labelled. The procedure was developed for this purpose.

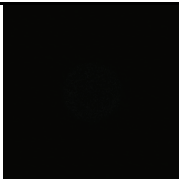
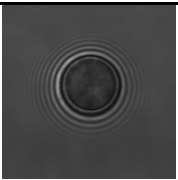
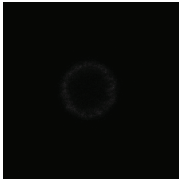
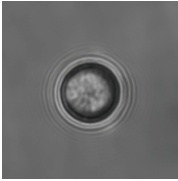
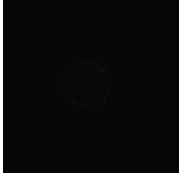
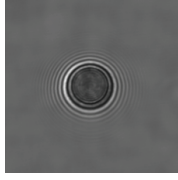

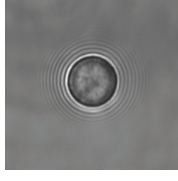

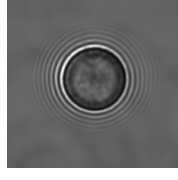
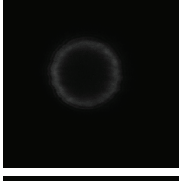
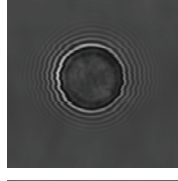
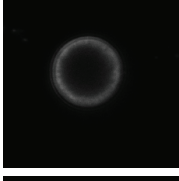
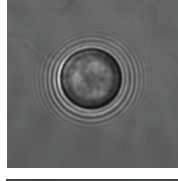
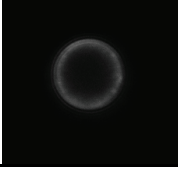
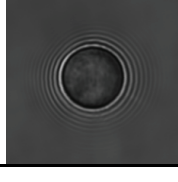
Carboxylated polystyrene beads with diameter 6 μm (Polybead Carboxylate Microspheres, Polysciences Inc) were labelled with pegylated quantum dots (Qdot 655 ITK amino, Invitrogen Molecular Probes, USA). A 50 mM solution of boric acid was made, and the pH was adjusted to 5,8 by addition of NaOH. 0,47 μl of the solution with polystyrene beads, corresponding to approximately 100 000 beads, was taken out into an eppendorf tube. The beads were diluted with 200 μl boric acid and centrifuged at 4000 rpm for 4 min (eppendorf centrifuge 5415R) at room temperature. The solution on top was pipetted off and replaced with 200 μl new boric acid. Centrifuging was repeated twice, and in the last step 500 μl of boric acid was added.

0,4 μl of the quantum dots was taken out and diluted with 200 μl 50 mM boric acid with pH adjusted to 8,3, resulting in an concentration of 16 nM. EDAC and quantum dots were added to the eppendorf tube containing the polystyrene beads in boric acid. To determine the concentrations of EDAC and quantum dots that would give the best result, eight samples with varying concentrations were prepared (Table 6). The first steps, as described above, were equal for all eight samples. The eppendorf tubes were covered in aluminium foil and shaken for approximately 24 hours.

A 10 mM Tris buffer was prepared by dissolving Trizma Base (Sigma Life Sciences) in mq-water. The pH was adjusted to 7,4 by addition of HCl. The polystyrene beads were washed in Tris buffer by centrifuging them at 4000 rpm for 4 min at room temperature and replacing the solution on top with 500 μl Tris buffer. This was repeated twice.

The fluorescently labelled polystyrene beads were investigated with a Leica TCS SP5 confocal microscope, together with the software LAS AF. The result is shown in Table 6. A 63x water immersion objective and an argon laser with 17 % power was used, with the three lines 458, 476 and 488 nm. The pinhole was 111,4 μm . The setup for the images was 1024x1024 pixels, 200 Hz and line average 4. For some beads a stack was obtained with the same specifications and 0,3 μm between each image in the z-direction.

Table 6: Fluorescence from 6 μm polystyrene beads labelled with Qdot 655 quantum dots. Different concentrations of EDAC and quantum dots were used during the procedure to label approximately 100 000 beads. Images to the left show the fluorescent signal from the beads, while the images to the right show the same beads in transmission microscopy, both obtained with Leica confocal microscope.

EDAC concentration (mg/ml)	Quantum dots mol/l)	Images of beads	
1	$5,4 \cdot 10^{-11}$		
1	$2,7 \cdot 10^{-10}$		
3	$5,4 \cdot 10^{-11}$		
3	$2,7 \cdot 10^{-10}$		
3	$4,8 \cdot 10^{-10}$		
3	$9,6 \cdot 10^{-10}$		
6	$4,8 \cdot 10^{-10}$		
6	$9,6 \cdot 10^{-10}$		

The four samples with the highest concentration of quantum dots all gave sufficient fluorescence, and the combination of 6 mg/ml EDAC and $4,8 \cdot 10^{-10}$ mol/l quantum dots to label 100 000 polystyrene beads with diameter 6 μm was chosen for the further work. To better match emission wavelength from the quantum dots with the filters in the TIRF microscope, the procedure was repeated with the chosen concentrations with quantum dots with a shorter emission wavelength (Qdot 585 ITK amino, Invitrogen Molecular Probes, USA).

3.5 TIRF measurements

The Observer D1 TIRF microscope from Zeiss was used for the measurements. An Andor iXon EMCCD camera was mounted to the side port of the microscope (Figure 19). This was controlled with the software Andor iXon, and the camera was cooled to -80°C to avoid dark current before it was be operated. An argon laser (LASOS Lasertechnik GmbH) provided a 488 nm wavelength beam that was used for excitation. The beads were viewed with an alpha Plan-Fluar 100x/1,45 oil immersion objective, with the oil Immersol 518 F. Filter set 74 from Zeiss was used, with excitation wavelengths 480 and 565 nm and emission wavelengths 525 and 616 nm (Figure 18). The critical angle is 61° for a specimen in water, and the TIRF measurement was performed at an angle of 63° .

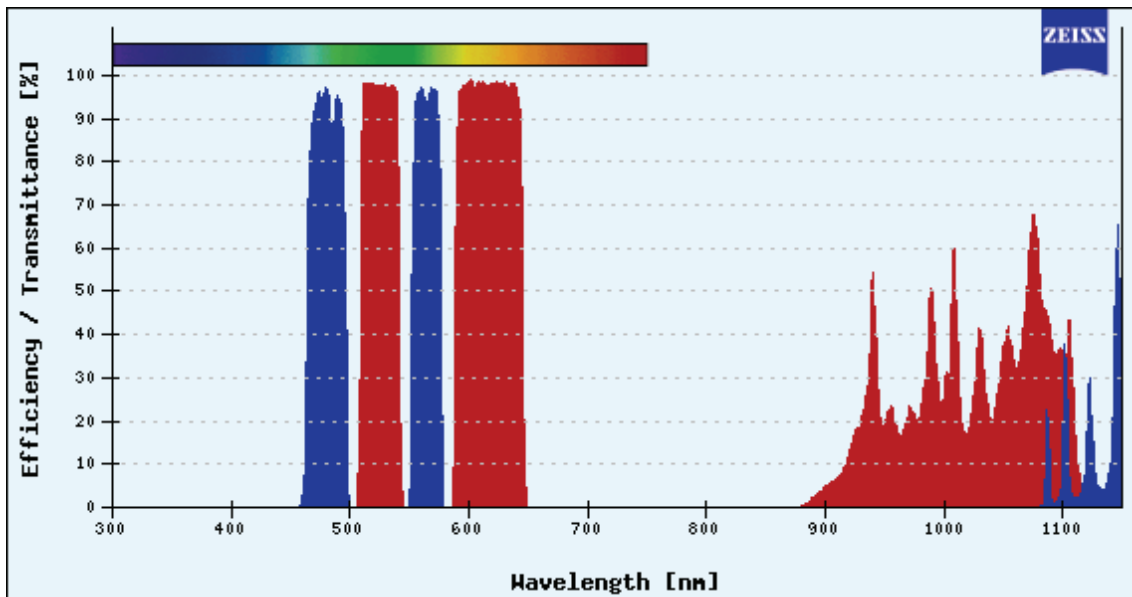


Figure 18: Excitation (blue) and emission (red) wavelengths for the filter set used in the TIRF measurements. The figure is from filter set 74 at the Zeiss webpage [34].

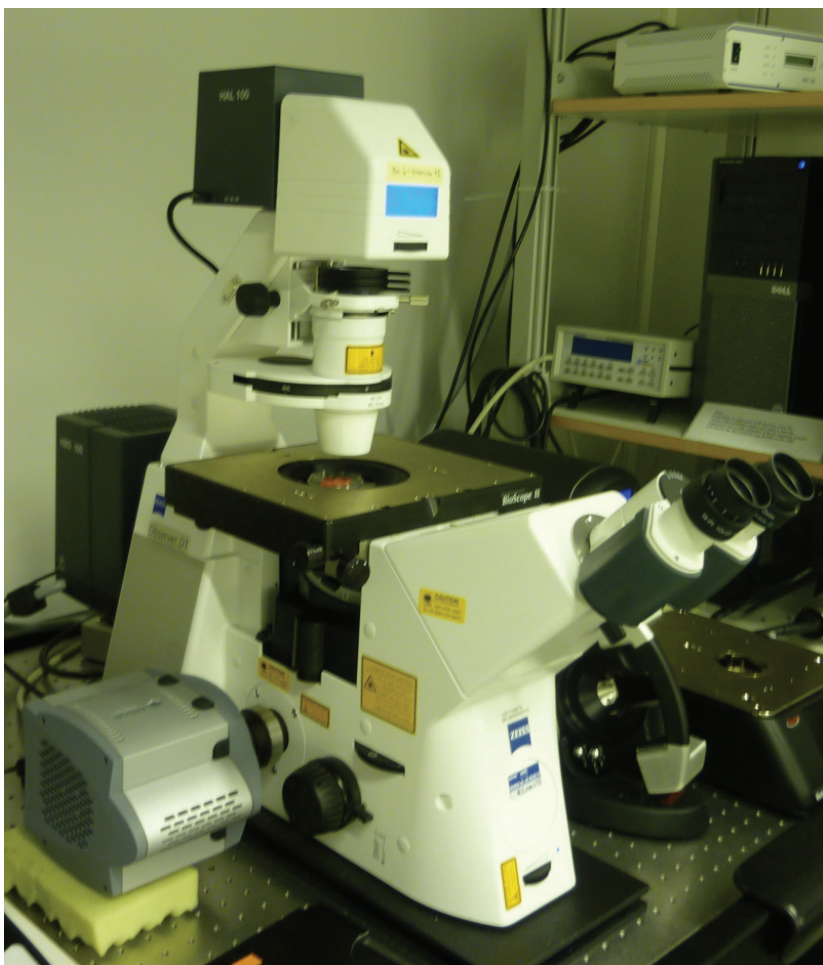
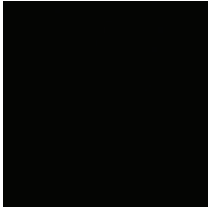
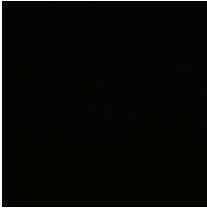

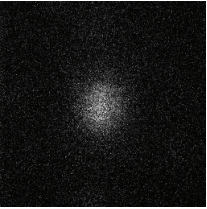
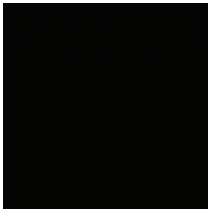
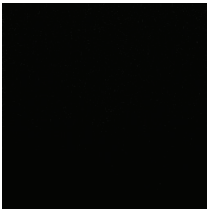

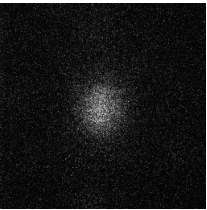
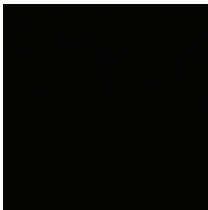
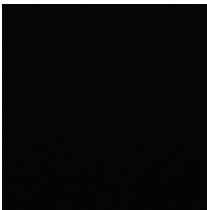
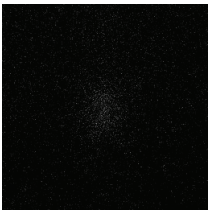
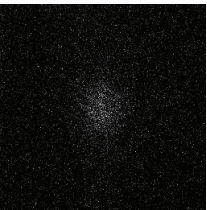
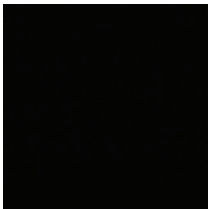

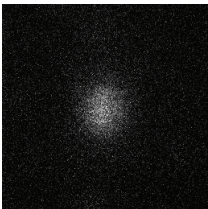
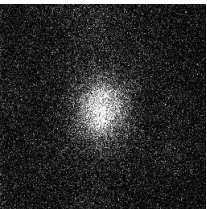
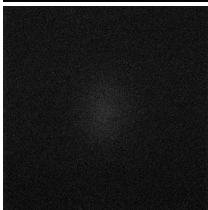
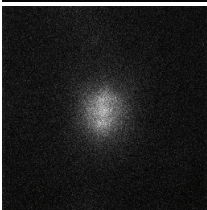
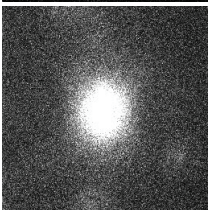
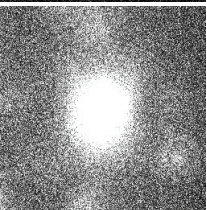


Figure 19: Zeiss Observer D1 TIRF microscope. The CCD camera is mounted to the side port of the microscope. The well with immobilized mucins is on the stage.

Before the TIRF experiments started, it was confirmed that there was no autofluorescence from the mucin layers. This was done by excitation with an Hg lamp. In addition, measurement series were performed repeatedly on one bead in order to determine possible photobleaching of the beads. This was done for four different beads, and no bleaching was observed.

The Andor iXon EMCCD camera counts the photo-electrons generated by the photons emitted from the fluorescent sample. The EM gain level is a linear scale and the gain is multiplied with the counts in order to increase the signal. Since no photobleaching of the beads were observed, the optimal conditions for measurements were determined by observation of one bead. The exposure time and EM gain level on the camera were varied and measurements performed. The result is shown in Table 7.

Table 7: TIRF images for 6 μm polystyrene beads labelled with Qdot 655 quantum dots suspended in 10 mM Tris buffer on a glass surface. The images are obtained with varying exposure times and EM gain levels on the EMCCD camera. The gray scale goes from 350 to 500 counts.

<u>EM gain level</u>	5	20	80	150
<u>Exposure time</u> (s)				
0,00001				
0,00081				
0,00251				
0,01081				
0,05001				

The fluorescently labelled beads, suspended in 10 mM Tris buffer, were placed in the empty silicone well on the TIRF glass surface. Kinetic series with 1000 frames were obtained, for reference and calibration. The exposure time was set to 0,01251 s and the EM gain level was 100. Shift speed was set to 1,7 μ s. This was repeated for the beads placed on the mucin layers with concentrations 1 mg/ml and 0,5 mg/ml. These two samples of mucin layers did not give a fluorescent signal in TIRF mode.

Another mucin layer was therefore prepared. The same procedure was used, with 0,05 mg/ml of both EDAC and PGM. The fluorescently labelled polystyrene beads were placed on the mucin layer and TIRF measurements were carried out with exposure time 0,01081 s, EM gain level 100 and shift speed 1,7 μ s. The kinetic series length was 1000 frames. The measurements were also performed on beads on a clean glass surface under the same conditions.

A mucin layer with mucin concentration 0,05 mg/ml was incubated with 0,5 mg/ml polyM alginate (PF83) to simulate the condition the lungs of CF patients. The experiment was repeated for this layer with the same conditions as for the mucin layer without alginate. To observe the effect of G-blocks in the solution covering the mucin-alginate layers, increasing concentrations of G-block solution was added. G-blocks ($DP_n \sim 10$, $F_G = 0,94$) were dissolved in filtered 10 mM Tris buffer with pH 7,4 to concentrations varying from 0,05 mg/ml to 2 mg/ml (see Table 1). TIRF measurements were performed under the same conditions as before in order to observe any difference in intensity.

The image series obtained was analysed in a program written in Interactive Data Language (IDL) by Bjørn Torger Stokke. The files were exported to ascii format before they were read by the program, which fitted the data to the theoretical double exponential intensity function, in accordance to Equation 8, given by

$$I = A[0] + A[1]e^{-A[2]z} + A[3]e^{-A[4]z}, \quad (11)$$

where $A[0]$ is the background intensity. The parameters were analysed to obtain the penetration depth of the field from $A[2]$ and the intensity from the bead given by $A[1]$, corresponding to the parameters in Equation 2. The analysis was done first for beads on a glass surface to calibrate the parameters and to find I_0 in Equation 2, before intensity data from beads bead on a mucin layer was analysed. The intensity for a bead on a mucin layer is converted to a distance by inserting

the obtained values into the theoretical expression for the decaying intensity (Equation 2).

3.6 AFM nanoindentation experiments

JPK ForceRobot 300 was used for the AFM nanoindentation experiments (Figure 20). The measurements were performed by Gjertrud Maurstad. On the tip of the cantilever was a polystyrene bead with diameter 4,5 μm . The spring constant was measured before the experiments. The sample surfaces was the mucin layers prepared on the mica slides immersed in filtered 10 mM Tris buffer (See Table 1). A $10 \times 10 \mu\text{m}$ grid was defined on the sample surface, and 6×6 measuring points were chosen within this grid. 10 force curves were obtained for each measuring point.

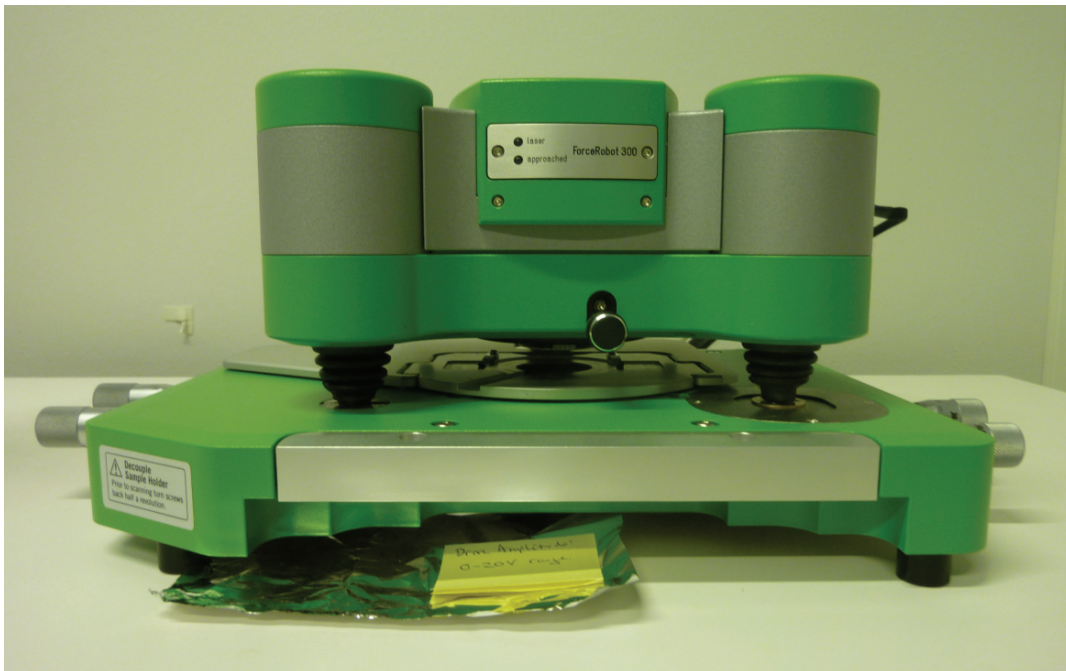


Figure 20: JPK ForceRobot 300 used for AFM indentation experiments.

To simulate the condition of mucus in a CF-affected lung, the mica slides with mucin layers were incubated with alginate. The alginate solution was prepared as described for the TIRF measurements. The buffer was filtered through a syringe filter with pore size 0,2 μm before use, in order to avoid interaction during the force measurements. The slides were incubated in two different concentrations of alginate; 0,5 mg/ml and 2 mg/ml. After incubation the mica slides were rinsed with the filtered Tris buffer. Nanindentation experiments were performed as for pure mucin layers.

It was investigated how addition of G-blocks to the solution covering the mucin layers incubated in alginate would affect the penetration depth of the bead and interactions with the layer. G-block solutions were prepared as for the TIRF measurements, with filtered Tris buffer. G-blocks were then added in increasing concentration, from 0,05 mg/ml to 2 mg/ml, to the mucin-alginate layers (see Table 1), and nanoindentation was performed as before.

The JPK Data Processing software was used to analyse the force curves obtained from the AFM nanoindentation experiments. A Hertz-fit was performed to obtain Young's modulus from each curve. The samples had a mucin layer on top of a mica slide, and this resulted in force curves with two points of slope change. The distance between these points were read from the curves to determine the thickness of the mucin and alginate layers (Figure 11).

4. Results

4.1 Alginate particles

The alginate beads produced with the electrostatic bead generator was found to have diameters varying from 50-200 μm , which is too large to be used in the TIRF measurement. Some of the smaller beads were droplet shaped. To see if the size could be reduced, they were immersed in DMC or 96 % ethanol for several days. Some decrease in size was observed, mostly for the larger beads (Figure 21). However the reduction was still insufficient for the beads to be used in TIRF measurements.

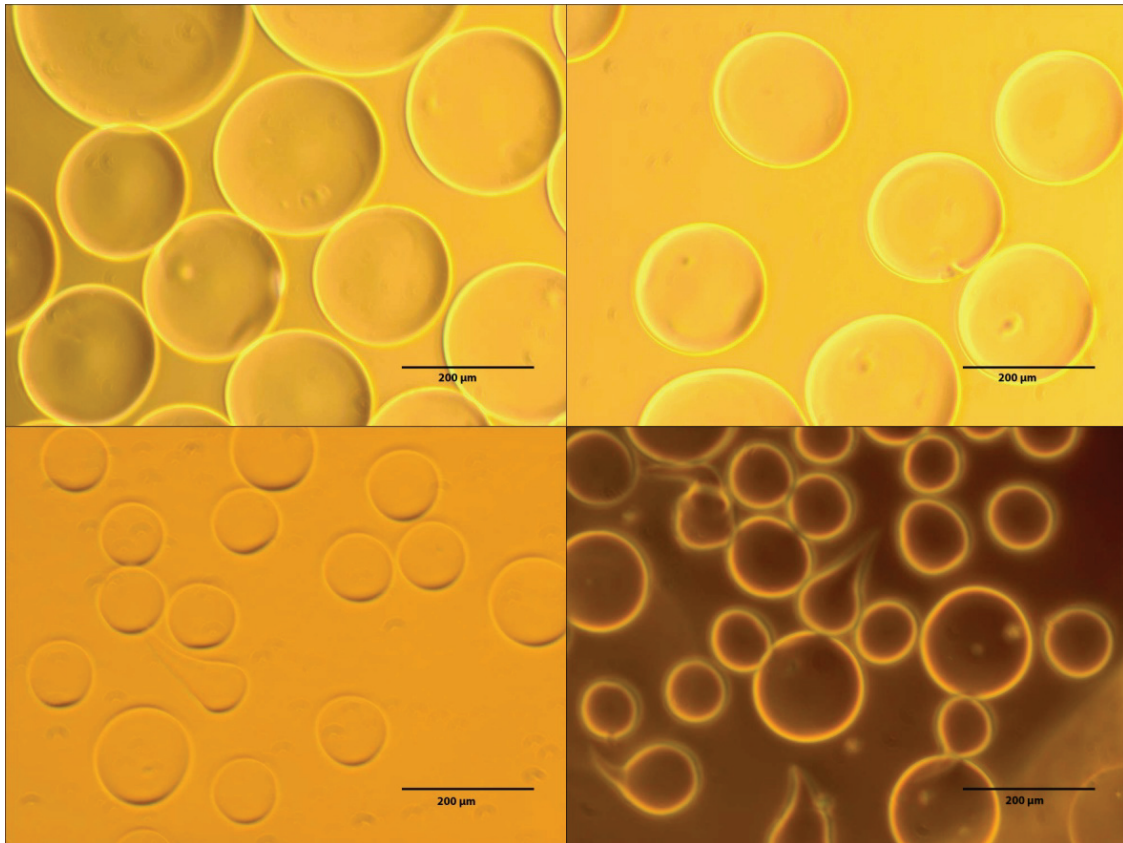


Figure 21: Alginate beads produced with electrostatic bead generator from a 2 % w/v alginate solution. The upper left image shows the larger beads after production and to the left are the beads after 91 hours in 96 % ethanol. The bottom left picture shows the small alginate beads after production. To the right are the beads after 46 hours in DMC. The scale bars are 200 μm .

Alginate particles were also produced by microfluidic techniques. With a device with T-shaped design and channel dimensions 10 x 50 μm in the droplet formation area, beads with diameters in the size range 10 μm were produced (Figure 22). The size of the beads is not monodisperse due to instabilities in the flows during production. Some examples of the beads are shown in Figure 23.

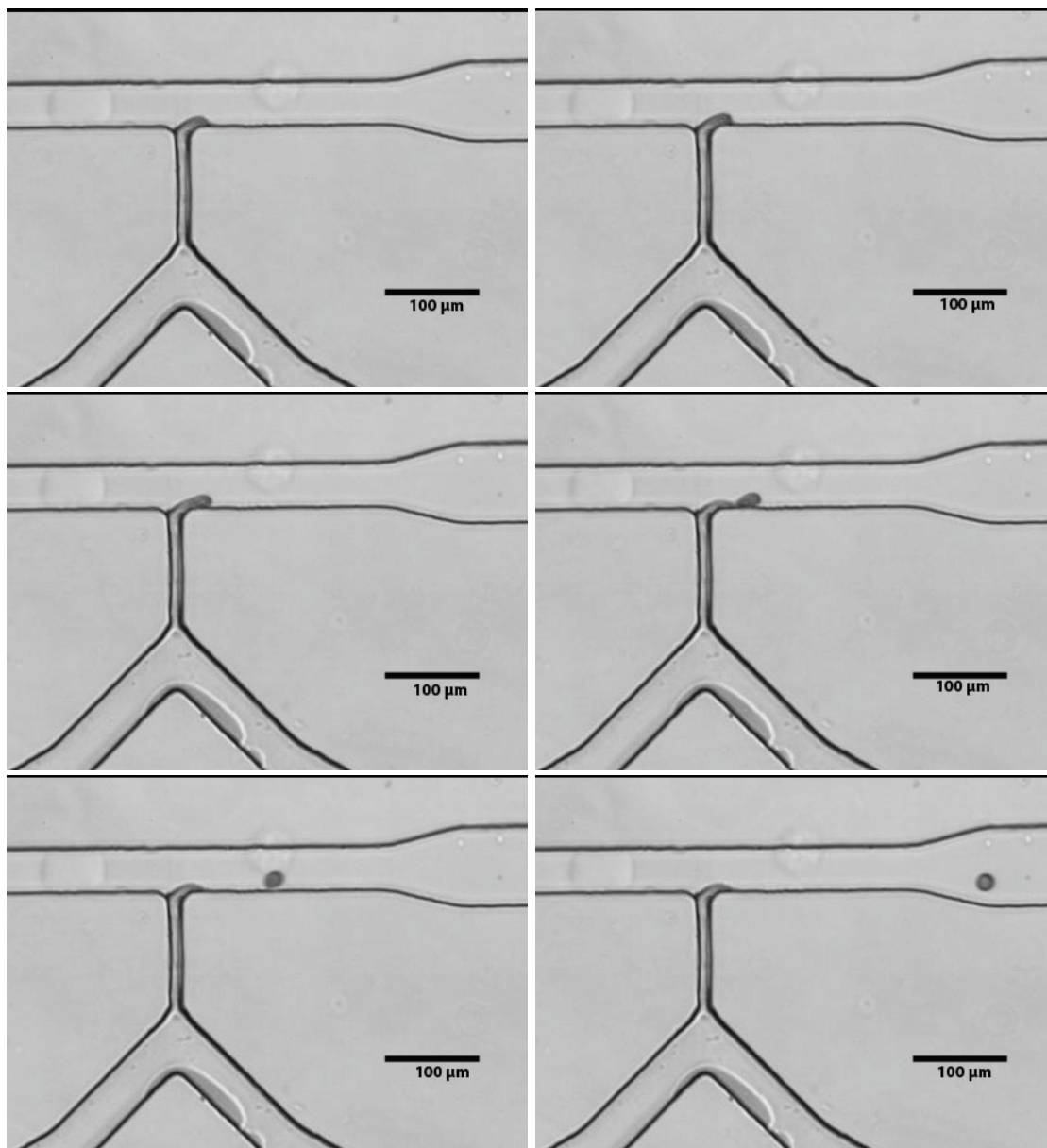


Figure 22: Production of alginate beads in a microfluidic device with a T-shaped design. The 2 % w/v alginate solution comes in from the bottom left channel, while a 10 mM calcium solution comes in from the bottom right channel. The two solutions mix in a narrow channel before the droplets are formed. Oleic acid with 2 % w/w Span 80 comes in from the left and breaks the dispersed phase into beads.

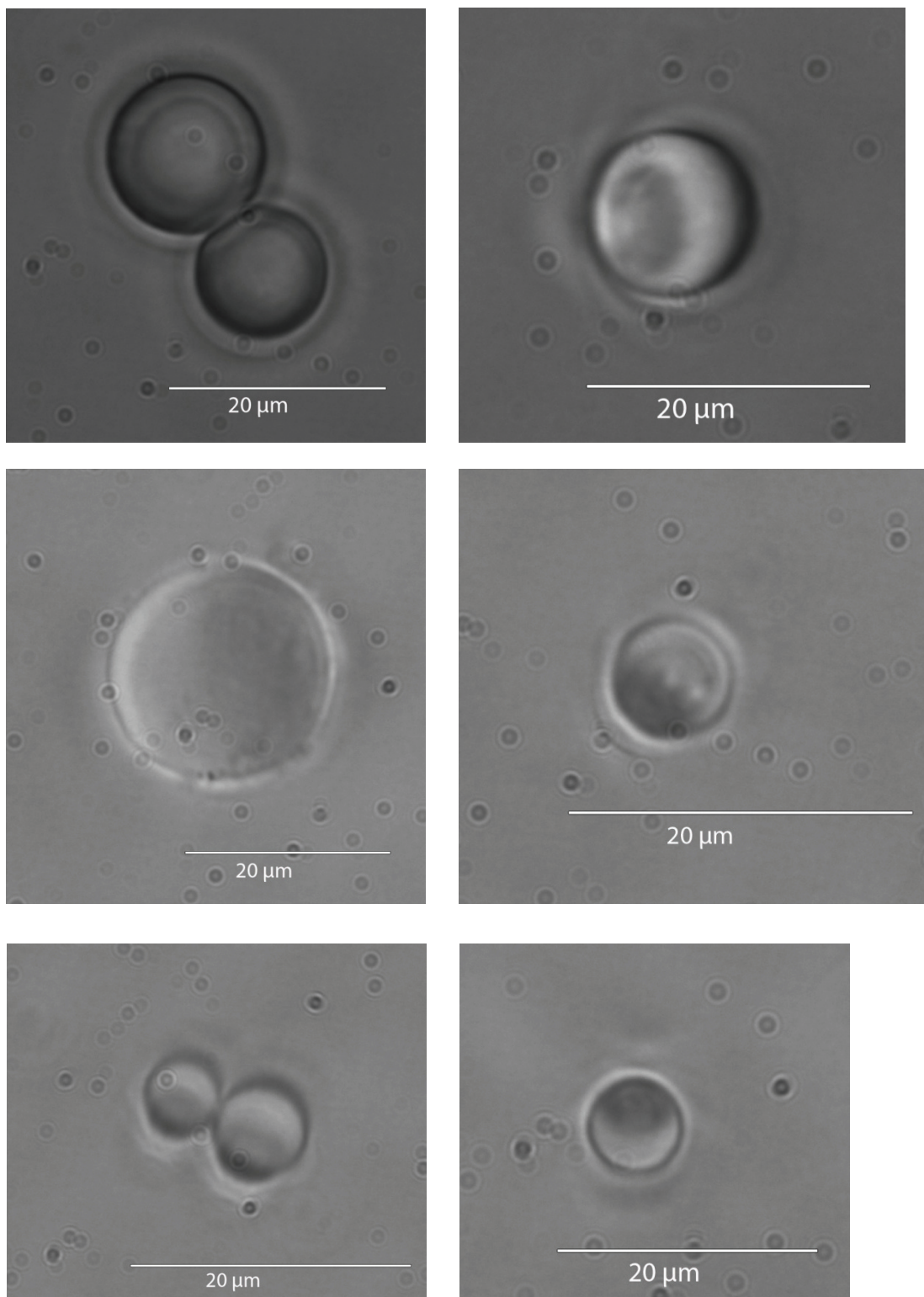


Figure 23: Images of alginate beads produced with microfluidic techniques at two different occasions. The beads in the top row images are produced with 50 mM CaCl_2 , while the rest are produced with 10 mM CaCl_2 . All beads are made with 2 % w/v alginate and oleic acid with 2 % w/w Span 80 in a T-device with three inlets and dimension $10 \times 50 \mu\text{m}$ in droplet formation area.

4.2 TIRF measurements

Intensity profiles of beads were measured using TIRF microscopy. 6 μm polystyrene beads labelled with Qdot 655 quantum dots gave an easily observable intensity when placed on a glass surface (Figure 24). However, when the beads were placed on a mucin layer with concentrations 1 mg/ml and 0,5 mg/ml, no fluorescence was observed in TIRF mode with the focus on the glass surface.

For the mucin layer with concentration 0,05 mg/ml a weak signal was observed from some of the beads in TIRF mode (Figure 24).

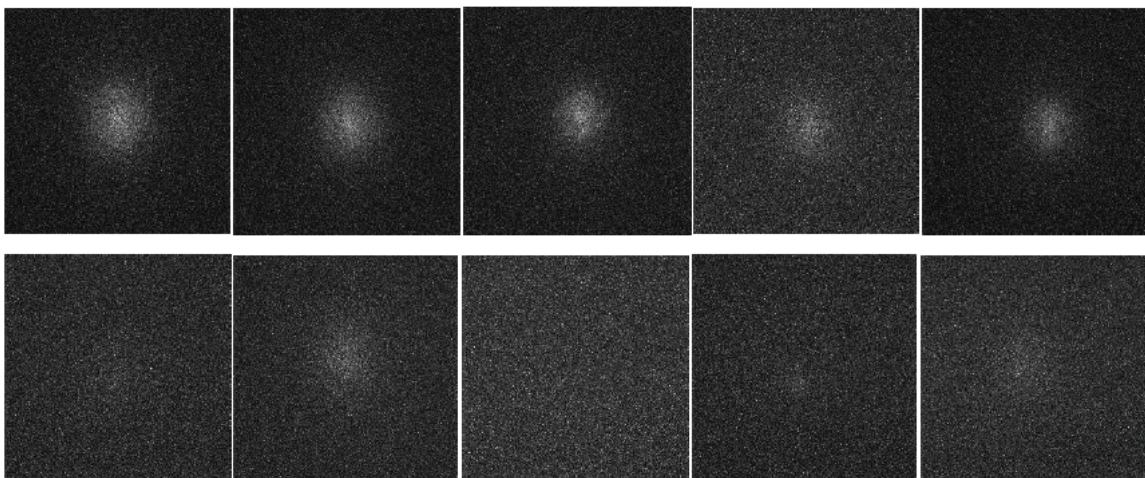


Figure 24: The top row images show the signal obtained in TIRF mode from five 6 μm polystyrene beads, fluorescently labelled with Qdot 655 quantum dots, on a clean glass surface. The signal obtained from beads on a mucin layer with concentration 0,05 mg/ml in TIRF mode is shown in the bottom row. For both cases the exposure time was 0,01081 s, EM gain level was 100 and the shift speed 1,7 μs . The gray scale was dynamic to obtain the best possible image.

The data series obtained for beads on glass and beads on mucin were analysed, and the intensity profiles were fit to a double exponential (Equation 11). Scatter plots of the parameters versus χ^2 from the fit are shown in Appendix C. Figure 25 shows histograms for the distribution of intensities I_0 for beads on a glass surface. The mean values of these distributions were calculated and the results are shown in Table 8. Before the mean value was calculated, parameters with A[1] set to the initial value or zero or with very high values of A[1] or χ^2 were filtered out. The average A[1] is $104,5 \pm 27,4$, which was used as the intensity at $z=0$. This intensity value was used for comparison when the height of the beads on the mucin layers was determined.

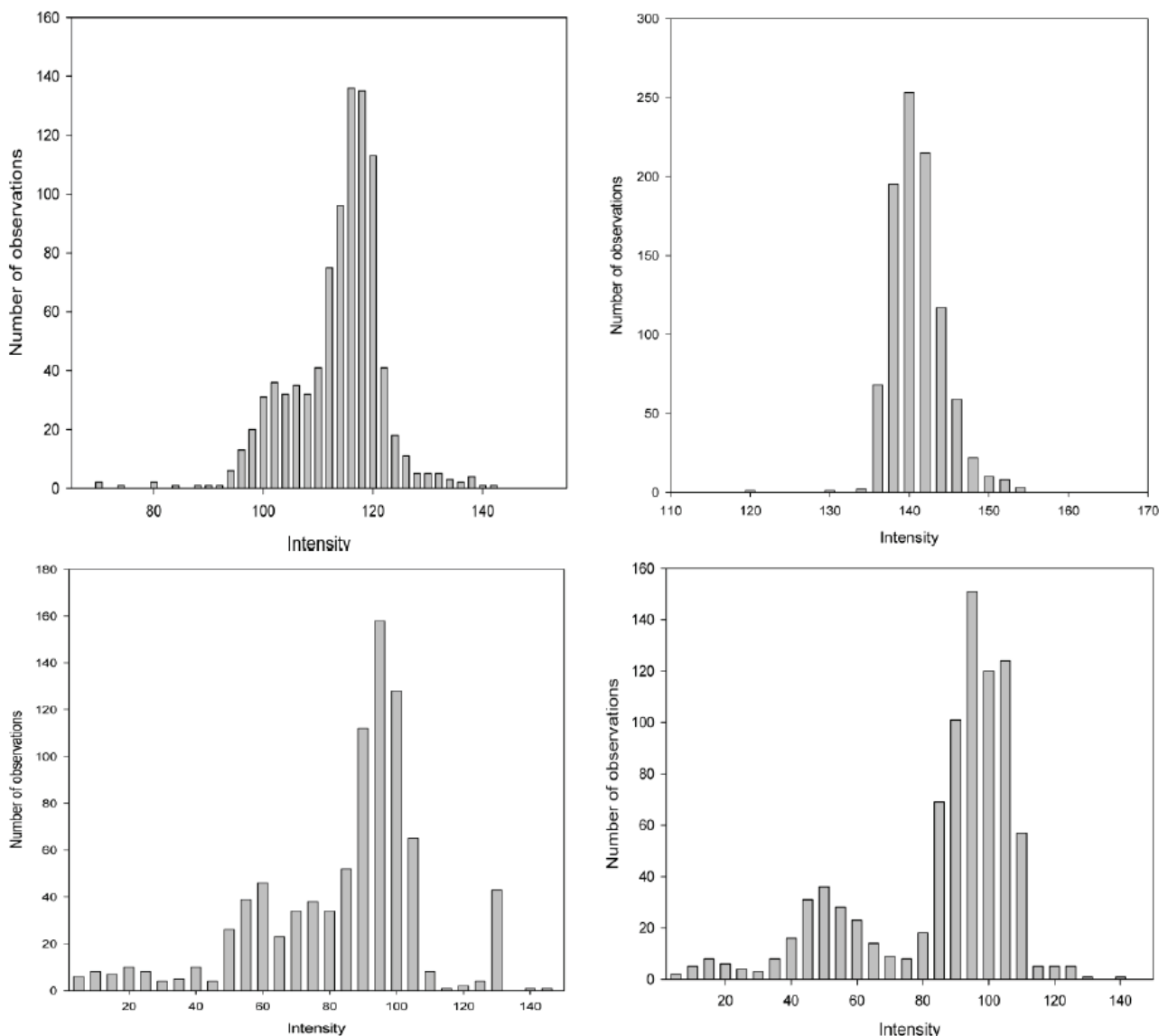


Figure 25: Histograms showing the distribution of the parameter $A[1]$ from the fit to a double exponential to TIRF data for four different beads on a glass surface. The parameters that were set to the initial value of 120 and those with high χ^2 were filtered out.

Table 8: Mean value and standard deviations for the intensities $A[1]$ for beads on a glass surface. The average of these was used for comparison with beads on a mucin layer.

Bead number	Mean value $A[1]$	Standard deviation $A[1]$
1	112,2759	14,00739
2	139,9909	3,263768
3	82,04405	25,27222
4	83,87728	24,26018

The penetration depth of the evanescent field was also calculated from the TIRF data. The parameter $A[2]$ is the inverse of penetration depth in pixels. Figure 26 shows histograms for the distribution of $A[2]$ for beads on glass. The parameter data were filtered before the mean value was calculated. Parameters with $A[2]$ set to the initial value or with high χ^2 were filtered out. Table 9 summarizes the mean values and standard deviations of the distributions. The average of these is $0,102 \pm 0,038$, which corresponds to a penetration depth of the field of $1,53 \mu\text{m}$.

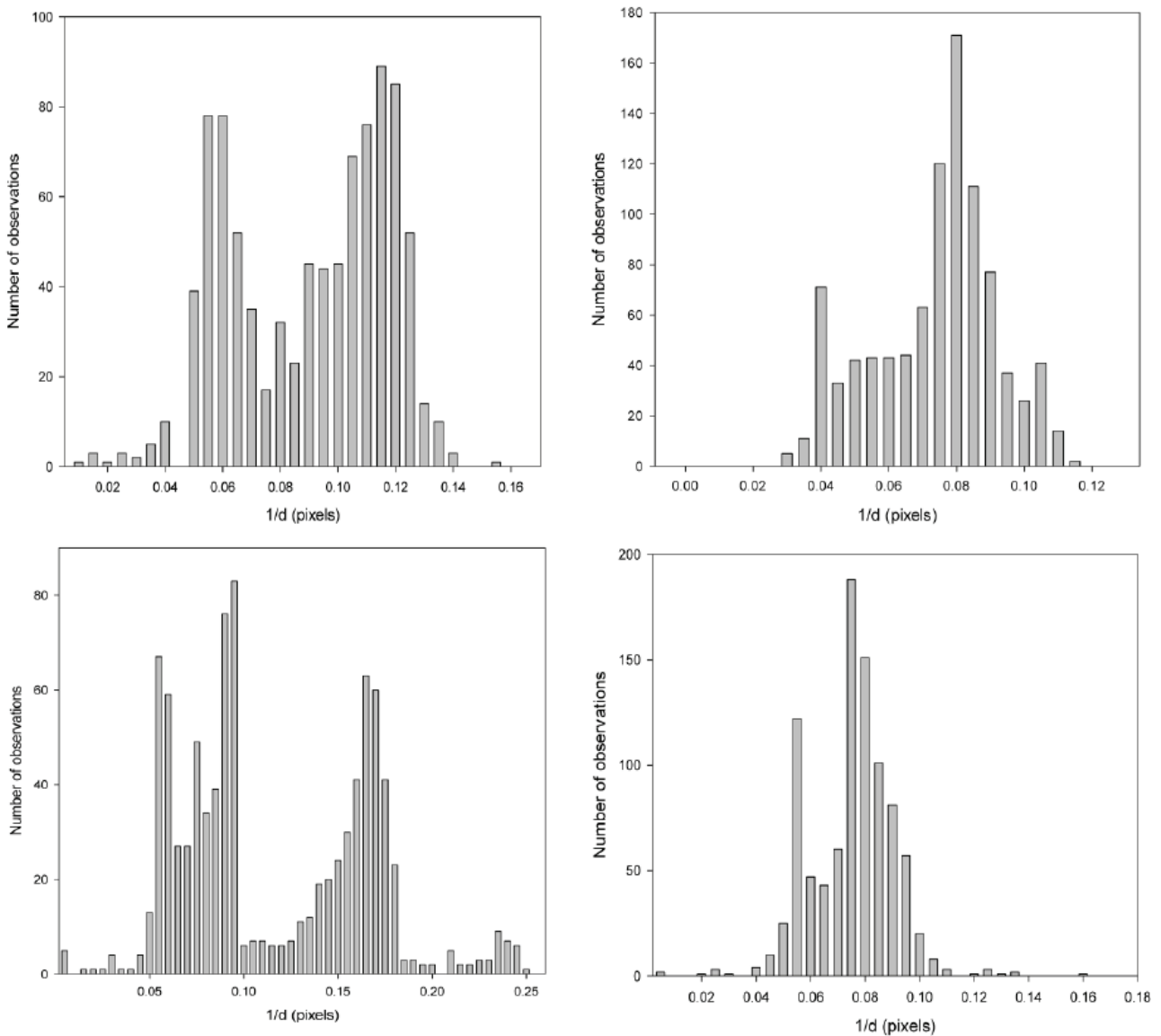


Figure 26: Histograms showing the distribution of the parameter $A[2]$ in the fit to a double exponential to TIRF data for beads on a glass surface. The parameters set to the initial value $0,054$ or with high χ^2 were filtered out.

Table 9: Mean value and standard deviations for the inverse penetration depth $A[2]$ for beads on a glass surface.

Bead number	Mean value $A[2]$	Standard deviation $A[2]$	Penetration depth (μm)
1	0,08699	0,028754	1,79
2	0,07141	0,018387	2,18
3	0,15800	0,298695	0,99
4	0,09023	0,180353	1,73

The same analysis was performed for the series of beads on a mucin layer with mucin concentration 0,05 mg/ml. The histograms for the distribution of $A[1]$ are shown in Figure 27. The data was filtered in the same way as for beads on glass, before the mean values of the distributions were calculated. The average intensity and penetration depth from the calibration on the glass surface was used together with the average intensity for a bead on a mucin layer to calculate the height of the bead above the surface from Equation 2 (Table 10). It is clearly larger variations in the intensities obtained from beads on a mucin layer.

The penetration depth of the evanescent field was also found from the data of a bead on a mucin layer. The analysis was the same as for the beads on a glass surface. The results are shown in Figure 28 and table 11.

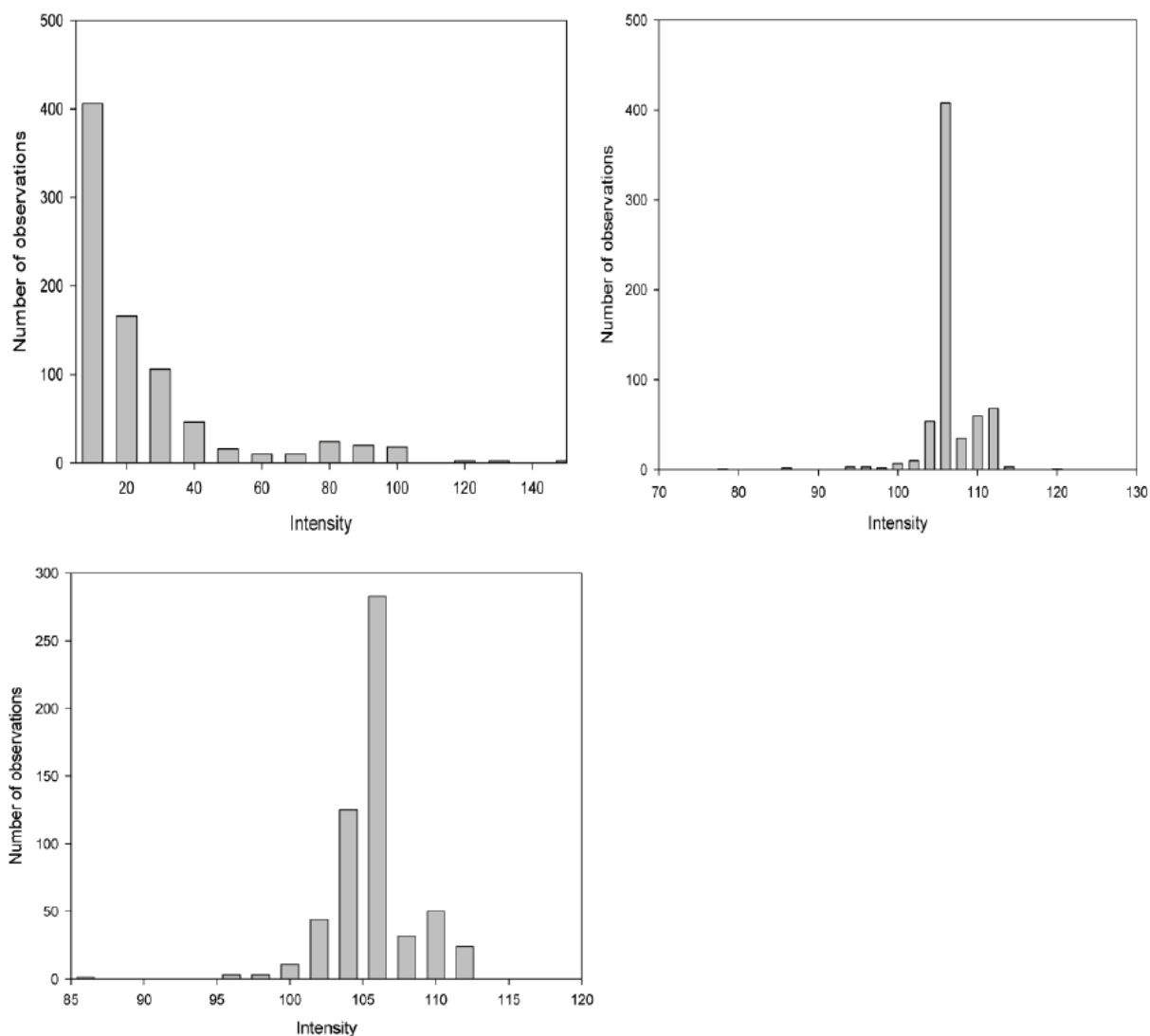


Figure 27: Histograms showing the distribution of the parameter $A[1]$ in the fit to a double exponential to TIRF data for beads on a mucin layer with mucin concentration 0,05 mg/ml. The parameters that were set to the initial value of 120 and those with high χ^2 were filtered out.

Table 10: Mean value and standard deviations for the intensities $A[1]$ for beads on a mucin layer with mucin concentration 0,05 mg/ml. The height is calculated from the average intensities and penetration depth.

Bead number	Mean value $A[1]$	Standard deviation $A[1]$	Height (nm)
1	21,6753	32,3193	2407
2	103,3665	13,4233	17
3	98,1728	23,5165	96

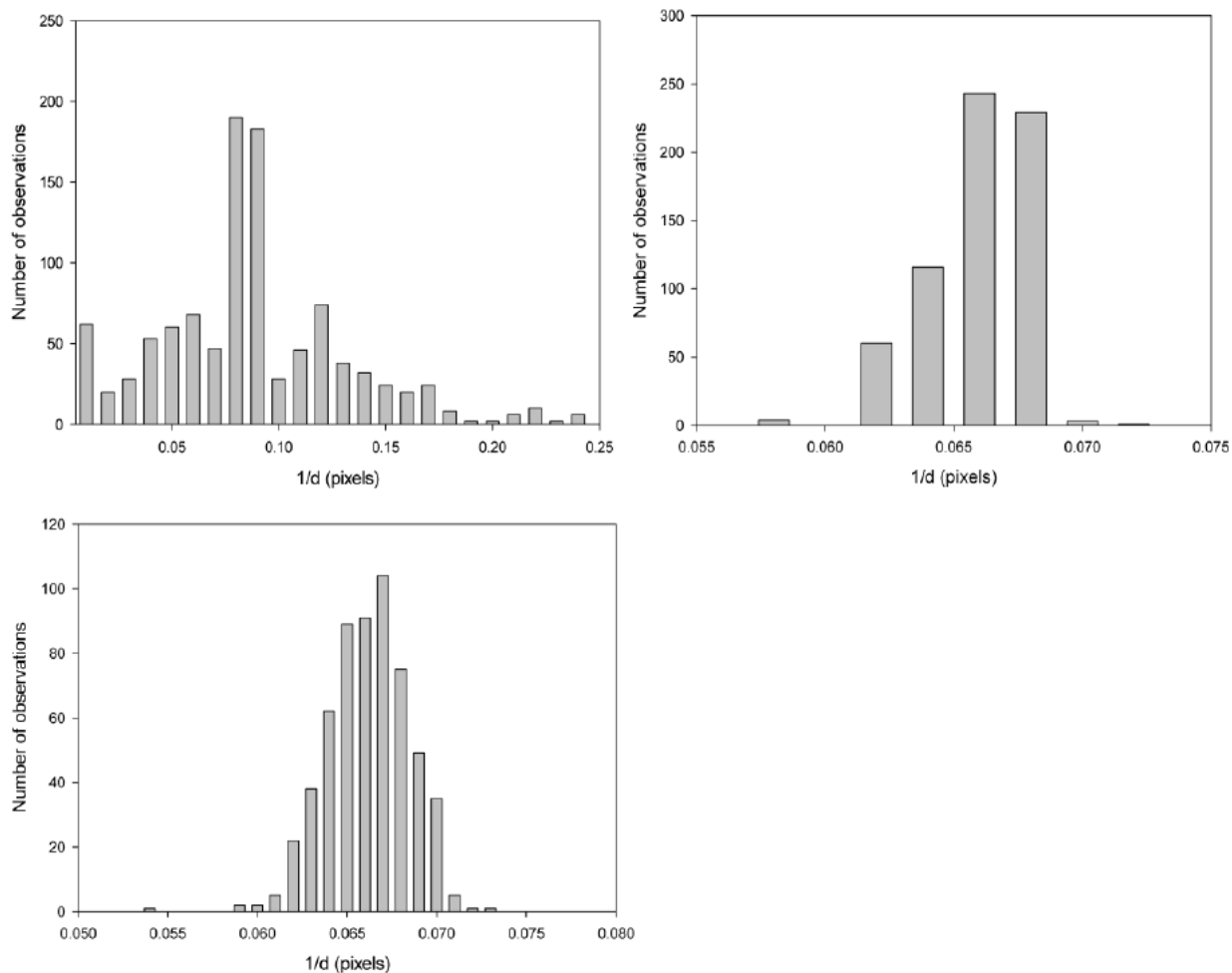


Figure 28: Histograms showing the distribution of the parameter $A[2]$ in the fit to a double exponential to TIRF data for beads on a mucin layer. The parameters that were set to the initial value of 0,054 and those with high χ^2 were filtered out.

Table 11: Mean value and standard deviations for the inverse penetration depth $A[2]$ for beads on a mucin layer.

Bead number	Mean value $A[2]$	Standard deviation $A[2]$	Penetration depth (μm)
1	0,08499	0,04949	1,84
2	0,05912	0,01845	2,64
3	0,06439	0,01057	2,42

The low concentration mucin layer with 0,05 mg/ml mucin, was incubated with 0,5 mg/ml alginate to make a model for the mucus barrier in the lungs of CF patients. This clearly gave less fluorescent signal from the beads than the mucin layer alone. The addition of G-block seemed to increase the fluorescence in some cases, however the uncertainty between the beads are larger than the intensity differences observed. No conclusions regarding the effect of G-blocks can be drawn from this experiment. An overview of the results is shown in Table 12.

Table 12: Intensity signals obtained in TIRF mode with focus on the glass surface, exposure time 0,01081 s and EM gain level 100. The images are of 6 μm polystyrene beads, labelled with Qdot 655 quantum dots, on a mucin-alginate layer with 0,05 mg/ml mucin and 0,5 mg/ml alginate. The effect of addition of G-block to the solution covering the layer is shown for five different beads for each G-block concentration. The gray scale was dynamic to obtain the best possible image.

G-block concentration (mg/ml)	0	0,05	0,1	0,5	2

4.3 AFM nanoindentation experiments

AFM nanoindentation experiments were performed on mucin layers on mica slides. The AFM tip was a 4,5 μm polystyrene bead. Force curves for mucin layers with and without alginate and G-blocks of various concentrations (see Table 1) were obtained.

Examples of force curves for the 2 mg/ml mucin layer with and without 0,5 mg/ml alginate and G-blocks are shown in Figure 29. The curves have no clear change in slope to determine the thickness of the layer. However, approximate values were obtainable. Each sample was measured in 36 points and the variation in the force-distance curves is shown in Appendix D. There are not large differences between different measuring points on the samples, which indicate that the samples are quite homogenous.

The retraction curves show unspecific adhesion interactions between the polystyrene bead and the mucin layers. The curves in Figure 29 show that there are great interactions between the bead and pure mucin layers. The layers incubated with alginate interacts less with the bead, and addition of G-block shows further reduction in the unspecific interactions. This effect is also observed for the mucin layer with mucin concentrations 0,5 mg/ml and to less degree for the 1 mg/ml mucin layer.

Young's modulus which describes the elasticity of a material was found from Hertz-fits to the force curves. The layer thickness was obtained from reading out the distance between the points of slope change on the force curves. There is no great effect observed for these parameters for the incubation with alginate and the addition of G-blocks to the solution. It seems that the layer thickness is slightly reduced when G-blocks are added for the 2 mg/ml mucin layers with alginate. Young's modulus is quite stable for each series, with some exceptions. The result is summarized in Table 13.

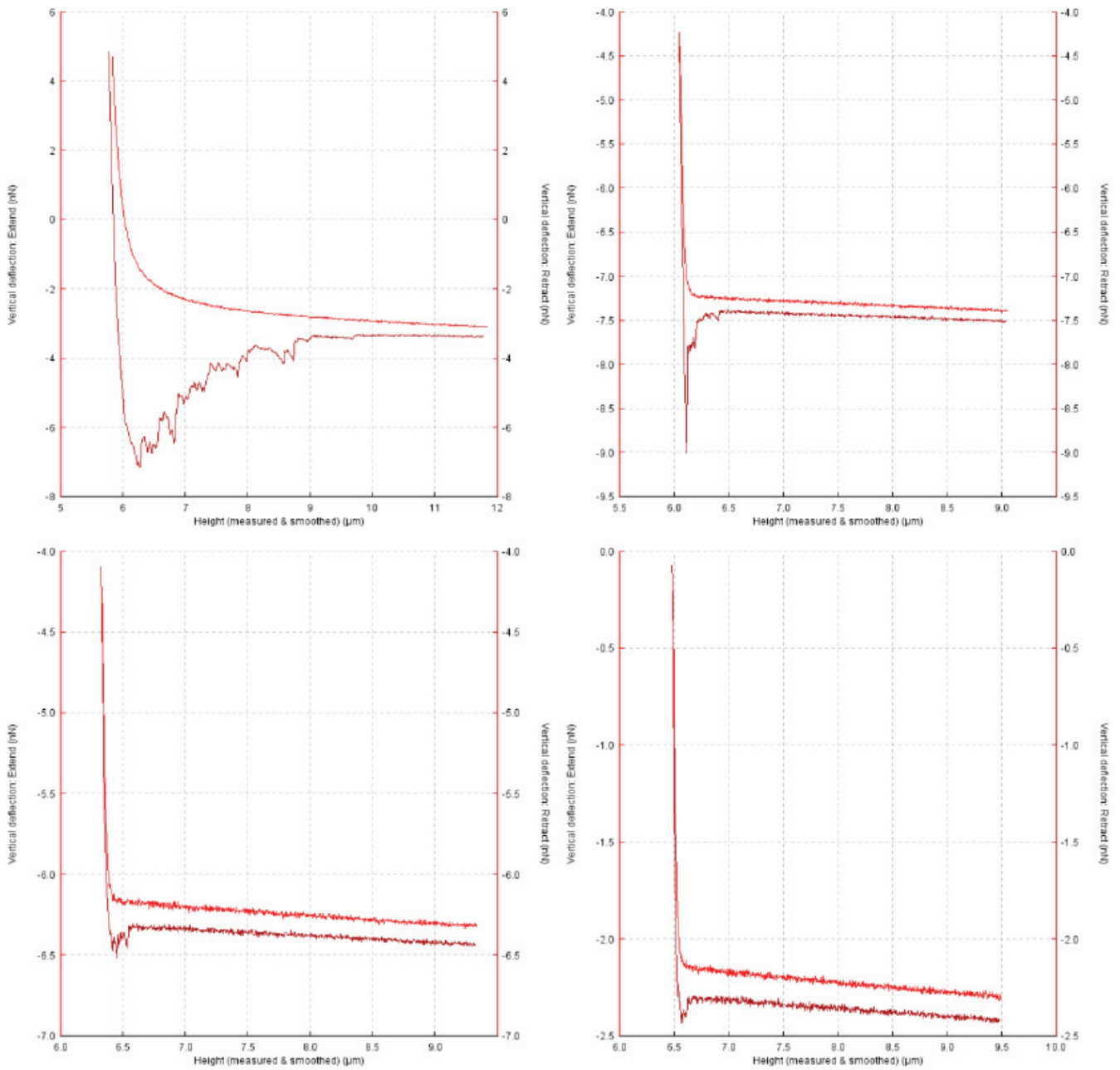


Figure 29: Force-distance curves from the AFM nanoindentation experiments with a 4,5 μm spherical polystyrene tip. The top left curve is for a 2 mg/ml mucin layer, while the top right is for the same layer incubated in 0,5 mg/ml alginate. The two lower images are for the same samples with 0,5 mg/ml (left) and 2 mg/ml (right) G-blocks in the solution.

Table 13: The average Young's modulus with standard deviation and approximate layer thickness obtained from 360 force curves from AFM nanoindentation experiments on mucin layers with alginate and G-blocks.

Mucin concentration (mg/ml)	Alginate concentration (mg/ml)	G-block concentration (mg/ml)	Young's modulus (Pa)	Layer thickness (nm)
2	0	0	2451 ± 2086	1000
2	0,5	0	30540 ± 23982	100
2	0,5	0,05	5895 ± 3496	60
2	0,5	0,1	5855 ± 3553	70
2	0,5	0,5	8478 ± 5496	100
2	0,5	2	9801 ± 5739	150
2	2	0	2606 ± 1861	100
2	2	0,05	2783 ± 2406	100
2	2	0,1	3511 ± 2378	70
2	2	0,5	3031 ± 1998	80
2	2	2	2959 ± 2123	80
1	0	0	11632 ± 4944	30
1	2	0	6625 ± 2435	40
1	2	0,05	6416 ± 3468	50
1	2	0,1	5356 ± 2975	60
1	2	0,5	6991 ± 3121	40
1	2	2	-	-
0,5	0	0	38795 ± 13603	40
0,5	0,5	0	6492 ± 3419	50
0,5	0,5	0,05	8087 ± 9458	50
0,5	0,5	0,1	6196 ± 3501	40
0,5	0,5	0,5	6186 ± 4009	40
0,5	0,5	2	7463 ± 5617	40

5. Discussion

5.1 Immobilization of mucins

During the immobilization of mucins to the glass surface in the silicone wells very small amounts were used. These were hard to control accurately, which make concentration of mucins uncertain. The mucin solution was left 15 min for the mucin to dissolve, but it was hard to observe if the mucin and EDAC had dissolved in the small volumes. This would affect the homogeneity of the mucin layer.

The lowest concentration on the mucin layers used in the TIRF measurements, 0,05 mg/ml, is too low to be a realistic model of the mucus barrier. The concentration might be too low to produce a homogeneous mucin layer. Typically a tenfold lower concentration is used when a small droplet is dried for imaging of single mucin molecules [9]. However it was only at 0,05 mg/ml concentration an intensity signal was obtained in TIRF mode. The great variations observed in intensity from the beads on this layer are probably due to a heterogeneous mucin layer.

5.2 Production of alginate beads

During production of alginate beads using microfluidics it has previously been challenging to obtain a stable droplet formation [21]. It was clear that addition of surfactant to the continuous phase stabilized the flows and facilitated the formation of the beads. This has also been shown by Dreyfus et al. [35].

Small particles were produced, but still with significant heterogeneity in size. The lack of monodispersity is most likely due to the instability during the bead formation. Stability was easier to obtain in devices with larger channel dimensions in combination with surfactant in the continuous phase. The effect of the surfactant seemed to be less important for the smaller channels, and the system is perhaps more easily disturbed when the channel dimensions are reduced.

Dimethyl carbonate (DMC) can be used as the continuous phase. DMC is nontoxic and environmentally friendly and qualifies as a green reagent [26]. According to Cooper White et al. alginate beads will shrink when exposed to

DMC, due to water diffusing from the beads out to the organic solvent [36]. This was also observed in the microfluidics project work [21]. In the microfluidic system the beads were exposed to DMC as they were made and before gelation took place. This is necessary because diffusion of water out of the bead and crosslinking are competing processes [36]. DMC could be used to obtain even smaller beads. However, the shrinking effect might not be as large for the microfluidic system used to obtain 10 μm beads due to the early introduction of calcium.

5.3 Labelling of beads with quantum dots

Covalent coupling of quantum dots with the shorter emission wavelength to polystyrene beads did not give good results. No fluorescence was detected for the procedure and concentrations established for the Qdot 655 quantum dots. As the emission wavelength of quantum dots is determined by their size, and therefore the Qdot 585 quantum dots are smaller, the procedure was repeated with up to ten times the established concentration of quantum dots. The fluorescence was still weak, and the problem could have been the increased pH in the linking solution due to large amounts of quantum dots added. A more concentrated solution with quantum dots was therefore prepared, and the procedure was repeated. This time there was fluorescence, but it was unevenly distributed among the polystyrene beads. Due to all these problems the quantum dots with emission wavelength 655 nm were chosen, and the appropriate filter set for the TIRF was used.

Preliminary micrographs of the fluorescently labelled polystyrene beads obtained with the Leica confocal microscope showed some artefacts. The bottom surface of the beads looked spherical, but on the top surface there seemed to be shadows around the sphere. This could be due to a refractive index mismatch between the water and the polystyrene beads which have a refractive index $n = 1,6$ (Polysciences, Technical data sheet 238). The beads were therefore subsequently imaged using vectashield, a mounting medium with refractive index $n = 1.457$. This resulted in less blurred images of the beads. This conclusion was strengthened by the images taken with the Zeiss microscope, which showed the same artefacts using the same type of laser and water objective as used with the Leica microscope.

In Table 6 one can clearly see that the fluorescence is mainly on the outside of the beads, apart from some autofluorescence from the polystyrene beads.

Although there is a certain thickness of the fluorescent layer, this suggests that the assumption used for Equation 6 for the intensity from the beads imaged in TIRF microscopy in general is correct.

5.4 TIRF measurements

To obtain a correct intensity measurement using TIRF microscopy it is important to focus on the right plane. The focal plane should coincide with the glass solution interface. For the control sample, with a bead directly on the glass, the focus should be on the bottom surface of the bead. However for the beads hovering above the mucin layer it is more difficult to locate the appropriate focus. The fluorescence intensity will be weaker for larger distances between the surface and the bead, but with wrong focus the measured intensity and distance would be incorrect. It is also important to avoid other light sources than the fluorescence from the sample during the measurements. This is due to the very sensitive EMCCD camera used to obtain the image series.

The exposure time for each image is reduced as much as possible to avoid averaging over fluctuations of the bead. The low exposure time is compensated by increasing the EM gain on the camera. However, high gain will also increase the noise in measurement. Therefore it is important to find a balance between these two parameters.

It is hard to determine the exact value of the penetration depth in a TIRF experiment. The refractive index of the sample is often heterogeneous and the incidence angle can be uncertain. This is due to possible scattering of incidence light that could cause the sample to be illuminated with a variety of angles around the critical angle for total internal reflection [5]. With an excitation wavelength of 488 nm, incidence angle 63° and refractive indices 1,33 for the aqueous buffer and 1,52 for the glass surface, the theoretical penetration depth is about 300 nm. However, the calculated value from the TIRF measurements suggests a much longer penetration depth of about 1,5 μm . This indicates that the measurements were not ideal.

Artefacts, probably due to scattering, were observed during TIRF measurements with polystyrene beads on the mucin layers. Fluorescence was observed if the focus was set to the middle of the bead instead of the glass surface. Scattering can also be a problem if the fluorescently labelled beads have a different refractive index than the surrounding solution, as observed during fluorescence

labelling of the polystyrene beads.

Scattering might also explain the two peaks observed in the histograms for intensity and inverse penetration depth of the evanescent field obtained from the fit to a double exponential of the TIRF data. Another explanation could be that the beads fluctuate between two heights. This could be further investigated by calculating the potential energy distribution, as described in Equation 10.

The mathematical function developed to describe the intensity profile did not fit well with the measurements. This could be due to scattering artefacts on the measured intensity profiles. However the double exponential expression for the intensity profile found by Mattheyses et al. [5], which does take into account the scattering effects, was used as basis for the analysis. The poor fit of the mathematical function to the TIRF data could also contribute to large variations in the parameter distributions and the great difference between theoretical and measured penetration depth of the evanescent field.

The TIRF measurements on the two mucin layers prepared with mucin concentrations 1 mg/ml and 0,5 mg/ml were not of sufficient quality to perform the analysis. A bead was found and the microscope was focused on the glass surface, but when the microscope was switched to TIRF mode, no intensity was detectable over the noise. Measurements performed on a bead on the glass surface gave series of intensity profiles under the exact same conditions. This indicates that the mucin layer is thicker than the penetration depth of the evanescent field, and that it acts like a barrier, preventing the beads from reaching the surface. Alternatively the barrier is too dense for the beads to be excited by the evanescent field. Weaker intensity from the beads was predicted, but since it was too weak for the distance from the bead to the glass surface to be measureable, the effect of alginate and G-blocks could not be measured with these concentrations of mucins.

Another reason that could explain the lack of intensity is that the penetration depth of the evanescent field was too short. The field is important during TIRF measurements, and it is hard to determine accurately, as discussed above. However, adjusting the angle of incidence will change the depth of the field. When the beads were on the mucin layer, the microscope was in TIRF mode and the focus was set correctly, the angle of incidence was adjusted. This did not result in any more fluorescence from the beads.

This problem was investigated further by observing the beads on the layer with mucin concentration 0,5 mg/ml in the Zeiss LSM 510 confocal microscope. Images were obtained in order to determine the distance between the glass surface and the bead. This indicated that the bead was close to the surface. However, the resolution in the z-direction was 570 nm, which is larger than the theoretical penetration depth of the evanescent field. The beads could therefore still be outside the field in TIRF and within the z-value closest to the surface in confocal microscopy, and so the test was inconclusive.

The intensities obtained in the TIRF measurements differ from bead to bead. This is due to uneven labelling of the beads. Some of the beads have areas with brighter aggregates of quantum dots. However it is a clear difference in intensity between the beads on a glass surface and the beads on the mucin layer. There are also larger differences in intensity between the beads on the mucin layer. This is probably a result of an inhomogeneous layer rather than uneven fluorescence labelling of the beads.

An alternative to TIRF is to do the measurements using reflection interference contrast microscopy (RICM) [4]. This technique is based on analysing the interference patterns of the light reflected from the sample, often detected with a CCD camera. It is similar to TIRF as it provides an intensity profile that is dependent on the distance between a surface and an object. In addition both methods need knowledge about the refractive index of the sample to provide accurate measurements of the distance. In the case of a micrometer sized bead excited by the evanescent field created in TIRF, only the bottom half of the bead has to be considered, due to the relatively short penetration depth of the field. When using RICM reflections from the whole sample has to be considered, and repeating interference patterns can be challenging. On the other side, the bead does not have to be fluorescent for measurements with RICM, and the difficulty with uneven labelling is avoided. Studies similar to the TIRF measurements performed here has been done using RICM [37].

5.5 AFM nanoindentation experiments

AFM nanoindentation experiments were performed in order to find the thickness of the mucin layers, and to investigate the effect of alginate and G-blocks. However, when performing Hertz-fit to force-distance curves the thickness of the sample is usually known. Since there should be two changes in slope on these curves, the fit was done to the first point of change. However, the curves were

often without distinct changes, and sometimes with more than two. This made the analysis very difficult, and caused the large variation in Young's modulus. The thicknesses of the layers that were found are also very approximate due to the difficulties with defining the points where the slope changes.

Despite these problems in the analysis of the force curves, it seems clear that the thicknesses of the layers in most cases are smaller than both the theoretical and measured penetration depth of the evanescent field in TIRF. The AFM indentation experiments therefore indicate that the layer thickness of the samples should not be a problem during TIRF measurements. The thickness observed from the force curves are larger than the thickness of individual mucin molecules, which are in the size range of 5-10 nm [11].

5.6 Particle transport

Even though the thickness and elasticity of the samples seemed to be relatively unaffected by the addition of alginate and G-blocks, it was a clear reduction in unspecific adhesion interactions between the bead and the layers. Especially addition of G-blocks to the solution reduced the interactions. This indicates that the mucins interact more with the alginate chains and the G-blocks than with the bead, which further suggests that a particle can move more freely through the layer when G-blocks are added to the solution.

The bacterium *Pseudomonas aeruginosa* produces alginate mostly containing M-blocks with acetyl groups [2]. This indicates that this alginate does not interact with mucins through G-blocks. From the AFM nanoindentation experiments it seems that G-blocks can compete with alginate, which suggests that G-blocks interact more strongly with mucins than polyM alginate. The particles produced by microfluidic techniques are made of alginate. These will contain G-blocks like the ones added to solution to compete with the alginate produced by *Pseudomonas aeruginosa* in the mucus layer in lungs of CF patients [2]. This might cause a problem when using the alginate particles for drug delivery systems, as the G-blocks of the particles could interact with mucins. However, it is likely that this is avoided since G-blocks in the beads are interacting with calcium.

Although many studies focus on the transport through the mucus layer to deliver drugs, there are also some that investigate the possibility of adhering the particles to the mucus to obtain drug release over extended periods of time [3]. This is an

alternative strategy for drug delivery if the mucus barrier is too hard to overcome.

5.7 Future perspectives

The microfluidic system for production of alginate beads needs to be developed further. Even though beads are produced at satisfactory small sizes, the size distribution is too large. This is due to the instability of flows during production. This problem might be solved by using a flow well that can more accurately control the amounts of solution that is pushed through the device. Filtering of the solutions before they are used in the channels might also increase the stability. Higher stability would also increase the reproducibility of the beads. The shape of the produced beads is also an issue that needs further investigation. Addition of D-Mannitol to the calcium solution might be helpful for production of spherical beads [38]. However, it seems that spherical beads are obtained when devices with inlet for calcium are used.

The alginate beads produced in the microfluidic devices should further be fluorescently labelled. It should be possible to use the same procedure as for the polystyrene beads, with some adjustments to the concentrations. The same measurements that were carried out for the polystyrene beads on mucin layer could then be done, together with other investigations to determine if the alginate particles can be used for medical applications and transport through the mucus barrier.

For TIRF to give accurate measurements of the penetration depth of beads into mucin layers, further adjustments to the mucin concentration would have to be done in order to obtain a homogenous layer that is not too thick or dense to obtain a signal from the beads. The incubation time of the mucin solution could also affect how many molecules are linked to the surface. The thickness of the mucin layers should also be more accurately determined in order to increase the accuracy of TIRF measurements.

In addition to adjusting conditions during the TIRF measurement to obtain reproducible results, the analysis needs further improvement. The theoretical expression, initial values of the parameters or other adjustments could be done to obtain a better fit to the experimental data.

6. Conclusions

This study has shown that it is possible to produce alginate microparticles using microfluidics. Beads with diameters in the size range 10 μm were produced. The size of the particles is mainly determined by the size of the channels, but also the flow rate ratios of the solutions. Monodispersity of the size is dependent on a stable system, which in many cases is hard to obtain. The shape of the beads after gelation is also an issue. It was easier to obtain spherical particles in a device where the calcium solution is introduced right before the droplet formation. However, the flows in this system were in general harder to stabilize than the flows in devices with inlets for only two solutions.

It has also been shown that it is possible to measure the penetration depth of a bead into a mucin layer using TIRF. It is however dependent on low concentration of mucins to obtain a signal from the fluorescent beads. High concentrations of the mucin results in a layer that is too thick or too dense for the particles to be excited from the evanescent field. For accurate measurements of the distance between the beads and the surface, the technique is also dependent on even fluorescence from the beads and a homogeneous mucin layer.

AFM nanoindentation experiments indicate that the thicknesses of the mucin layers are smaller than the theoretical penetration depth of the evanescent field. The force curves also showed that both the thickness and the elasticity are relatively unaffected by the incubation with alginate and addition of G-blocks. However, the force curves show that there are adhesion interactions between a polystyrene bead and the mucin layers, which are reduced when the layers interact with alginate, and further reduced when G-blocks are added. Addition of G-blocks could therefore have a positive effect on the particle transportation in the lungs of CF patients.

References

1. Hattrup CL, Gendler SJ: **Structure and function of the cell surface (tethered) mucins**. *Annual Review of Physiology* 2008, **70**:431-457.
2. May TB, Shinabarger D, Maharaj R, Kato J, Chu L, Devault JD, Roychoudhury S, Zielinski NA, Berry A, Rothmel RK *et al*: **Alginate Synthesis by Pseudomonas aeruginosa: a Key Pathogenic Factor in Chronic Pulmonary Infections of Cystic Fibrosis Patients**. *Clinical Microbiology Reviews* 1991, **4**(2):191-206.
3. Khanvilkar K, Donovan MD, Flanagan DR: **Drug transfer through mucus**. *Advanced Drug Delivery Reviews* 2001, **48**:173-193.
4. Limozin L, Sengupta K: **Quantitative reflection interference contrast microscopy (RICM) in soft matter and cell adhesion**. *ChemPhysChem* 2009, **10**:2752-2768.
5. Mattheyses AL, Axelrod D: **Direct measurement of the evanescent field profile produced by objective-based total internal reflection fluorescence**. *Journal of Biomedical Optics* 2006, **11**:014006-014001-014007.
6. Taylor C, Draget KI, Smidsrod OA: **Use of oligouronates for treating mucus hyperviscosity**. In: *The Patent Cooperation Treaty*. 2007.
7. Bansil R, Turner BS: **Mucin structure, aggregation, physiological functions and biomedical applications**. *Current opinion in colloid and interface science* 2006, **11**:164-170.
8. McMaster TJ, Berry M, Corfield AP, Miles MJ: **Atomic force microscopy of the submolecular architecture of hydrated ocular mucins**. *Biophysical Journal* 1999, **77**:533-541.
9. Stokke BT, Elgsaeter A, Skjrak-Brjek G, Smidsrød O: **The molecular size and shape of xanthan, xylinan, bronchial mucin, alginate, and amylose as revealed by electron microscopy**. *Carbohydrate Research* 1987, **160**:13-28.
10. Hong Z, Chasan B, Bansil R, Turner BS, Bhaskar KR, Afdhal NH: **Atomic force microscopy reveals aggregation of gastric mucin at low pH**. *Biomacromolecules* 2005, **6**:3458-3466.
11. Lai SK, Wang Y-Y, Hida K, Cone R, Hanes J: **Nanoparticles reveal that human cervicovaginal mucus is riddled with pores larger than viruses**. *PNAS* 2010, **107**(2):598-603.
12. Lai SK, O'Hanlon DE, Harrold S, Man ST, Wang Y-Y, Cone R, Hanes J:

- Rapid transport of large polymeric nanoparticles in fresh undiluted human mucus** *PNAS* 2007, **104**(5):1482-1487.
13. McGill SL, Smyth HDC: **Disruption of the mucus barrier by topically applied exogenous particles.** *Molecular Pharmaceutics* 2010, **7**(6):2280-2288.
 14. Lieleg O, Vladescu I, Ribbeck K: **Characterization of particle translocation through mucin hydrogels** *Biophysical Journal* 2010, **98**:1782-1789.
 15. Stephen AM, Phillips GO, Williams PA: **Food polysaccharides and their applications.** Boca Raton, FL: CRC/Taylor & Francis; 2006.
 16. Chan HW-S (ed.): **Biophysical methods in food research:** Blackwell Scientific Publications; 1984.
 17. Mørch ÝA: **Novel Alginate Microcapsules for Cell Therapy - a study of the structure-function relationships in native and structurally engineered alginates.** *Doctoral theses.* Trondheim: Norwegian University of Science and Technology; 2008.
 18. Dominguez-Espinosa G, Synytska A, Drechsler A, Gutsche C, Kegler K, Uhlmann P, Stamm M, Kremer F: **Optical tweezers to measure the interaction between poly(acrylic acid) brushes.** *Polymer* 2008, **49**:4802-4807.
 19. Tønnesen HH, Karlsen J: **Alginate in drug delivery systems.** *Drug Development and Industrial Pharmacy* 2002, **28**(6):621-630.
 20. Hori Y, Winans AM, Irvine DJ: **Modular injectable matrices based on alginate solution/microsphere mixtures that gel in situ and co-deliver immunomodulatory factors.** *Acta Biomaterialia* 2009, **5**:969-982.
 21. Myklatun A: **Exploring microfluidics as a possible strategy for preparation of micronized alginate gel beads.** *Project work.* Norwegian University of Science and Technology; 2010.
 22. De Geest BG, Sanders NN, Sukhorukov GB, Demeester J, De Smedt SC: **Release mechanisms for polyelectrolyte capsules.** *Chemical Society Reviews* 2006, **36**:636-649.
 23. Chuah AM, Kuroiwa T, Kobayashi I, Zhang X, Nakajima M: **Preparation of uniformly sized alginate microspheres using the novel combined methods of microchannel emulsification and external gelation.** *Colloids and Surfaces A: Physicochemical and Engineering Aspects* 2009, **351**:9-17.
 24. Strand BL, Gåserød O, Kulseng B, Espevik T, Skjåk-Bræk G: **Alginate-polylysine-alginate microcapsules: effect of size reduction on capsule properties.** *Microencapsulation* 2002, **19**(5):615-630.

25. Tumarkin E, Kumacheva E: **Microfluidic generation of microgels from synthetic and natural polymers**. *Chemical Society Reviews* 2009, **38**(8):2149-2496.
26. Tundo P, Selva M: **The Chemistry of Dimethyl Carbonate**. *Accounts of chemical research* 2002, **35**(9):706-716.
27. Prasad PN: **Bioimaging: Principles and Techniques**. In: *Introduction to biophotonics*. John Wiley & Sons Inc.; 2003.
28. [<http://www.microscopyu.com/articles/fluorescence/tirf/tirfintro.html>]
29. Prieve DC: **Measurement of colloidal forces with TIRM**. *Advances in Colloid and Interface Science* 1999, **82**(1-3):93-125.
30. Prasad PN: **Nanotechnology for Biophotonics: Bionanophotonics**. In: *Introduction to Biophotonics*. John Wiley & Sons, Inc. ; 2003.
31. Davies CdL, Stokke BT: **Biophysical Nanotechnologies - Lecture notes TFY 4265 Biophysical microtechniques**. In. Biophysics and Medical Technology, Department of Physics, NTNU; 2008.
32. JPK: **Data processing software manual - Version 3.4**. 2010.
33. Dagdas YS, Tombuloglu A, Tekinay AB, Dana A, Guler MO: **Interfiber ineractions alter the stiffness of gels formed by supramolecular self-assembled nanofibers**. *Soft Matter* 2011, **7**:3524-3532.
34. [<https://www.micro-shop.zeiss.com/?l=en&p=us&f=f>]
35. Dreyfus R, Tabeling P, Willaime H: **Ordered and disordered patterns in two-phase flows in microchannels**. *Physical Review Letters* 2003, **90**(14):144505.
36. Rondeau E, Cooper-White JJ: **Biopolymer Microparticle and Nanoparticle Formation within a Microfluidic Device**. *Langmuir* 2008, **24**:6937-6945.
37. Picart C, Sengupta K, Schilling J, Maurstad G, Ladam G, Bausch AR, Sackmann E: **Microinterferometric study of the structure, interfacial potential, and viscoelastic properties of polyelectrolyte multilayer films on a planar substrate**. *Journal of Physical Chemistry B* 2004, **108**:7196-7205.
38. Strand BL, Mørch ÝA, Espevik T, Skjåk-Bræk G: **Visualization of alginate-poly-L-lysine-alginate microcapsules by confocal laser scanning microscopy**. *Biotechnology and Bioengineering* 2003, **82**(4):386-394.

Appendix A

Data files

Alginate beads produced with electrostatic bead generator: Alginate beads produced with the electrostatic bead generator are imaged with Olympus IX70 microscope and the Olympus camera. The filenames identify the alginate concentration used to produce the beads and whether the beads are large, medium or small, based on the filtering of bead solutions and if they contain blue dextran. The names also identify the medium and time the beads have been shrunk in. The objective used is also identified in the file name.

Computer: Microfluidics by Olympus IX70 microscope

Files: Documents and Settings / Alginate beads

Microfluidic videos: Videos were obtained with the high speed camera Photron Fastcam SA3 mounted to the Olympus IX70 microscope during production of alginate beads with the microfluidic system. The names of the files describe which design of the microfluidic device was used, which dispersed and continuous phases and concentrations in the system: device – dimensions – continuous phase – dispersed phase.

Computer: Microfluidics by Olympus IX70 microscope

Files: Documents and Settings / microfluidics / Microfluidics 2011

Alginate beads produced with microfluidics: Alginate beads produced with microfluidics devices were imaged with the Olympus camera through the Olympus IX70 microscope. The software AnalySIS was used. The names of the files describe the system that was made to produce the beads in the following system: device design – channel dimensions – continuous phase – dispersed phase.

Computer: Microfluidics by Olympus IX70 microscope

Files: Documents and Settings / microfluidics / Microfluidics 2011 / Alginate beads

Confocal microscopy: The 6 μm polystyrene beads were imaged with the Leica TCS SP5 confocal microscope, together with the software LAS AF, to check if the labelling with quantum dots was successful. A 63x water immersion objective and an argon laser with 17 % power was used, with the three lines 458, 476 and 488 nm. The pinhole was 111,4 μm . The setup for the images was 1024x1024 pixels, 200 Hz and line average 4. For some beads a stack was obtained with the same settings and 0,3 μm between each image in the z-direction. The letters in the file name corresponds to different concentrations of qdots and EDAC used during the labelling procedure (see Table 6). G is the one that was used further for TIRF measurements.

Computer: by Leica TCS SP5 confocal microscope

Files: (D:) / Brukere / Ahne / KulerQdot_A-G

Bleaching of labelled polystyrene beads: Five data series of one bead were obtained in TIRF mode with the Andor EMCCD camera mounted to the Zeiss Observer D1 microscope. This was done to observe possible bleaching of polystyrene beads fluorescently labelled with Qdot 655 quantum dots. The five series was performed with exposure time 0,01501 s, EM gain 81, shift speed 1,7 μs and kinetic series length 1000 frames.

Computer: by Zeiss Observer D1 TIRF microscope

Files: system(C:) / iXon Data / Ahne / kuler qdots movies / bleaching1-5

Exposure time and EM gain level for TIRF: Images and data series was obtained of one 6 μm polystyrene bead labelled with Qdot 655 quantum dots to determine optimal combination of exposure time and EM gain on the Andor EMCCD camera during TIRF measurements (see Table 7). The measurement was performed with exposure times 0,00001 s, 0,00081 s, 0,00251 s, 0,01081 s and 0,05001 s, corresponding to the numbers 1 to 5 in the file names. The shift speed was set to 1,7 and the EM gain was varied between 5, 20, 80 and 150. The kinetic series length was 1000 frames.

Computer: by Zeiss Observer D1 TIRF microscope

Files: system(C:) / iXon Data / Ahne / kuler qdots movies / single_emgain5-150_exptime1-5 and emgain5-150_exptime1-5

TIRF measurements on mucin layers: 6 μm polystyrene beads labelled with Qdot 655 quantum dots were used for TIRF measurements with the Zeiss microscope. Series were obtained with exposure time 0,01251 s, EM gain level 100, shift speed 1,7 μs and kinetic series length 1000 frames. Series were first obtained for the beads on a clean glass surface, and then for beads on mucin layers. The files are named to recognize the surface the beads are placed on. Files named mucin A corresponds to a mucin concentration of 1 mg/ml, while mucin B is 0,5 mg/ml and mucin C is 2 mg/ml.

Computer: by Zeiss Observer D1 TIRF microscope

Files: system(C:) / iXon Data / Ahne / Measurements 120511 and Measurements 160511

TIRF measurements with low concentration mucin layer: 6 μm polystyrene beads labelled with Qdot 655 quantum dots were used for TIRF measurements with the Zeiss microscope. Series were obtained with exposure time 0,01081 s, EM gain level 100, shift speed 1,7 μs and kinetic series length 1000 frames. The files are named to recognize the surface the beads are placed on; a glass surface or a mucin layer with concentration 0,05 mg/ml. Single images were also obtained. Same file number corresponds to same bead.

Computer: by Zeiss Observer D1 TIRF microscope

Files: system(C:) / iXon Data / Ahne / Measurements 230511

TIRF measurements with mucin layer incubated in alginate: 6 μm polystyrene beads labelled with Qdot 655 quantum dots were used for TIRF measurements with the Zeiss microscope. 0,5 mg/ml alginate was used to incubate the mucin layer. Series were obtained with exposure time 0,01081 s, EM gain level 100, shift speed 1,7 μs and kinetic series length 1000 frames. The G-block number identifies the concentrations, with 1 corresponding to 0,05 mg/ml etc. (see Table 1)

Computer: by Zeiss Observer D1 TIRF microscope

Files: system(C:) / iXon Data / Ahne / Measurements 010611

Analysed TIRF data: The TIRF series obtained with the Zeiss Observer D1 microscope and the Andor EMCCD camera were converted to ascii format and analysed with iXonReader256pro, which fitted the data to Equation 11. The files with the fitted parameters are called iXonReader256pro_mucin/glass.txt depending on the surface the TIRF measurements were performed on. The mucin layers were in all cases with mucin concentration 0,05 mg/ml.

Computer: in laboratory

Files: system (C:) / RSI / Data / TIRF

AFM nanoindentation experiments: An AFM tip with a polystyrene bead with diameter 4,5 μm was used to perform nanoindentation experiments of the mucin layers. The JPK ForceRobot 300 was used. Mucin concentrations of 0,5 mg/ml, 1 mg/ml and 2 mg/ml was tested. The mucin layers was also incubated with 0,5 mg/ml and 2 mg/ml alginate. Measurements were further carried out with addition of increasing concentrations of G-blocks, from 0,05 mg/ml to 2 mg/ml (see Table 1). The filenames are given to identify the concentrations of mucin, alginate and G-blocks.

Computer: in laboratory

Files: system (C:) / RSI / Data / AFM / 30052011 and 31052011

Appendix B

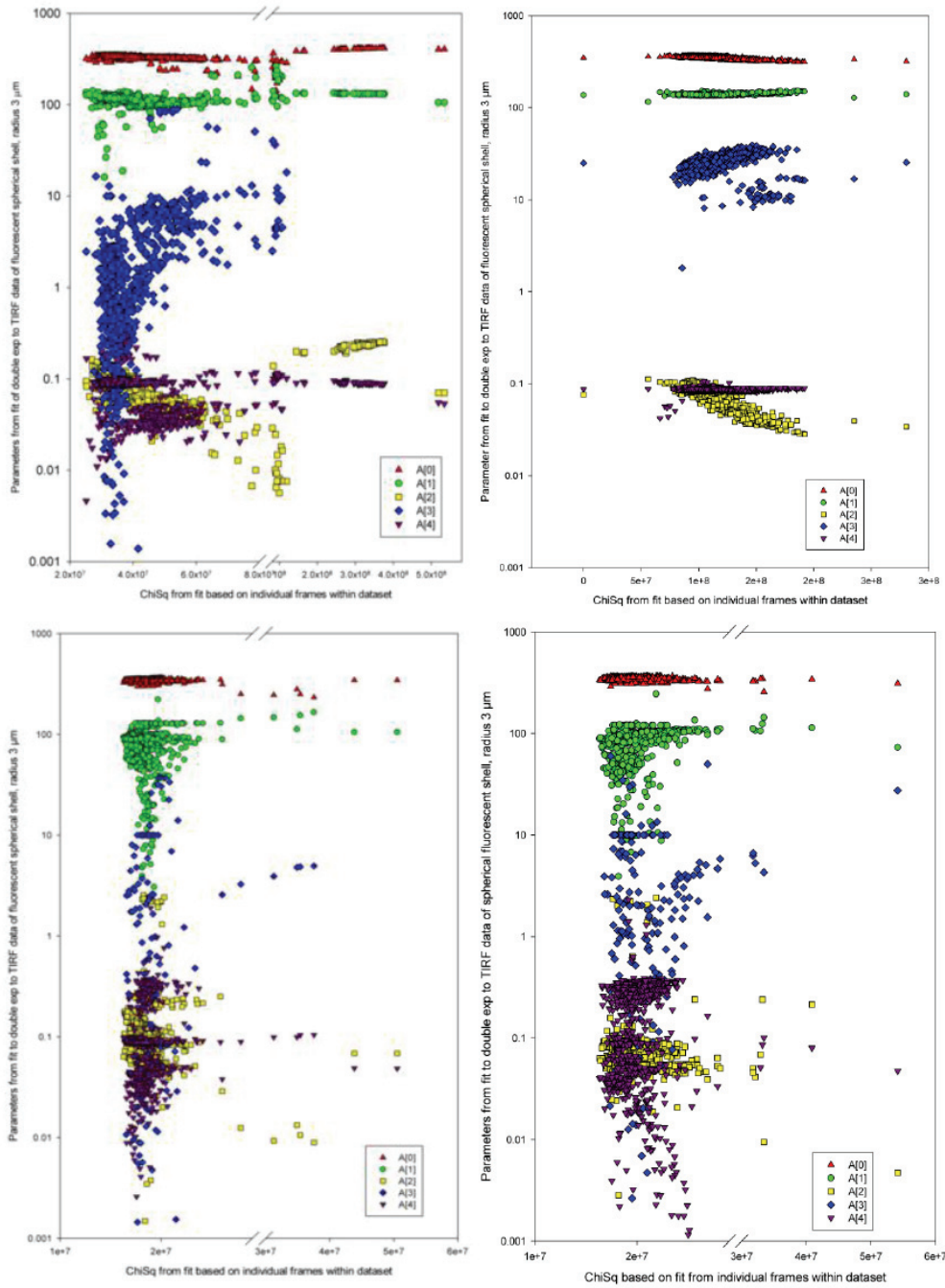
Table of abbreviations

AFM	Atomic force microscopy
CF	Cystic fibrosis
DETA	Trimethoxysilylpropyl-diethylenetriamine
DMC	Dimethyl carbonate
EDAC	1-(3-dimethylaminopropyl)-3-ethylcarbodiimide hydrochloride
EMCCD	Electron multiplication charged coupled device
IDL	Interactive data language
PDMS	Poly(dimethylsiloxane)
PGM	Pig gastric mucin
Qdot	Quantum dot
RICM	Reflection interference contrast microscopy
TIRF	Total internal reflection fluorescence

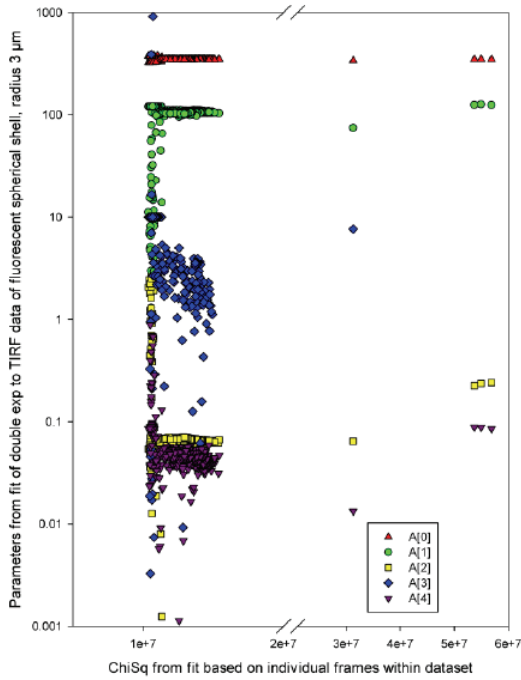
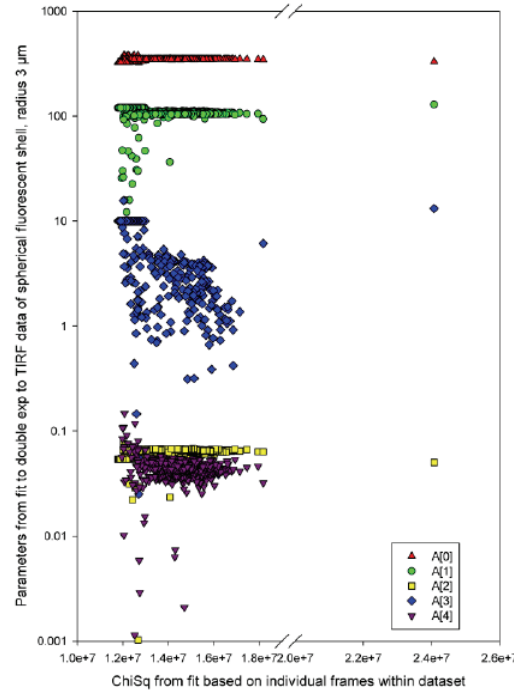
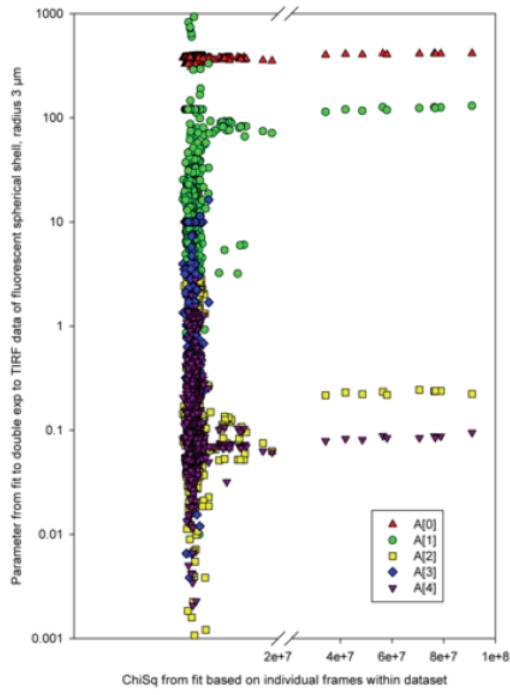
Appendix C

Scatter plots for parameter fit from TIRF analysis

Bead on glass surface



Bead on mucin layer



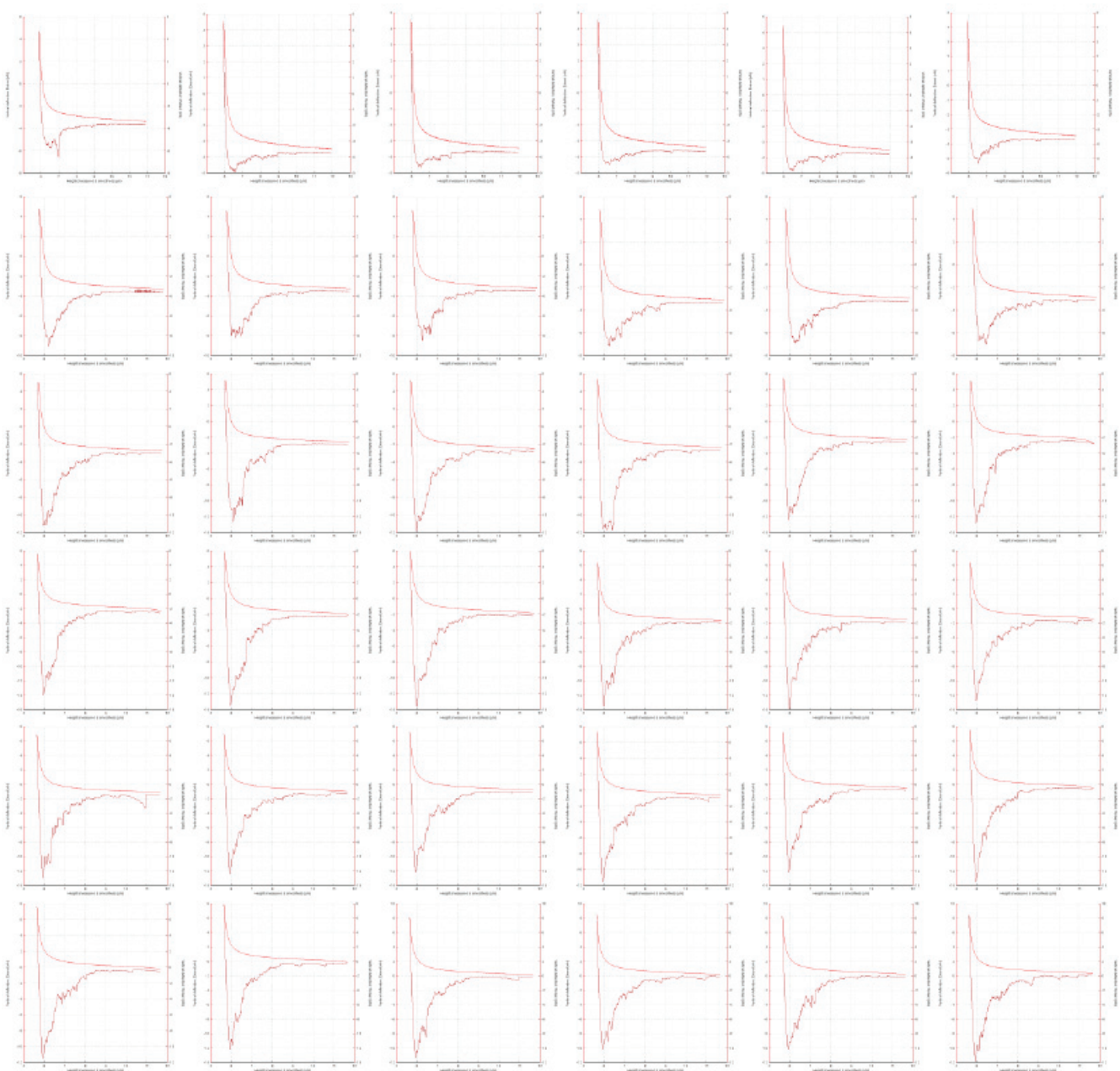
Appendix D

Force-distance curves from AFM nanoindentation experiments

2 mg/ml mucin

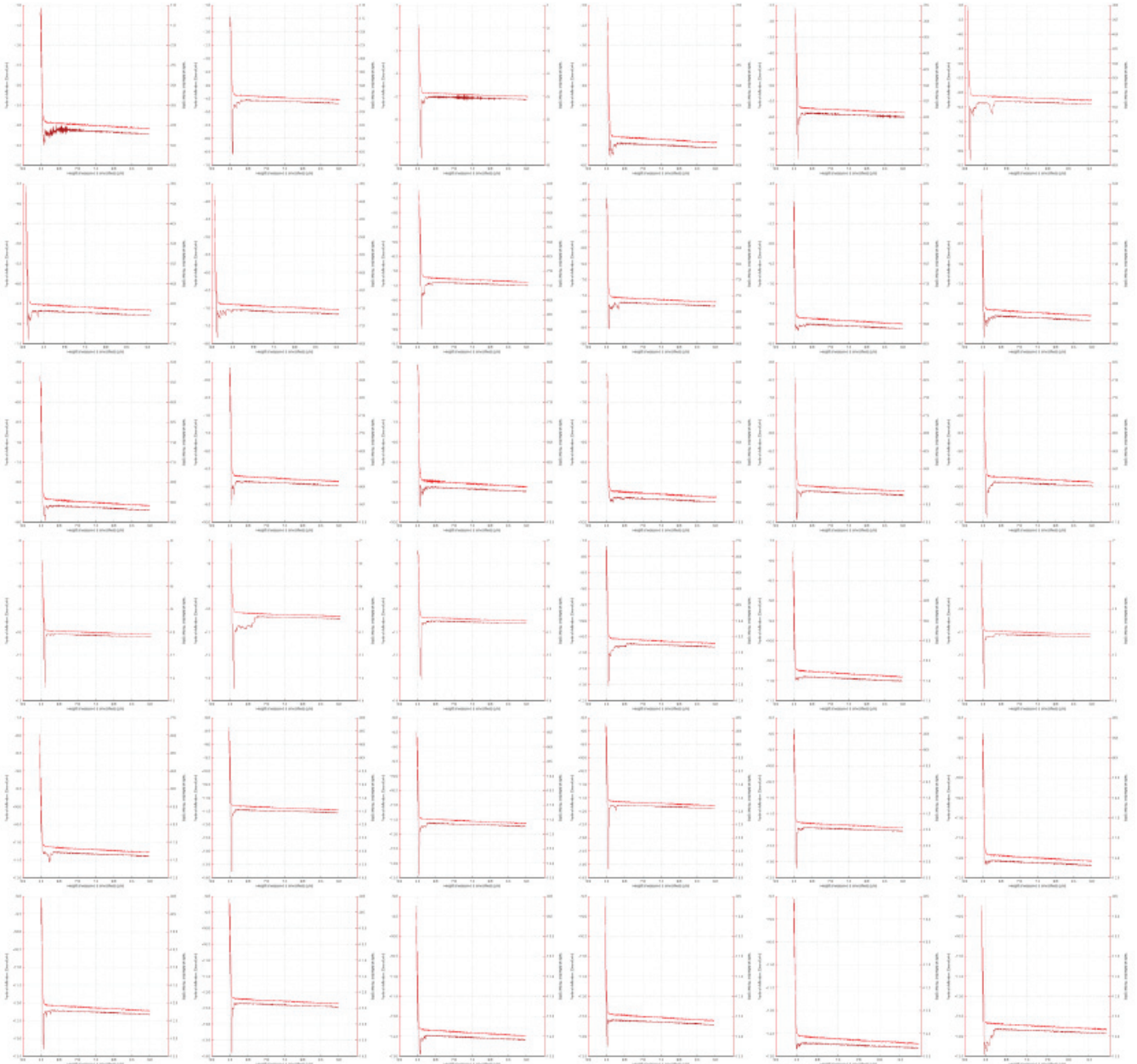
Spring constant: 0,1183 N/m

Deflection sensitivity: 43,85 nm/V



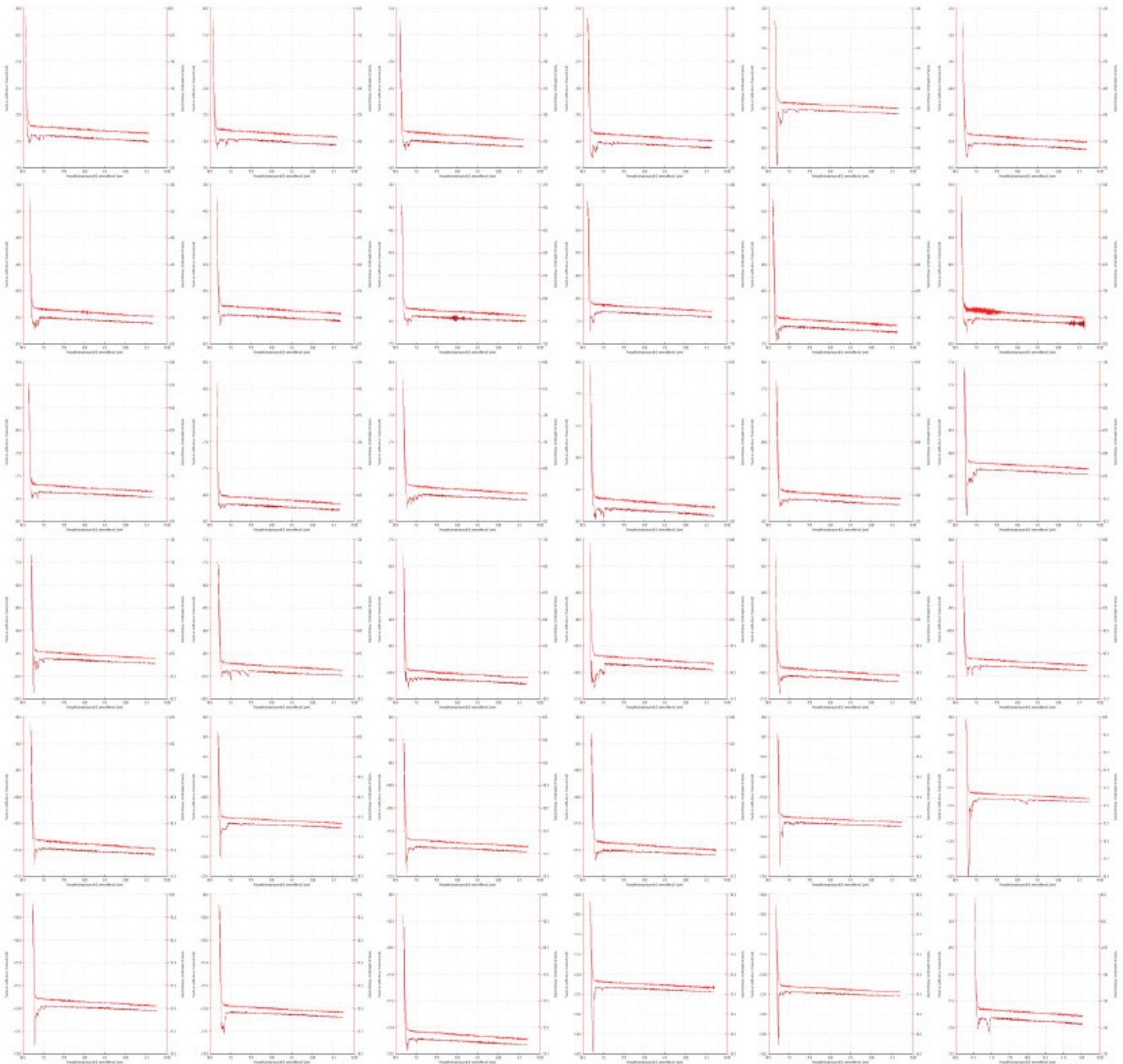
2 mg/ml mucin
0,5 mg/ml alginate

Spring constant: 0,0845 N/m
Deflection sensitivity: 49,53 nm/V



2 mg/ml mucin
0,5 mg/ml alginate
0,05 mg/ml G-blocks

Spring constant: 0,0845 N/m
Deflection sensitivity: 49,53 nm/V



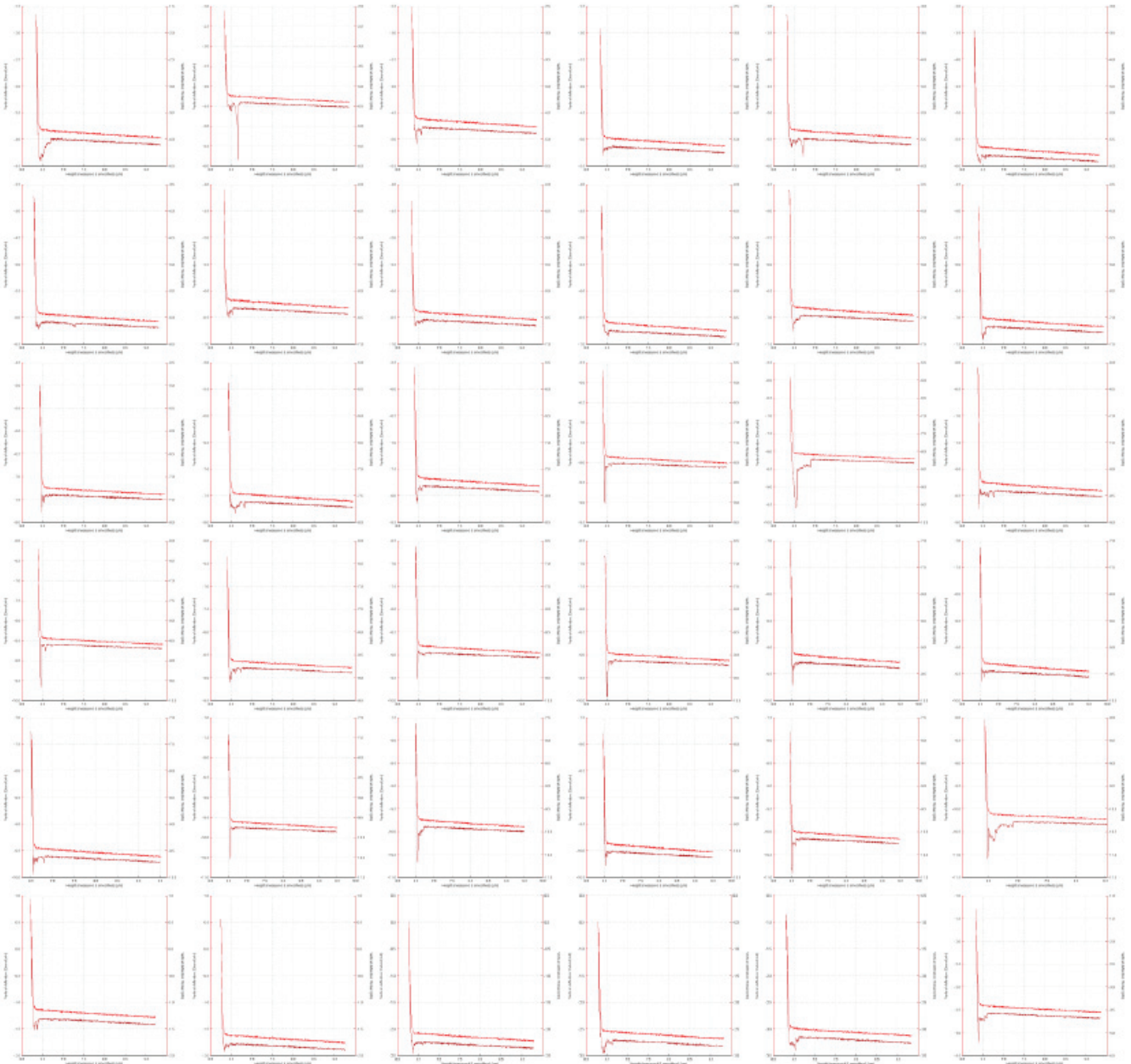
2 mg/ml mucin
0,5 mg/ml alginate
0,1 mg/ml G-blocks

Spring constant: 0,0845 N/m
Deflection sensitivity: 49,53 nm/V



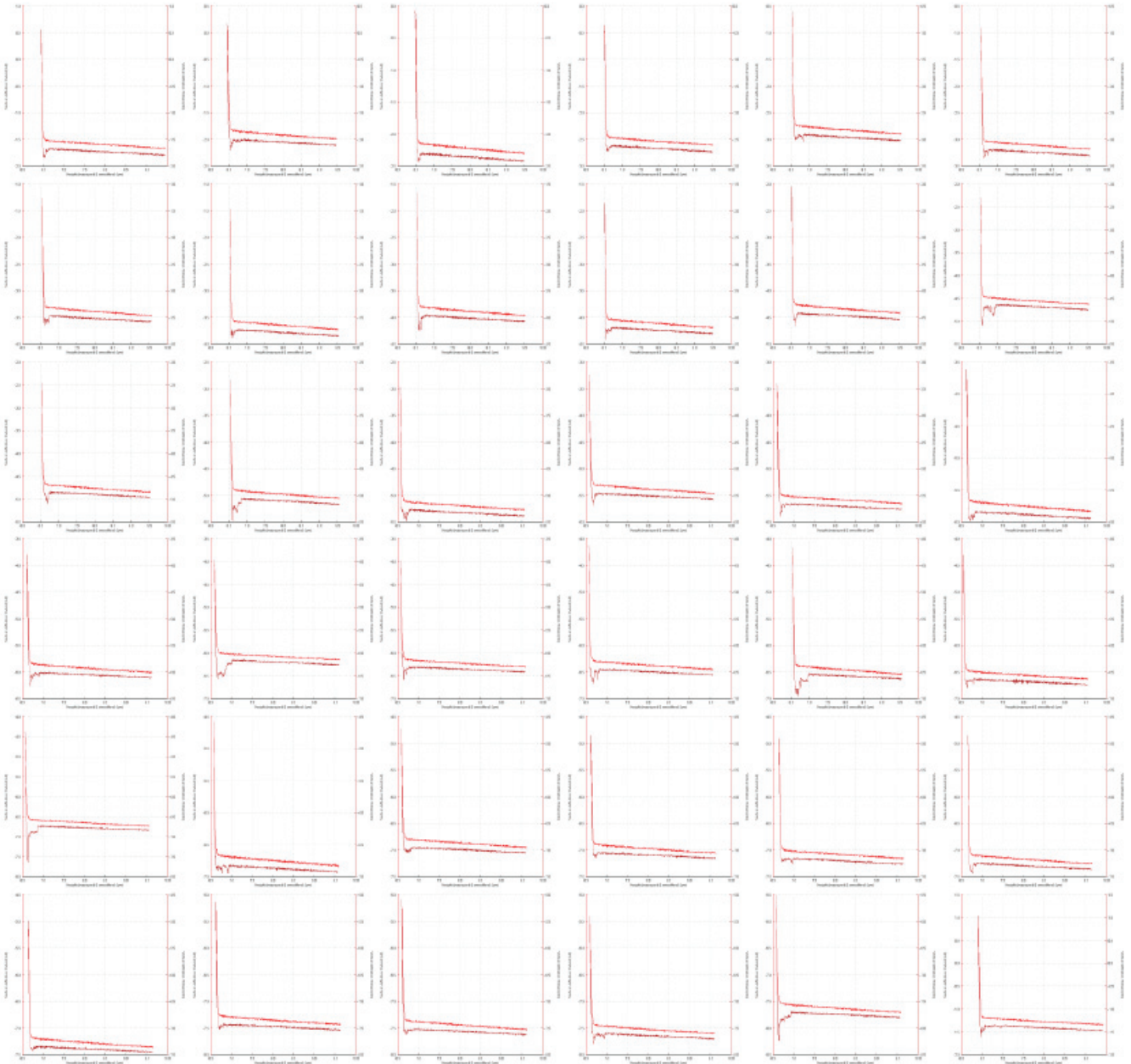
2 mg/ml mucin
0,5 mg/ml alginate
0,5 mg/ml G-blocks

Spring constant: 0,0845 N/m
Deflection sensitivity: 49,53 nm/V



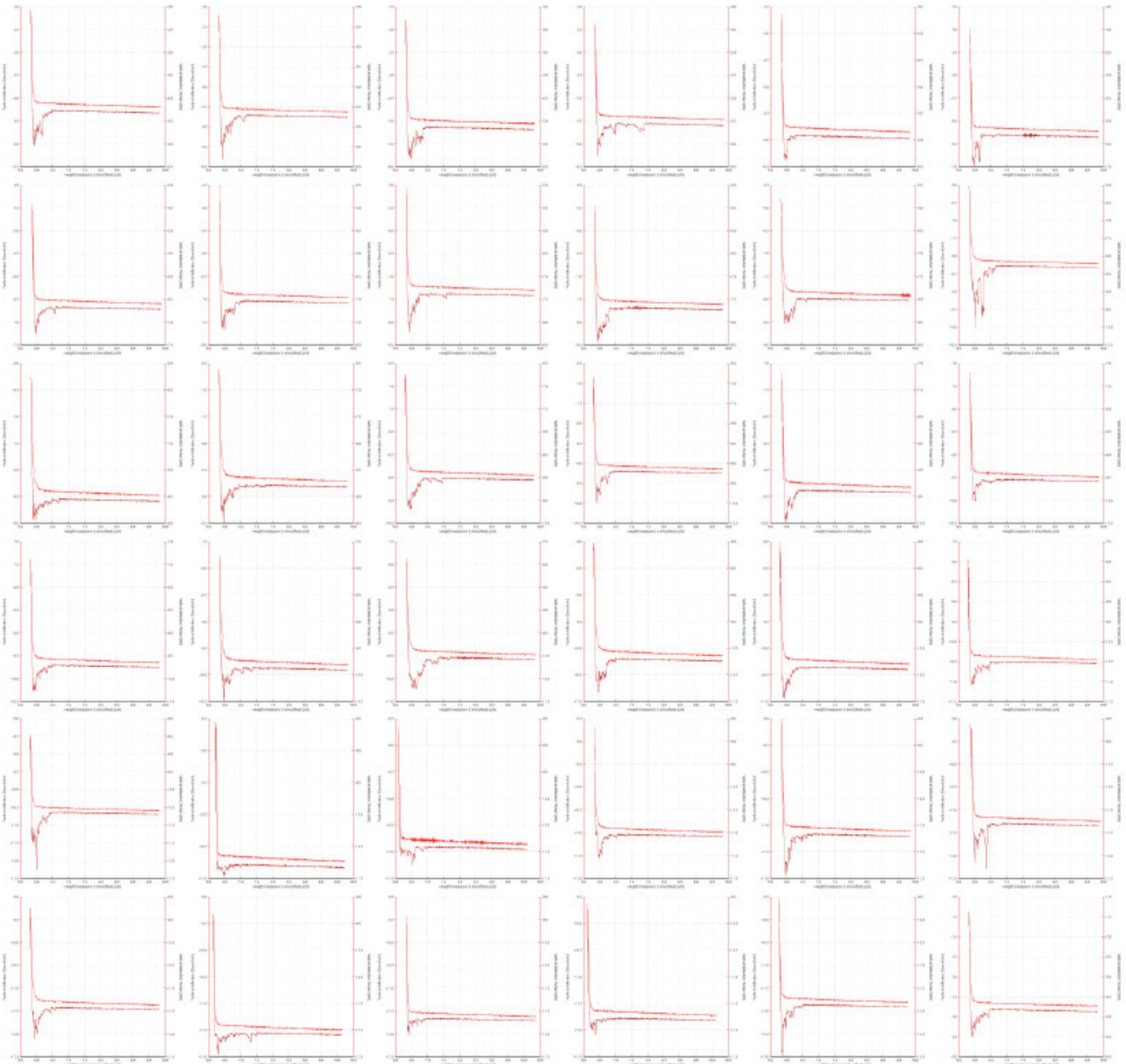
2 mg/ml mucin
0,5 mg/ml alginate
2 mg/ml G-blocks

Spring constant: 0,0845 N/m
Deflection sensitivity: 49,53 nm/V



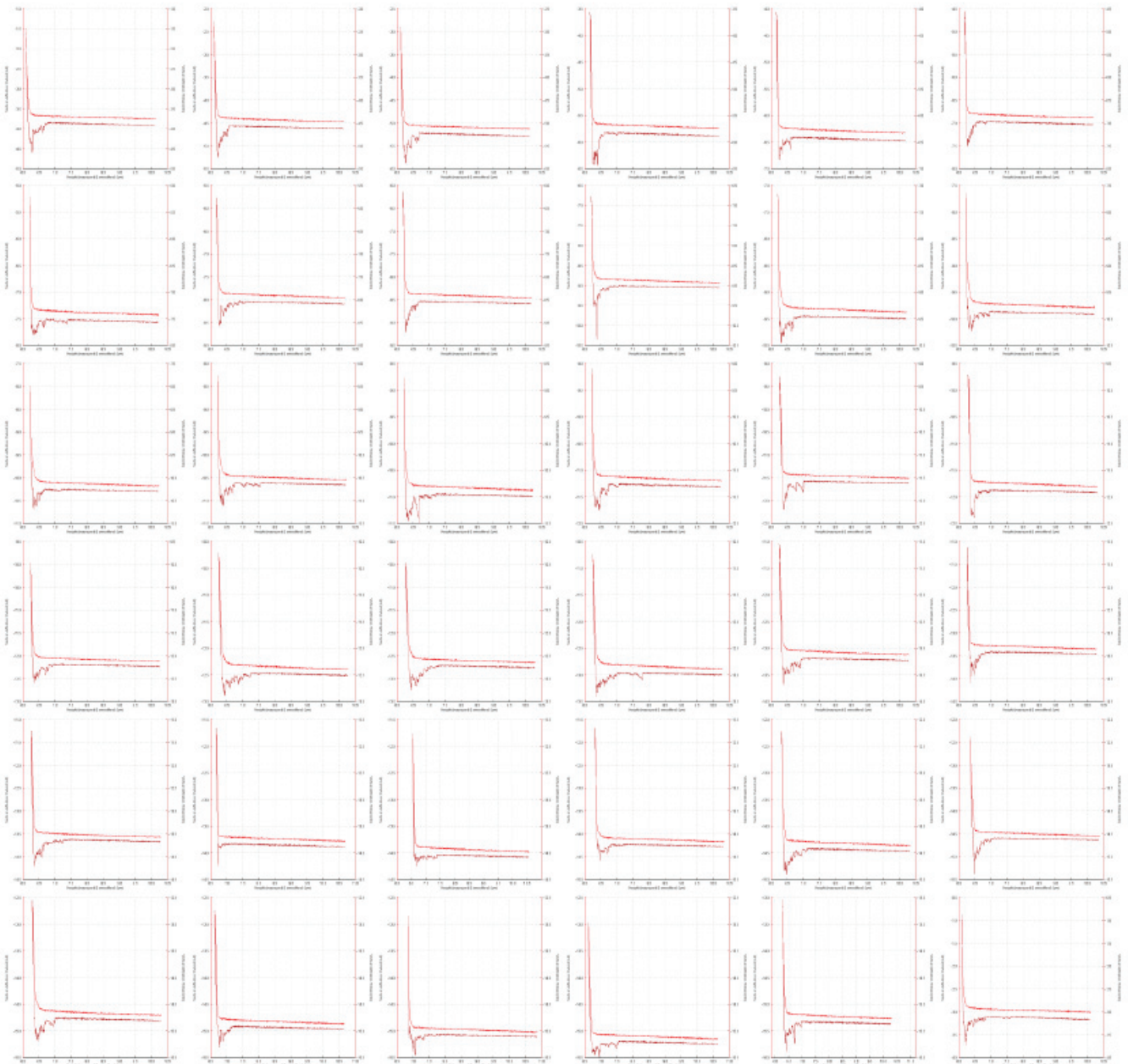
2 mg/ml mucin
2 mg/ml alginate

Spring constant: 0,0504 N/m
Deflection sensitivity: 58,73 nm/V



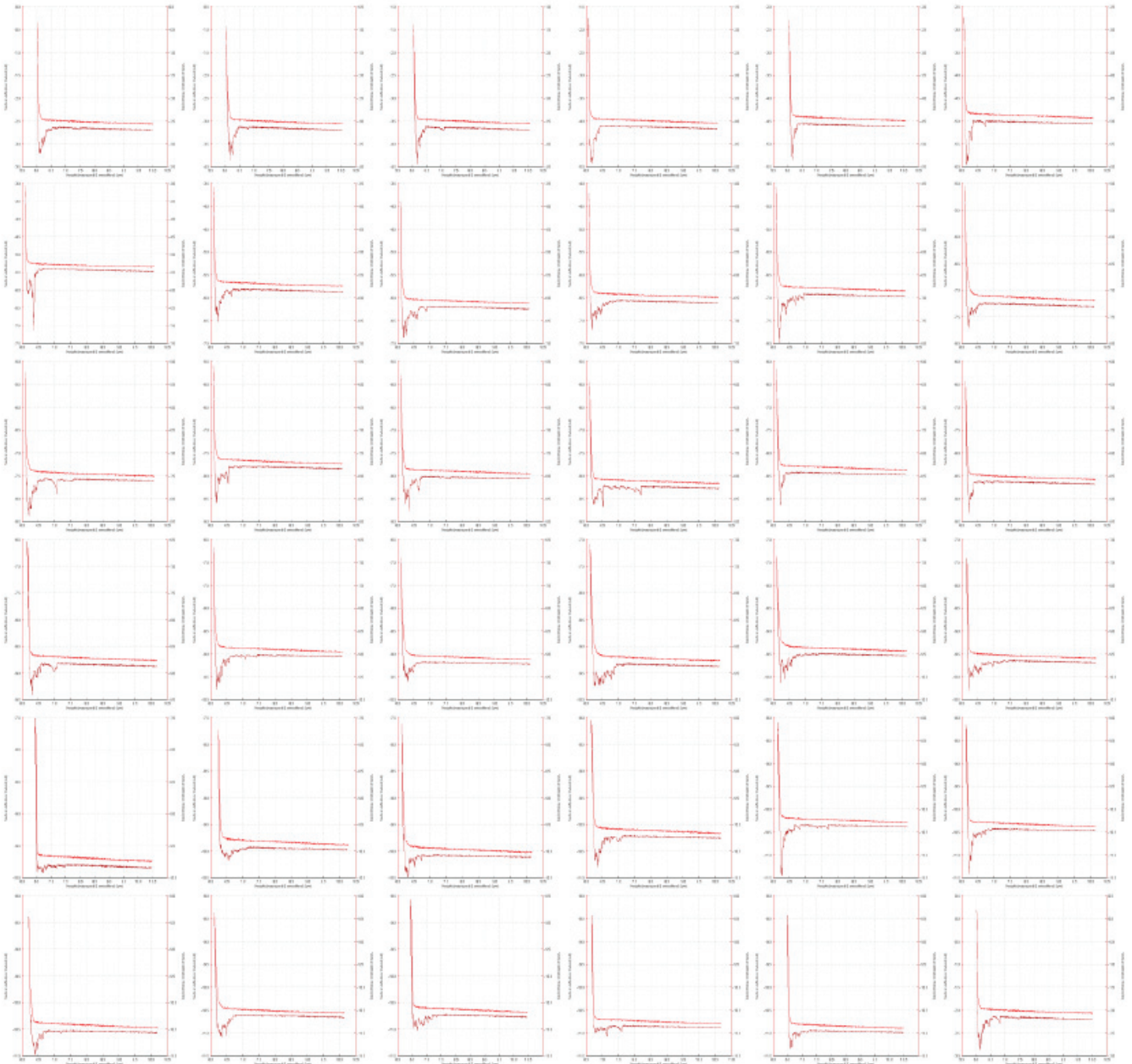
2 mg/ml mucin
2 mg/ml alginate
0,05 mg/ml G-blocks

Spring constant: 0,0504 N/m
Deflection sensitivity: 58,73 nm/V



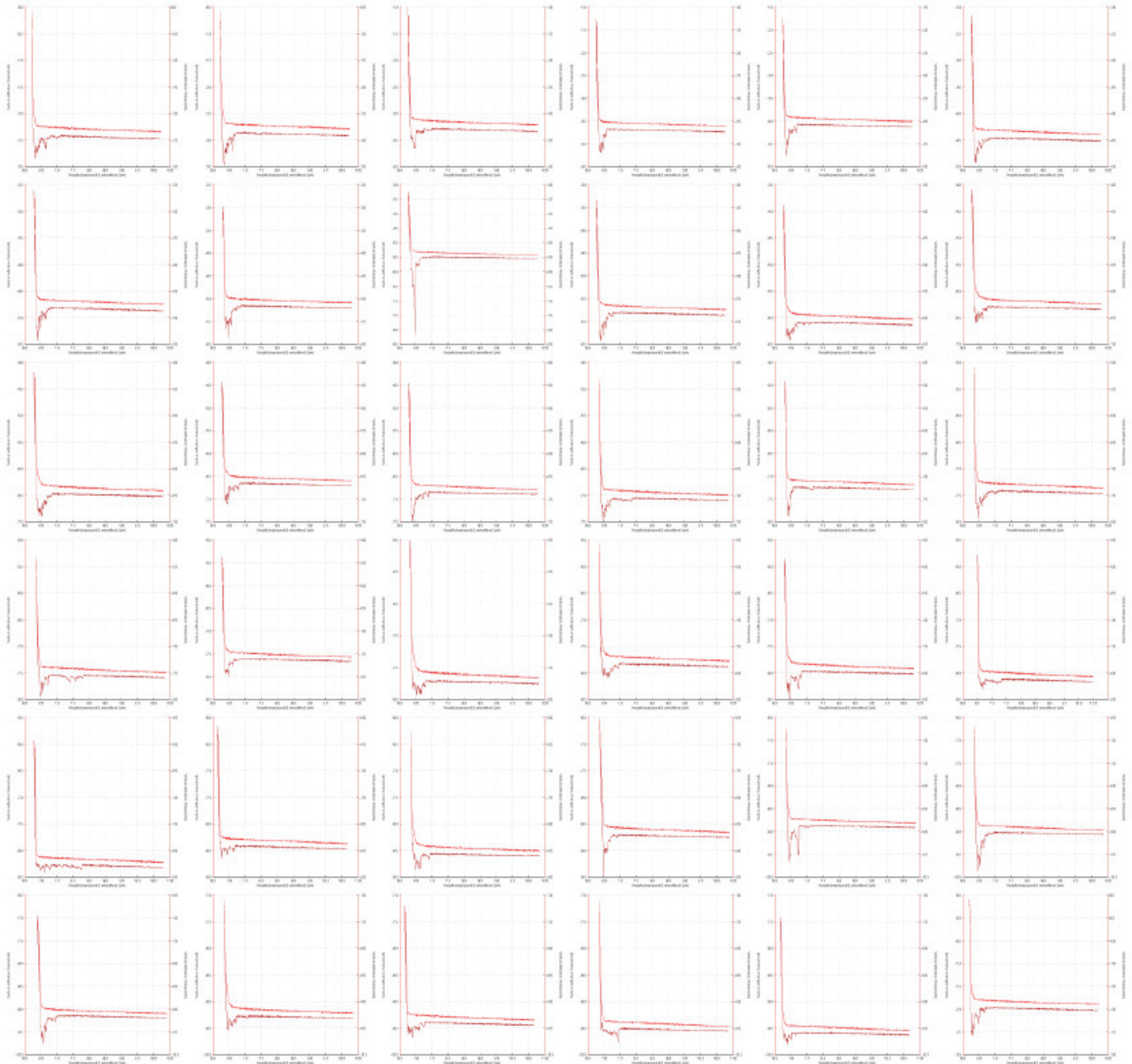
2 mg/ml mucin
2 mg/ml alginate
0,1 mg/ml G-blocks

Spring constant: 0,0504 N/m
Deflection sensitivity: 58,73 nm/V



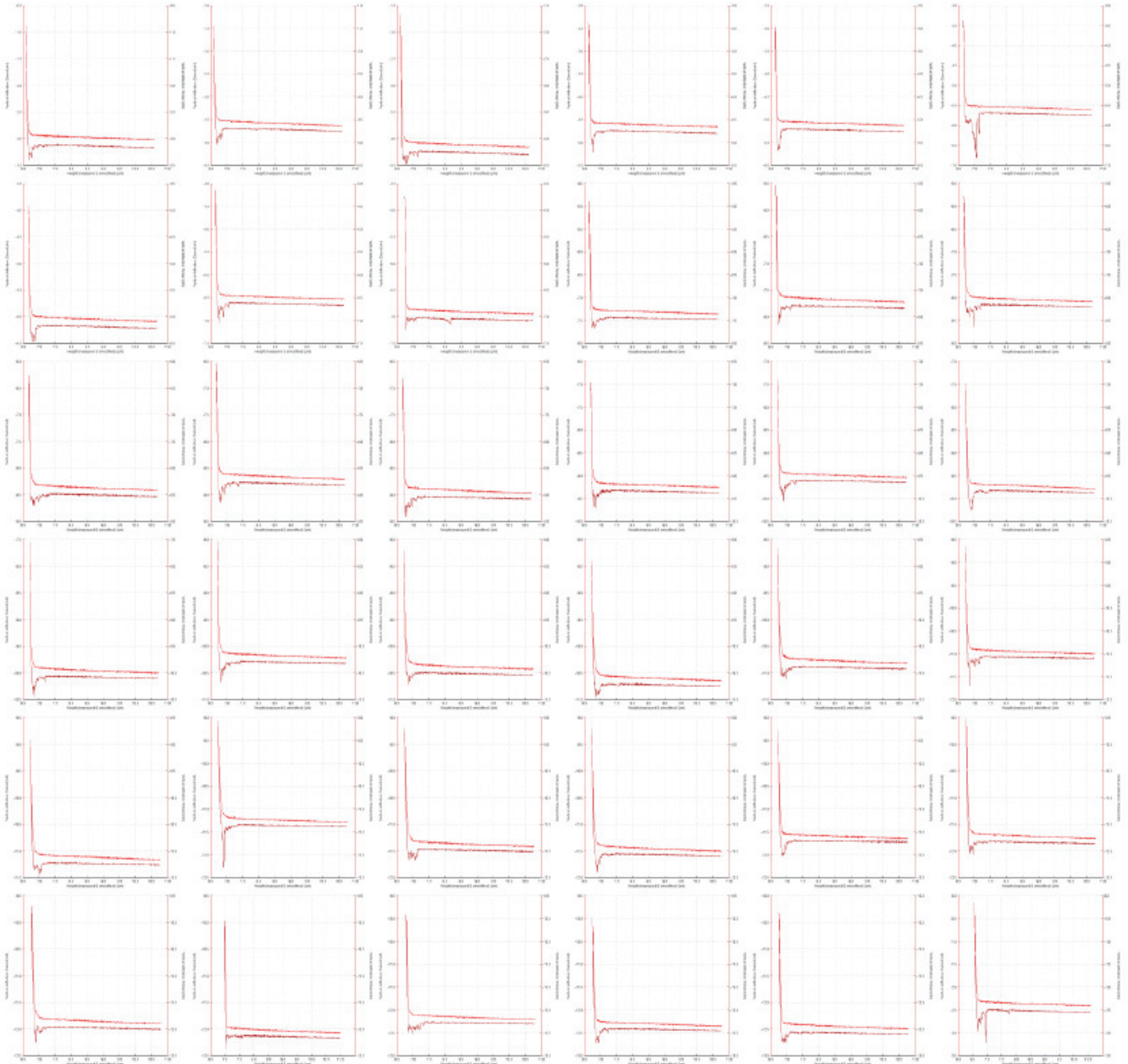
2 mg/ml mucin
2 mg/ml alginate
0,5 mg/ml G-blocks

Spring constant: 0,0504 N/m
Deflection sensitivity: 58,73 nm/V



2 mg/ml mucin
2 mg/ml alginate
2 mg/ml G-blocks

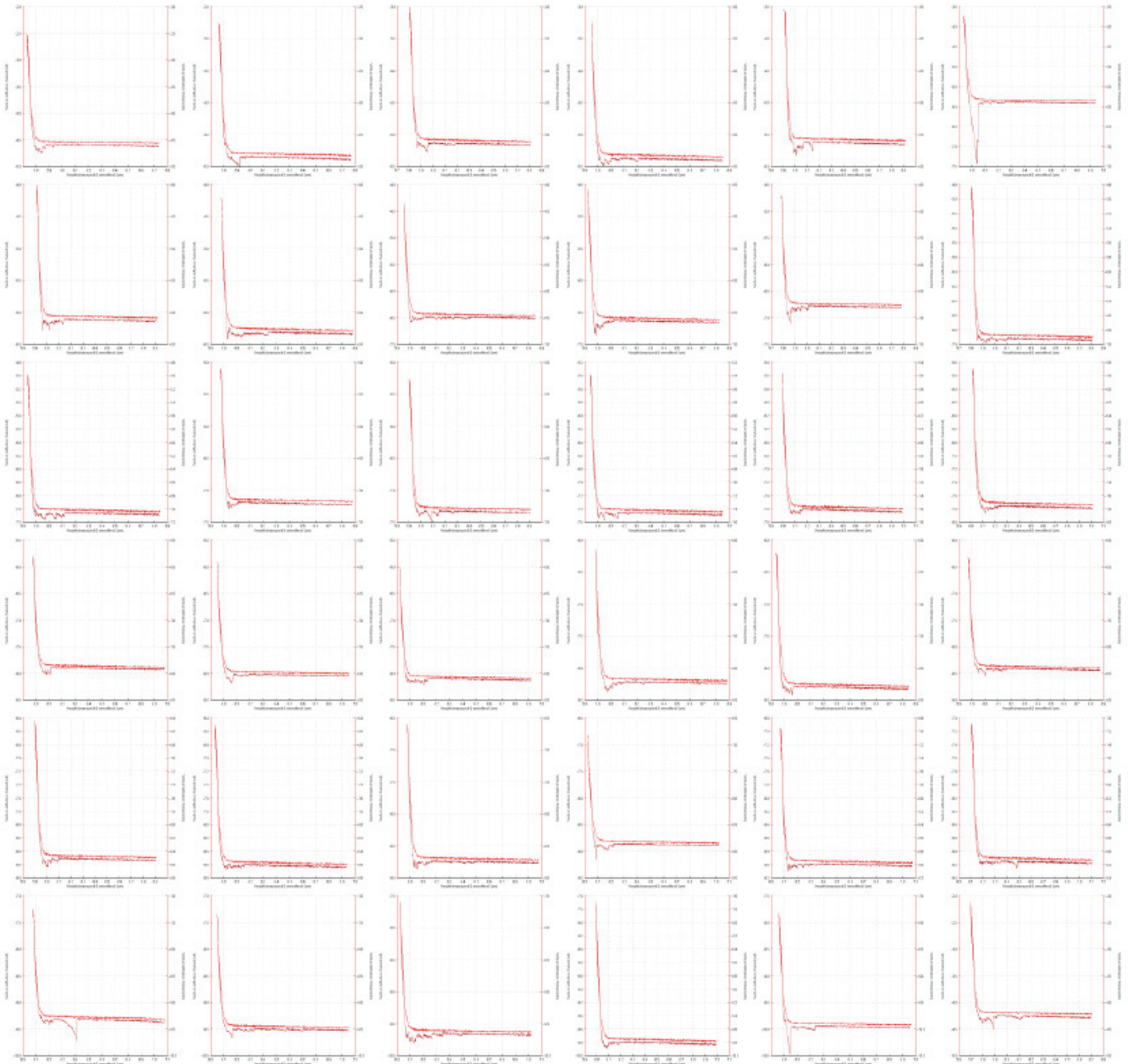
Spring constant: 0,0504 N/m
Deflection sensitivity: 58,73 nm/V



1 mg/ml mucin

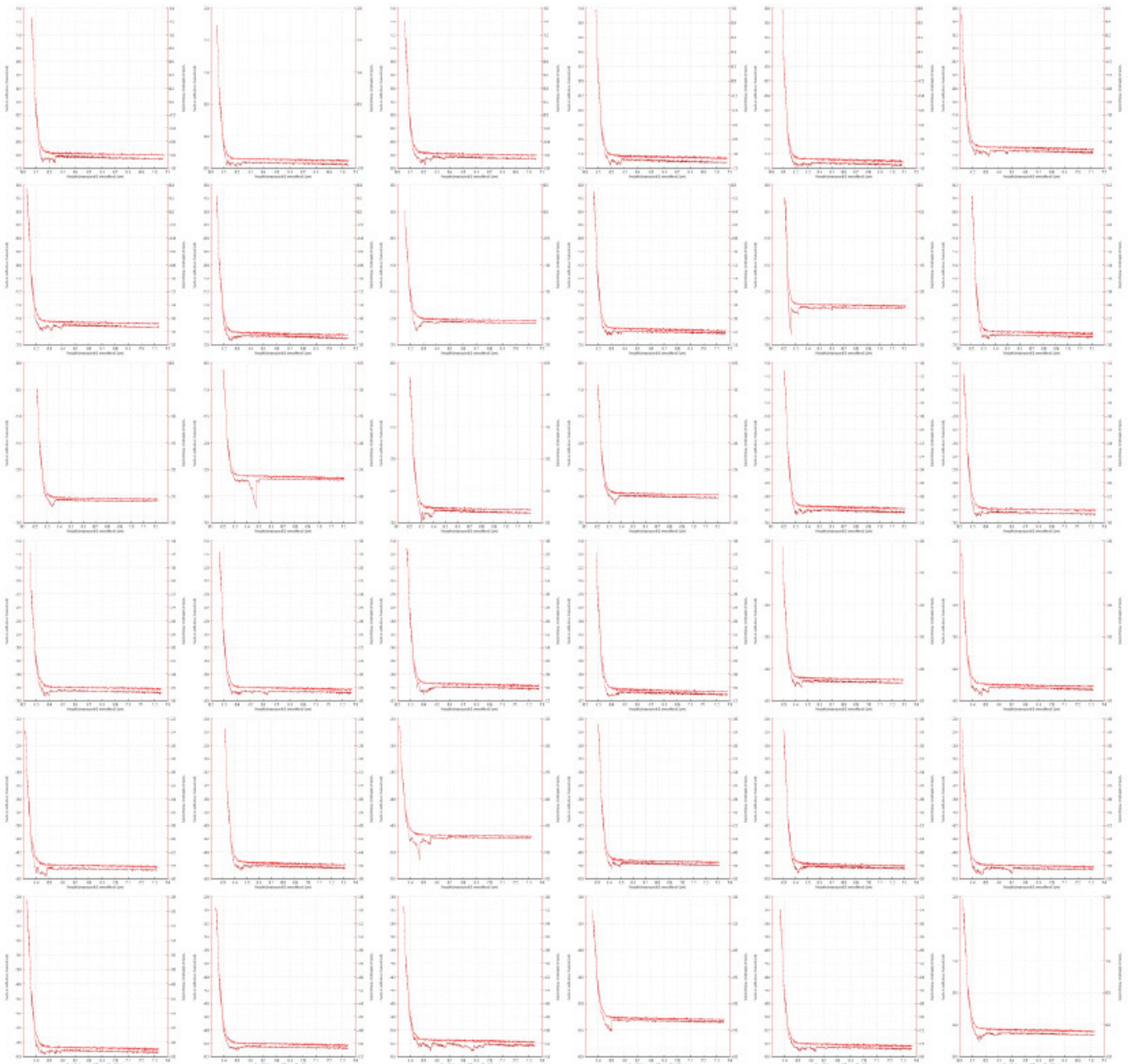
Spring constant: 0,0504 N/m

Deflection sensitivity: 66,77 nm/V



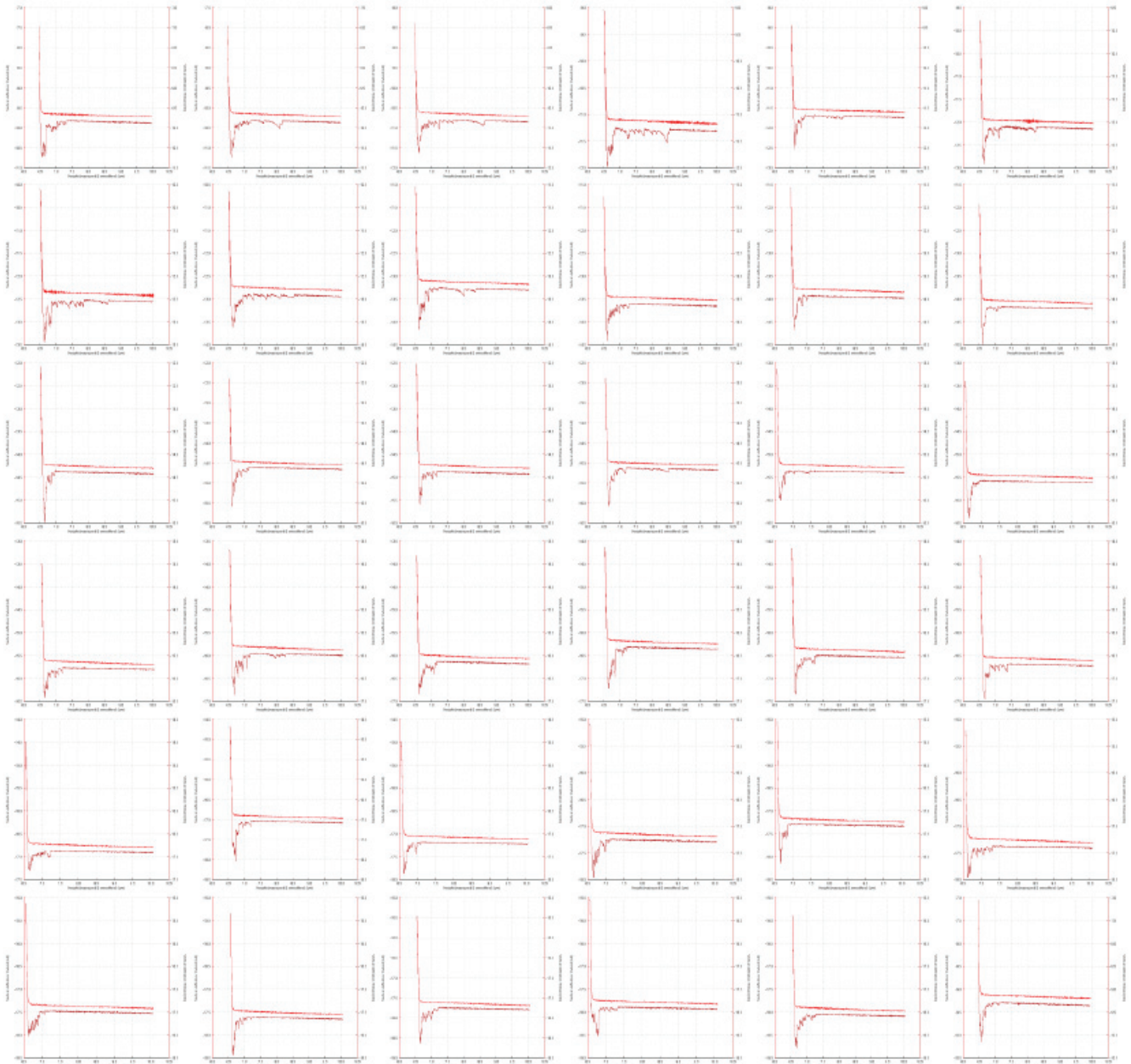
1 mg/ml mucin
2 mg/ml alginate

Spring constant: 0,0504 N/m
Deflection sensitivity: 66,77 nm/V



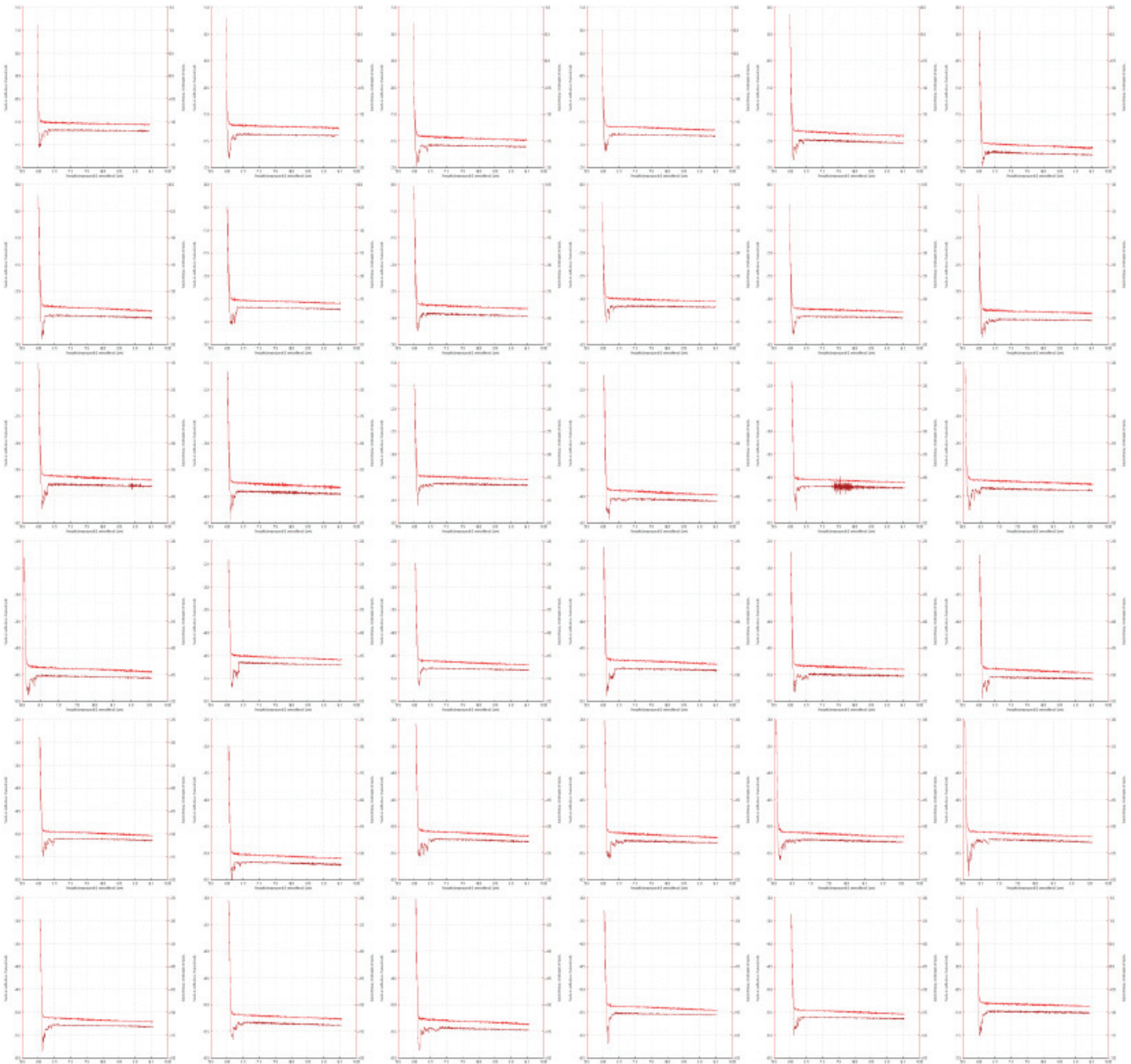
1 mg/ml mucin
2 mg/ml alginate
0,05 mg/ml G-blocks

Spring constant: 0,0470 N/m
Deflection sensitivity: 58,73 nm/V



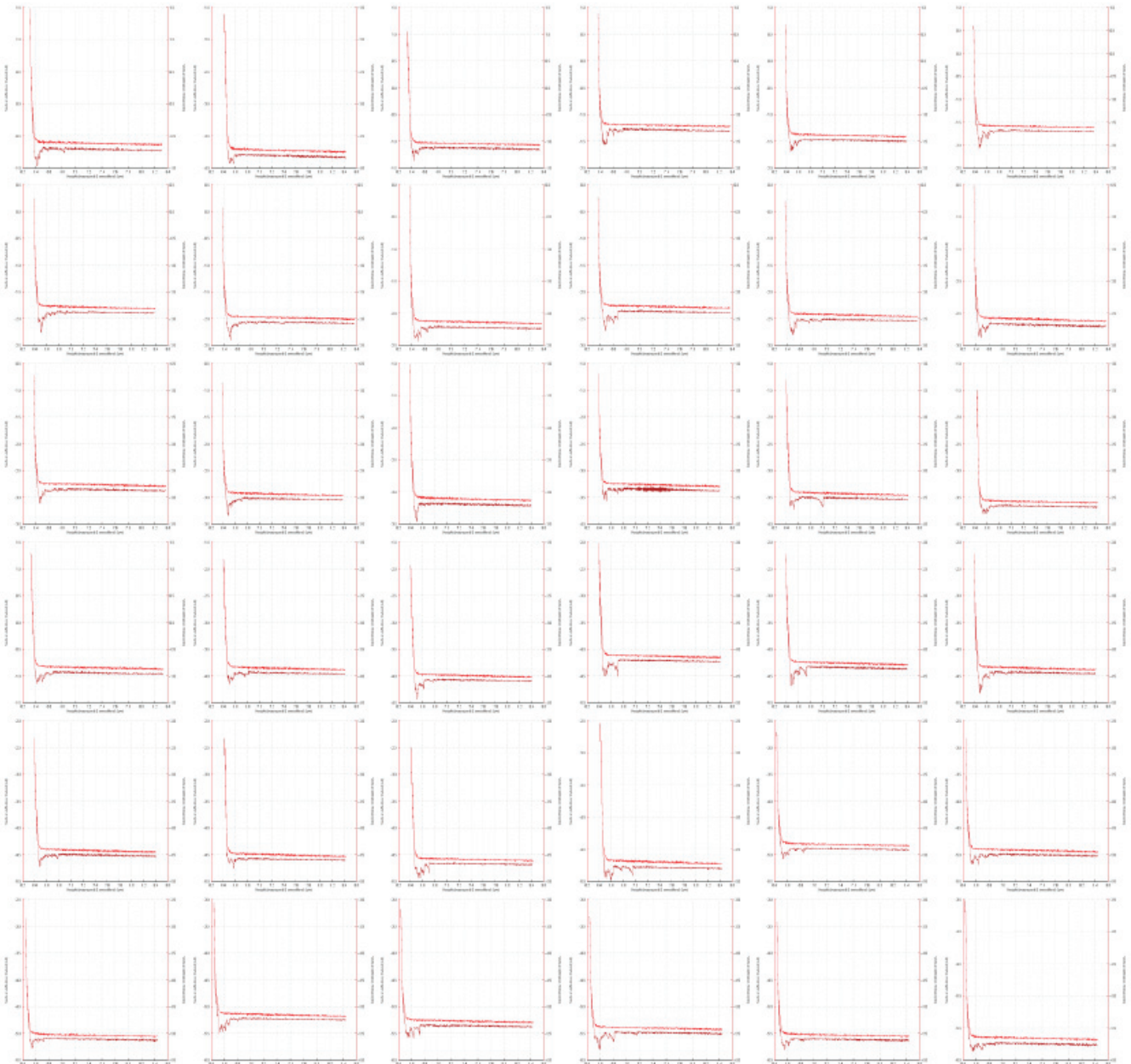
1 mg/ml mucin
2 mg/ml alginate
0,1 mg/ml G-blocks

Spring constant: 0,0470 N/m
Deflection sensitivity: 58,73 nm/V



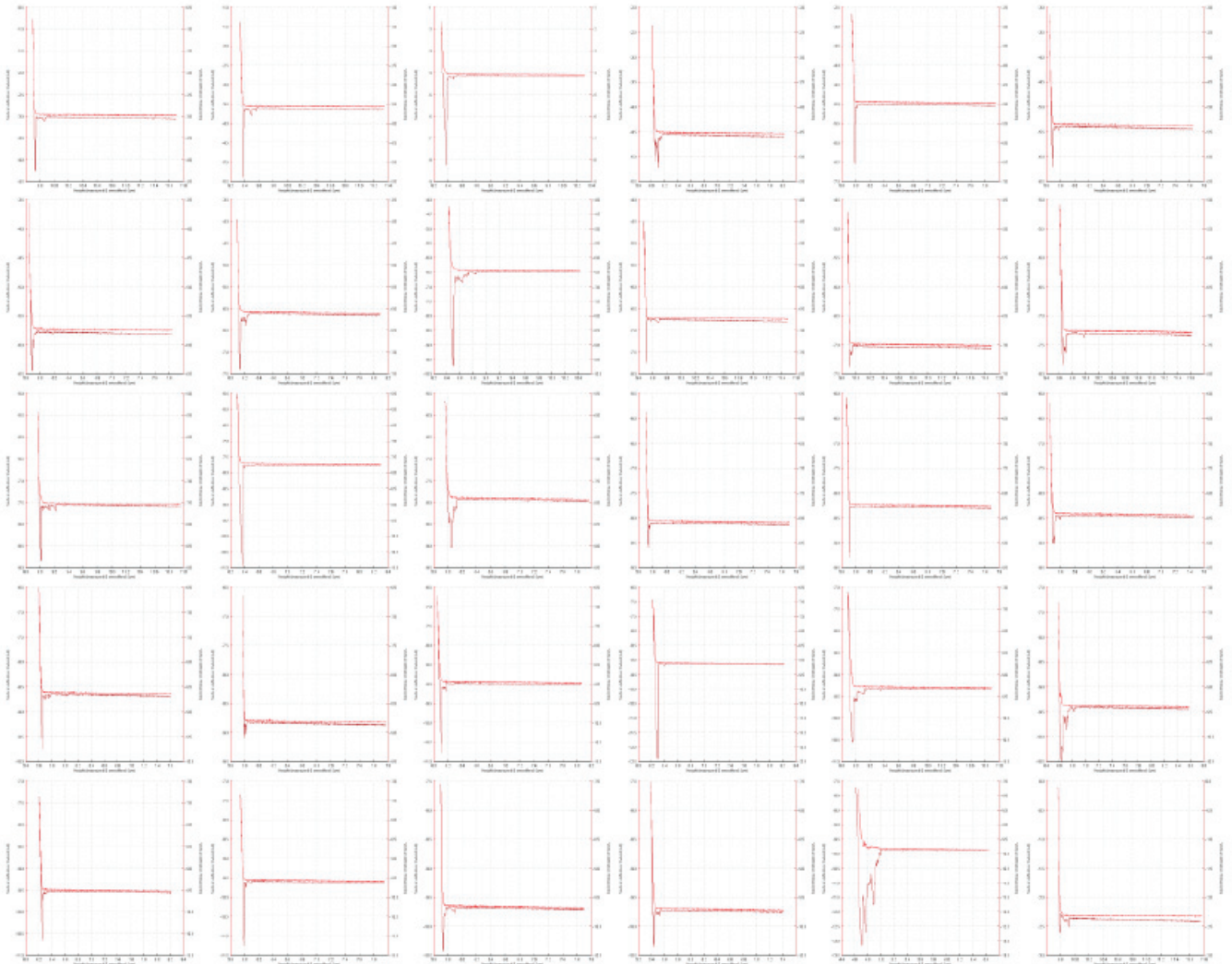
1 mg/ml mucin
2 mg/ml alginate
0,5 mg/ml G-blocks

Spring constant: 0,0470 N/m
Deflection sensitivity: 58,73 nm/V



1 mg/ml mucin
2 mg/ml alginate
2 mg/ml G-blocks

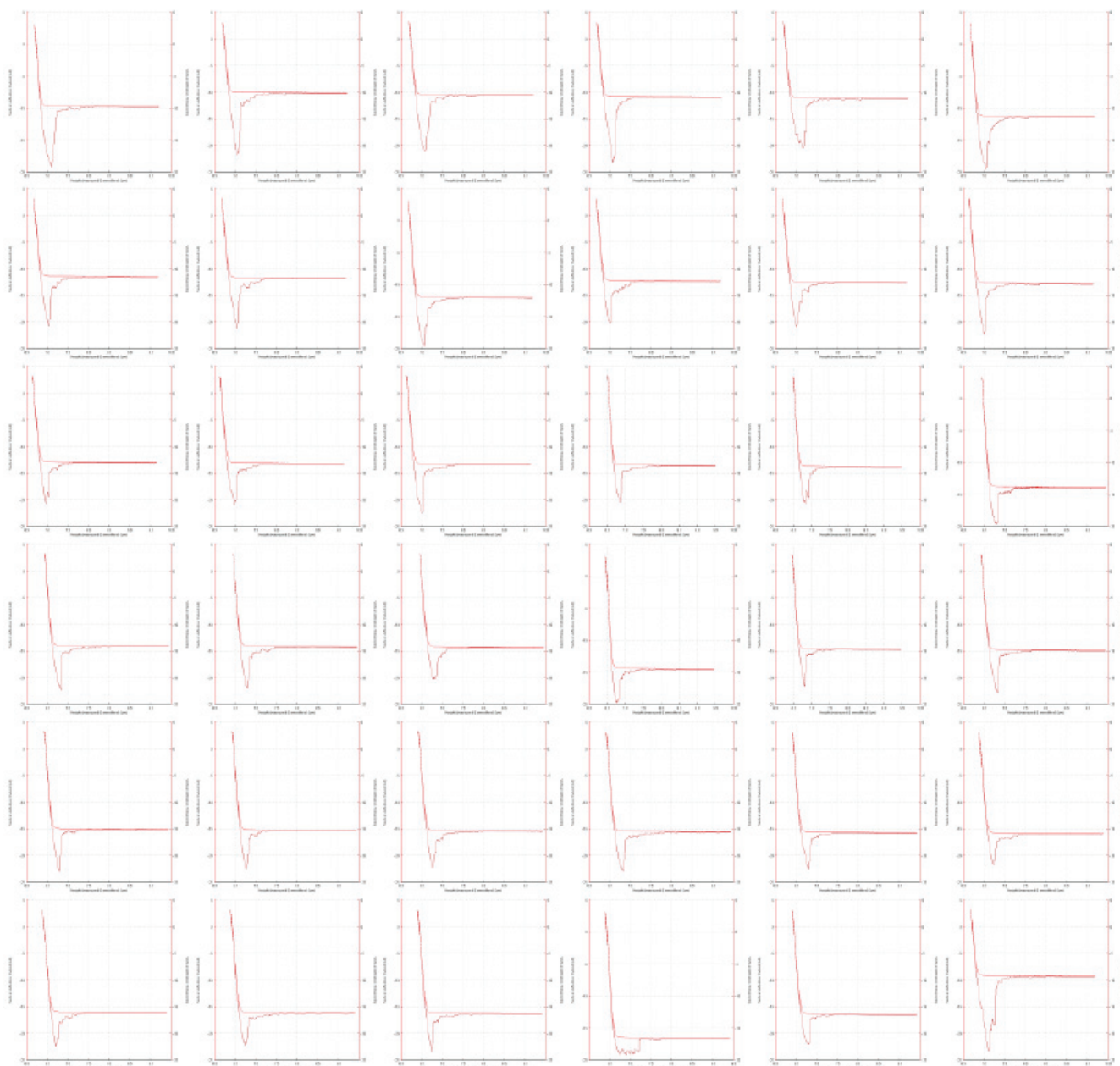
Spring constant: 0,0470 N/m
Deflection sensitivity: 58,73 nm/V



0,5 mg/ml mucin

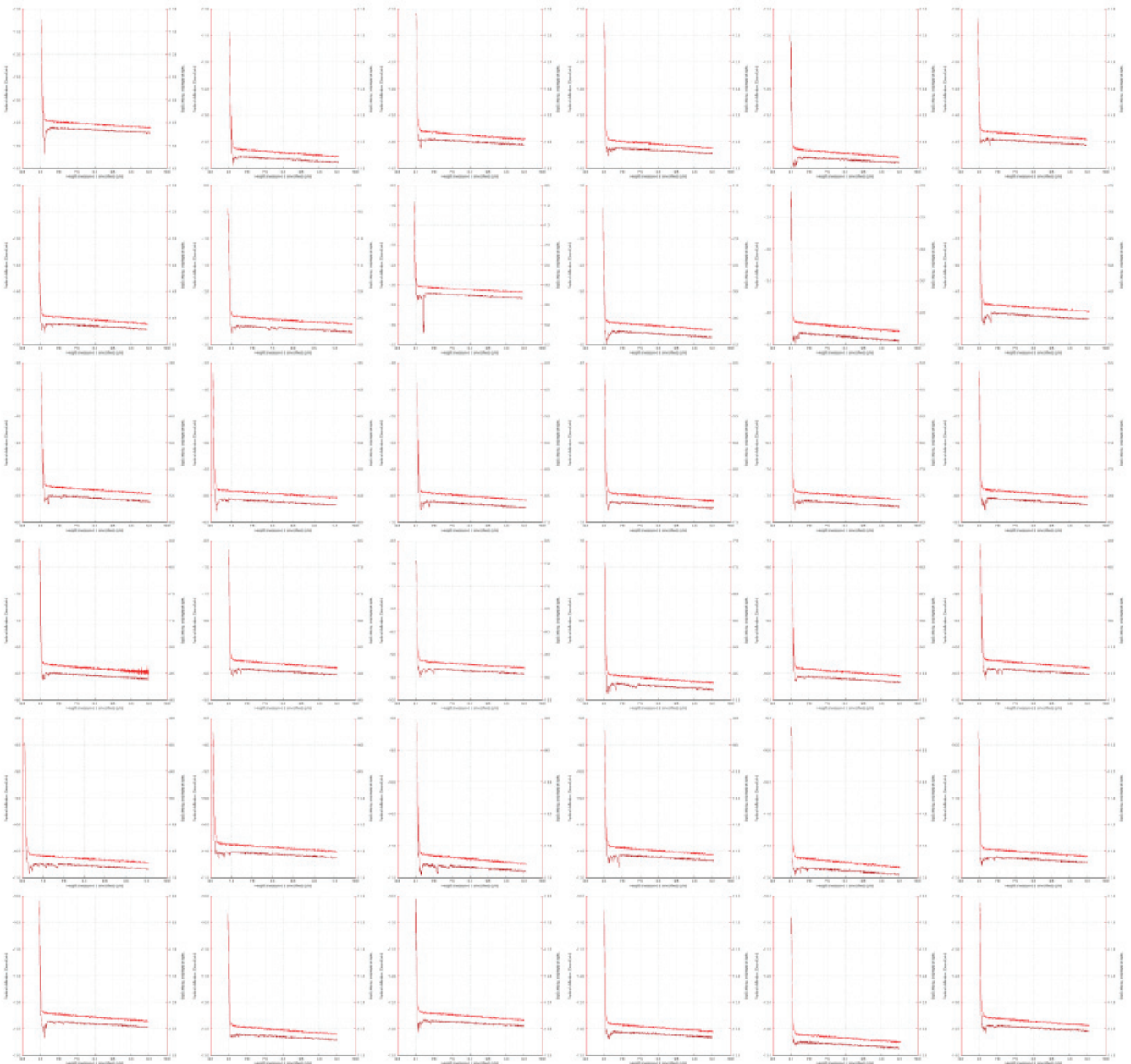
Spring constant: 0,0845 N/m

Deflection sensitivity: 49,53 nm/V



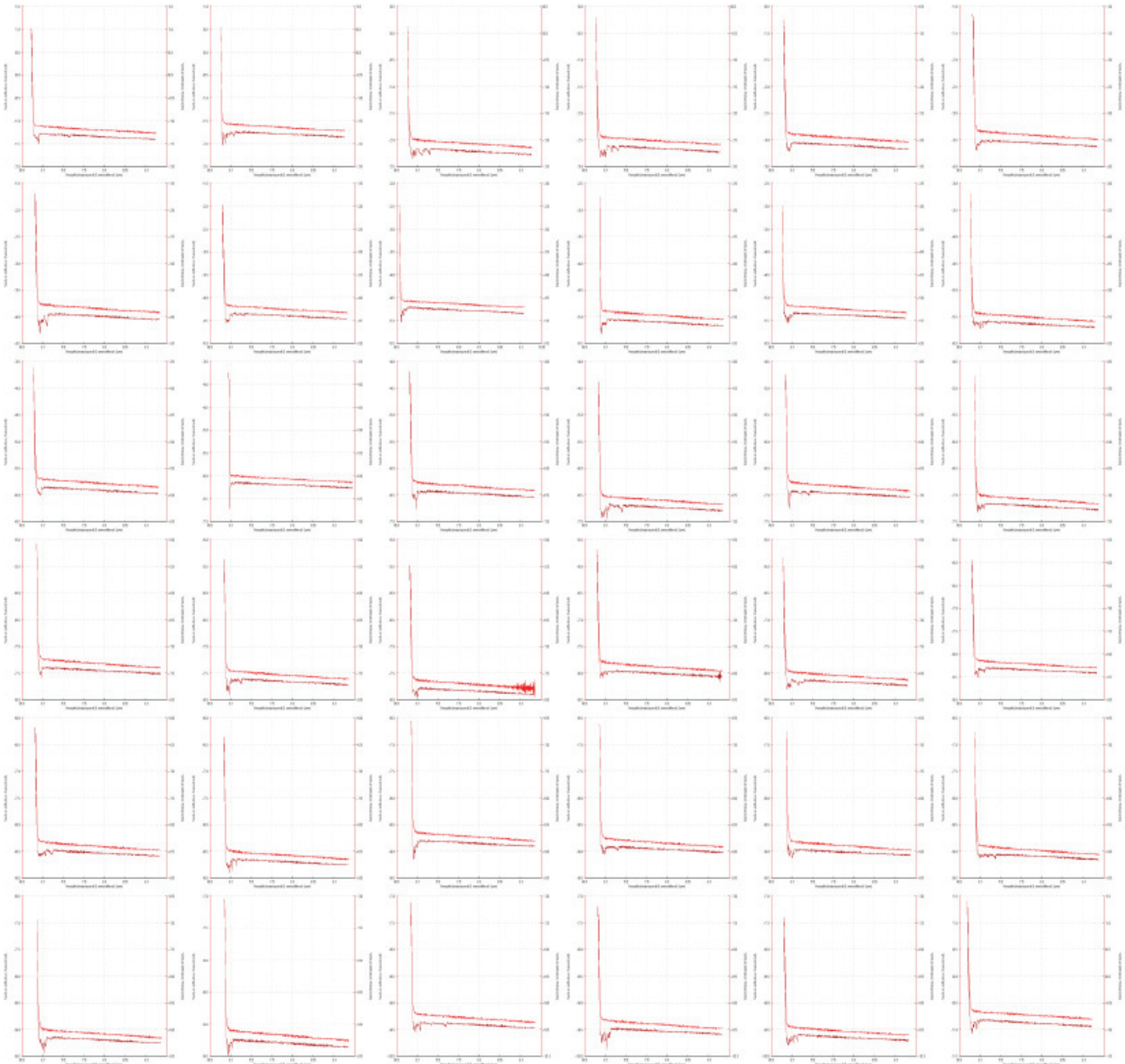
0,5 mg/ml mucin
0,5 mg/ml alginate

Spring constant: 0,0845 N/m
Deflection sensitivity: 49,53 nm/V



0,5 mg/ml mucin
0,5 mg/ml alginate
0,05 mg/ml G-blocks

Spring constant: 0,0845 N/m
Deflection sensitivity: 49,53 nm/V



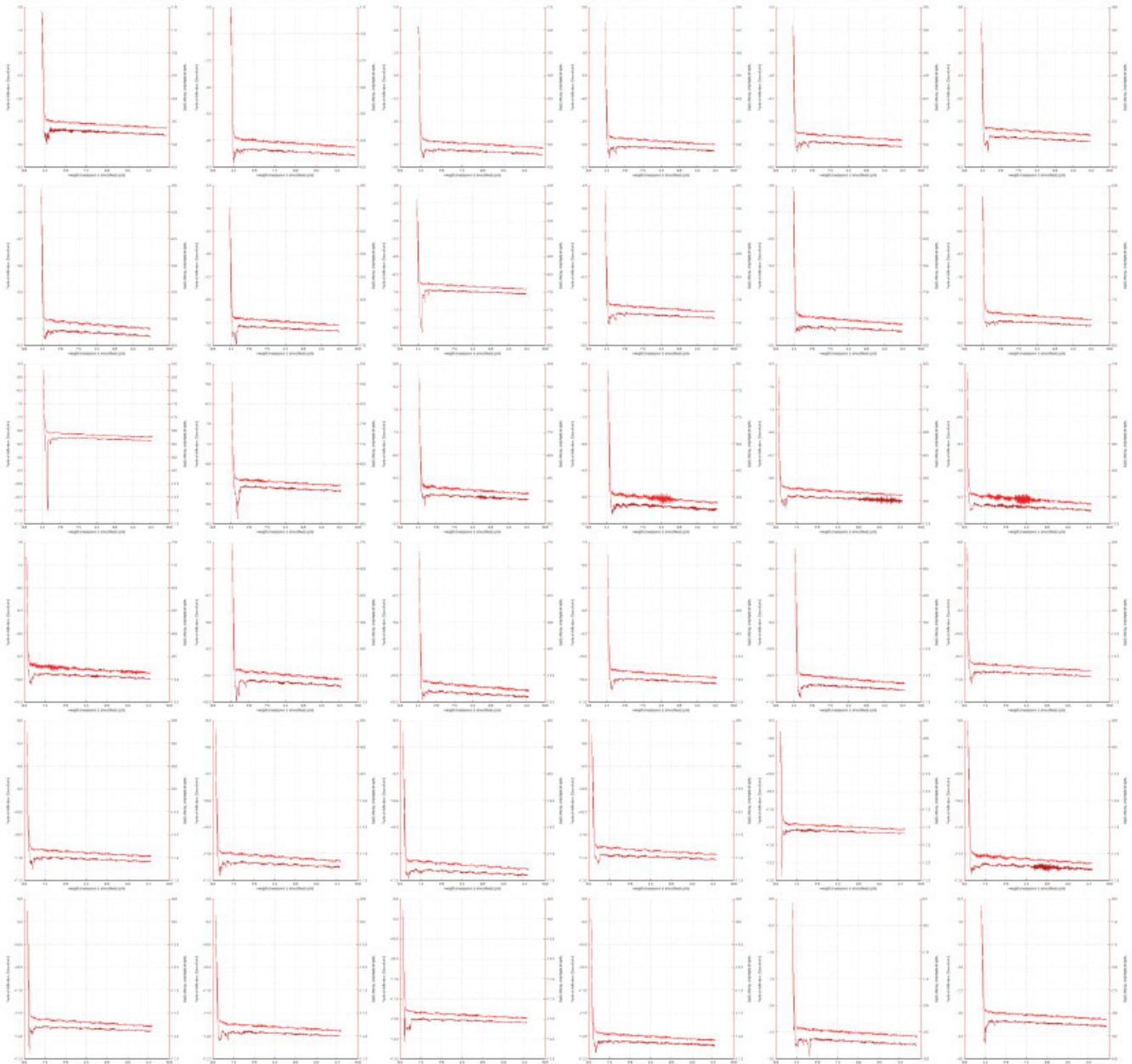
0,5 mg/ml mucin
0,5 mg/ml alginate
0,1 mg/ml G-blocks

Spring constant: 0,0845 N/m
Deflection sensitivity: 49,53 nm/V



0,5 mg/ml mucin
0,5 mg/ml alginate
0,5 mg/ml G-blocks

Spring constant: 0,0845 N/m
Deflection sensitivity: 49,53 nm/V



0,5 mg/ml mucin
0,5 mg/ml alginate
2 mg/ml G-blocks

Spring constant: 0,0845 N/m
Deflection sensitivity: 49,53 nm/V

